8-1974

Droplet Dynamics in Cooling Tower Plumes

Edison A. Picklesimer Jr.
University of Tennessee - Knoxville

To the Graduate Council:

I am submitting herewith a dissertation written by Edison A. Picklesimer Jr. entitled "Droplet Dynamics in Cooling Tower Plumes." I have examined the final electronic copy of this dissertation for form and content and recommend that it be accepted in partial fulfillment of the requirements for the degree of Doctor of Philosophy, with a major in Engineering Science.

William T. Snyder, Major Professor

We have read this dissertation and recommend its acceptance:

George C. Frazier, John H. Forrester, H. L. Weissberg, C. J. Remenyik

Accepted for the Council:
Dixie L. Thompson

Vice Provost and Dean of the Graduate School

(Original signatures are on file with official student records.)

To the Graduate Council:

I am submitting herewith a dissertation written by Edison A. Picklesimer, Jr., entitled "Droplet Dynamics in Cooling Tower Plumes." I recommend that it be accepted in partial fulfillment of the requirements for the degree of Doctor of Philosophy, with a major in Engineering Science.

William J Snyder
William T. Snyder, Major Professor

We have read this dissertation
and recommend its acceptance:

George C. Frazier

John H Forester

Harold J. Hawley

Carl J. Pennington

Accepted for the Council:

Dean A. Shirk
Vice Chancellor
Graduate Studies and Research

DROPLET DYNAMICS IN COOLING TOWER PLUMES

A Dissertation

Presented for the

Doctor of Philosophy

Degree

The University of Tennessee

Edison A. Picklesimer, Jr.

August 1974

ACKNOWLEDGEMENTS

The author wishes to take the opportunity to acknowledge the assistance he has received in accomplishing the present investigation. First, particular thanks are due to the Oak Ridge National Laboratory, the Carolina Power and Light Company, and the University of Tennessee for providing the financial assistance and computer time that made possible the research. Thanks are due to Dr. H. A. Smith and the Graduate Council for providing a N.D.E.A. Title IV Fellowship that made possible the continuation of the author's educational program. The efforts of each of the Faculty Advisory Committee, Dr. J. H. Forrester, Dr. G. C. Frazier, Dr. C. J. Remenyik, Dr. W. T. Snyder, and Dr. H. L. Weissberg, is gratefully acknowledged. Particular recognition is due for the Committee Chairman, Dr. W. T. Snyder, who is not only an inspiring teacher but also a personal friend to the students.

Particular attention is also drawn to the personal efforts, guidance, never ending support, faith, and numerous sacrifices made by the author's wife, Linda P. Picklesimer, children, Patrick and Kent, and parents.

ABSTRACT

Large cooling towers are becoming more common as a means of disposing of large quantities of waste heat from steam electric generating stations. Increased attention is being focused on how the effluents from these towers affect the environment. This research is concerned with the determination of the paths and ultimate deposition of salt laden drift drops exiting from a cooling tower by analyzing the basic droplet dynamics governing the transport of these droplets.

The equation of motion is developed for a liquid drift drop as it is transported through the atmosphere. A term appears in the equation of motion which has not been considered by previous authors. A finite difference technique is used to solve for the velocity and position of the drift drop at any time. Meteorological variables as well as cooling tower variables are considered in calculating the trajectory of the drift drop. A model is developed to account for the effects of dissolved chemicals on droplet evaporation rate.

The concepts presented in this paper have been incorporated into a model which predicts chemical deposition from evaporative cooling towers. The results of the model study show better agreement with experimental data than previous models.

TABLE OF CONTENTS

CHAPTER		PAGE
I.	INTRODUCTION	1
II.	LITERATURE REVIEW	5
	Basic Features of Cooling Towers	5
	General Plume Features	8
	Basic Plume Assumptions in the Literature	11
	Thermodynamics of Moist Air Mixing	16
	Drift Deposition Models in the Literature	23
III.	DEVELOPMENT OF THE EQUATION OF MOTION	34
IV.	DRAG COEFFICIENTS	39
V.	EVAPORATION OF DROPS	44
VI.	DROPLET VAPOR PRESSURE	51
VII.	PLUME BEHAVIOR	64
VIII.	SOLUTION OF THE EQUATION OF MOTION	72
	Finite Difference Solution	72
	Initial Conditions	75
	Sign on the Drag Term	76
IX.	DISCUSSION OF RESULTS	80
	Sample Calculation Using the Hosler, et.al., Model	94
	UT Model	99
	Discussion of Sample Calculation	102
X.	CONCLUSIONS	110

CHAPTER PAGE

BIBLIOGRAPHY.....112

APPENDIXES.....116

Appendix A.....117

Appendix B.....118

VITA.....122

LIST OF TABLES

TABLE		PAGE
2-1	Factors Affecting Transport and Deposition of Drift	24
6-1	Number of Particles in One Mole for Various Salts	58
6-2	Comparison of Freezing-Point Lowering by Ionic Electrolytes and by Non-Electrolytes in Water	59
9-1	The Pasquill Stability Classification	82
9-2	Meteorological Conditions Used in Sample Calculations	95
9-3	Cooling Tower Variables Used in Sample Calculations	96
9-4	Mass Distribution Using Hosler, et.al., Model	97
9-5	Maximum Height in Plume and Equilibrium Fall Height of Drops Using Hosler, et.al., Model	98
9-6	Deposition by Hosler, et.al., Model	100
9-7	Program Input	103
9-8	Input Cards for UT Program	104
9-9	Modified Mass Distribution For UT Model	105
9-10	Modified Wind Distribution	106

LIST OF FIGURES

FIGURE		PAGE
2-1.	Natural Draft Cooling Tower	6
2-2.	Mechanical Draft Cooling Tower	7
2-3.	Schematic Representation of Flow Near Cooling Tower Exit Plane	9
2-4.	Schematic of a Plume in Cross Flow	10
2-5.	Smokestack Plume Showing Hewett, Fay, and Hoult's Coordinates	14
2-6.	Vapor Mass Fraction Versus Temperature	18
2-7.	Heat Balance for Air-Vapor Mixture	20
2-8.	Height, h_e, a Drop of Initial Radius Must Fall To Reach the Equilibrium Size for Different Relative Humidities and Different Initial Salt Concentrations	29
2-9.	Correction Factor, CORRF, as a Function of Radius For Three Different Air Flow Velocities, w_o, from the Tower	30
2-10.	Nonogram for Salt Deposition Calculations ($h_r < h_e$)	31
2-11.	Nonogram for Salt Deposition Calculations (saturated droplets, $h_r > h_e$)	32

FIGURE PAGE

2-12. Nonograms for Salt Deposition Calculations (solid particles)..... 33

3-1. Drop at Time t and Time t + Δt..... 36

4-1. Drag Coefficient for Spheres as a Function of Reynolds Number..... 40

5-1. Ventilation Factor as a Function of Reynolds Number..... 50

6-1. Vapor Pressure Over a Flat Surface..... 52

6-2. Vapor Pressure Over a Curved Surface..... 53

6-3. Comparison of the Vapor Pressures of Pure Water, a One Molal (1 M) Solution, and a Two Molal (2 M) Solution..... 57

6-4. Van't Hoff Factor versus Concentration..... 60

6-5. Solubilities of Certain Solids at Different Temperatures..... 63

7-1. Plume Profile..... 66

7-2. Coordinate System..... 68

7-3. Model Parameters..... 70

8-1. Drift Drop in Plume..... 77

8-2. Drift Drop Moving Up in Ambient Air..... 78

8-3. Drift Drop Falling in Ambient Air..... 79

9-1. Drift Drop Trajectory..... 83

9-2. Drift Drop Trajectory Showing Effects of Initial Position..... 85

FIGURE PAGE

9-3. Drift Drop Trajectory Showing Effects of Salt Concentration..... 87

9-4. Drift Drop Trajectory Showing Effects of Stability Condition..... 88

9-5. Drift Drop Trajectory of Wistrom and Ovard..... 90

9-6. Drift Drop Trajectory by UT Model..... 91

9-7. Salt Precipitation Within a Drift Drop..... 93

9-8. Comparison of Deposition from Hosler, et.al., Model and UT Model.....101

9-9. Transfer of Chromium and Zinc to Vegetation from Cooling Tower Drift as a Function of Distance from the Tower. The Horizontal Lines (dashed) Indicate Levels of Concentration in Vegatation Remote from the Towers.....108

B-1. The Mixing of Air.....119

NOMENCLATURE

I. English Symbols

a	characteristic plume width, 2 times the standard deviation, meters
$\bar{a}$	acceleration, m/sec^2
A	plume cross-sectional area perpendicular to plume centerline, m^2
A_p	projected area of drop, m^2
b	buoyancy parameter = $(g/T_p)(T_p-T_e)$, m/sec^2
c	specie concentration, gm/gm mixture
C	a constant
c_p	specific heat at a constant pressure, cal/gm-°K
cf	convection coefficient
C_D	drag coefficient
d	distance, meters
D	diffusion coefficient, m^2/sec
F_D	drag force, newtons
$\bar{F}$	force, newtons
g	acceleration of gravity, m/sec^2
h	enthalpy, cal/gm
h_d	height a drop must fall to evaporate to a dry particle, m
h_e	height a drop must fall to achieve the equilibrium size, m
h_o	height of tower, m
h_p	height of plume, m
h_r	maximum height of drops in plume, m
Δh	plume rise = h_p-h_o, m
H	relative humidity

k	thermal conductivity, cal/m-hr-°K
L	latent heat of vaporization, Cal/gm
m	mass, gm, mixing ratio
M	mass of drop, gm
Mw	molecular weight, gm/gm-mol
n	van Hoff's factor
Pr	Prandtl number = C_p /k
P	pressure, newtons/m^2
Q	energy generated per unit volume of fluid, cal/m^3
Q'	source strength, m^3/sec
q	specific humidity (vapor mass fraction), gm H_2O vapor/gm dry air
$\bar{q}$	heat flux vector, cal/m^2-sec
Re	Reynolds number = $2P_3 (V_d-V_e)^2 Rd/$ e
R	radius, m
$\mathcal{R}$	universal gas constant, gm-cal/gm-mol-°K
r	radius, radial coordinate, m
SP	stability parameter
S	surface tension, newtons/m
s	distance along plume centerline, m
Sc	Schmidt number
t	time , seconds
T	temperature, °K
u	velocity parallel to plume centerline, m/sec
U	wind velocity, m/sec
v	velocity, m/sec

NOMENCLATURE (continued)

VF	ventilation factor
vr	velocity ratio
$\overline{V}$	velocity vector, m/sec
$\forall$	volume flux, m^3/sec
w	vertical velocity, m/sec
W	specie generation rate, gm/m^3-sec
x,y,z	coordinate positions (see Figure 21), m

II. Greek Symbols

α	thermal diffusivity, m^2/sec
ε	rate of entrainment, m^3/sec-ft
$\overline{\overline{\sigma}}$	stress tensor
σ	water mass fraction, gm H_2O liquid/gm dry air
ρ	density, gm/cm^3
γ	specific weight, newtons/m^3
ψ	stream function
θ	potential temperature
Φ	velocity potential
$\hat{\Phi}$	dissipation function
ν	kinematic viscosity of air, m^2/sec
ϕ'	angular coordinate (see Figure 7-2)
β	angle between u and x
θ'	angular coordinate (see Figure 7-2)

III. Subscripts

a	air
B	body force

NOMENCLATURE (continued)

c	solute dissolved in drop
d	drop
D	drag
e	environment
g	gas
l	liquid
o	cooling tower exit plane
p	plume
r	radial direction
s	saturated
v	vapor
x,y,z	coordinate directions
θ	θ' coordinate direction
∞	far away from the drop

CHAPTER I

INTRODUCTION

The disposal of waste heat associated with electric power generation is of great concern to the electric power generating industry and the general public. Because of the large amount of electricity produced in the United States, the electric power generating industry must dispose of large quantities of waste heat. It is necessary to dispose of 5.1 BTU/hr (.36 gm-cal/sec) of waste heat for every watt of generating capacity in today's design of a fossil-fueled steam electric power station and 6.8 BTU/hr (.48 gm-cal/sec) for every watt in a nuclear electric station. These figures are based on thermal efficiences of 40% and 33% for fossil and nuclear electric power plants respectively. Thus, a 1000 megawatt fossil station must dispose of 2000 megawatts of waste heat; a nuclear station of similar capacity must dispose of 2000 megawatts of waste heat.

The first natural draft cooling tower in the United States, Big Sandy near Louisa, Kentucky, began operation in December, 1962. Since this date there has been a rapid increase in the use of such cooling towers, and about 30 towers were in operation by January, 1974. Projections indicate that 40 to 60 towers will be completed by 1976. All the natural draft cooling towers currently operating are associated with the electric utility industry and serve coal-fired, steam electric stations, but about half of the future towers will serve nuclear stations.

The majority of future natural draft cooling tower installations will be located in the Northern Appalachian area of the United States.

There are a number of factors that currently favor the selection of cooling towers as an alternative means of disposing of waste heat. The two most prominent factors are present economics of power station siting and antipollution regulations pertaining to both thermal and air pollution. The electrical power generating industry is currently using rural sites for new stations and mine mouth locations for coal-fired units because the cost of overland power transmission may be more than offset by the lower rural property values and bulk fuel transportation costs. The antipollution regulations dictate the use of either mechanical or natural draft cooling towers. The climatic conditions favorable to the efficient use of natural draft towers are low ambient temperatures. This factor previously has limited the use of natural draft towers to Europe where the low ambient temperatures prevail in the winter when power demand is at its peak. In the United States peak power demand is in the summer due to the widespread use of air conditioners. As a result, mechanical draft units are favored in the United States. However, comparison of the environmental effects of the two types of cooling towers favor the selection of natural draft towers in certain situations, especially for areas where good dispersion of vapor is necessary.

The Chalk Point natural draft cooling towers in Maryland are typical of the towers currently in operation in the United States. The Potomac Electric Power Company (PEPCO) selected natural draft cooling towers for its new fossil Units 3 and 4 (630 MWe each) since the existing Chalk Point Units already use up to 30% of the Patuxent River flow. The

Chalk Point Unit 3 tower is of particular interest because it will be the first hyperbolic natural draft cooling tower in Maryland and the first in the United States to use salt water when it goes on line in 1974. (The Unit 4 tower is scheduled to begin operation in 1975.)

Although cooling towers alleviate the problem of thermal input to the aquatic environment, they can pose problems of their own (i.e., drift, fog, downwind icing, precipitation enhancement, and blowdown.) Most important, little is known about the potential effects a brackish water tower could have on surrounding vegetation, particularly tobacco, a commercially important crop in the Chalk Point area (tobacco is known to be very chloride sensitive).

The Chalk Point Unit 3 tower is expected to dissipate a heat load of $3.5X10^9$ Btu/hr at design conditions, equivalent to about 1000 MW. This heat discharge to the atmosphere is accompanied by an equally impressive quantity of water, about 5200 gpm due to evaporation, the primary heat transfer mechanism. Of greatest immediate concern, however, is the "salt water drift," droplets of saline water carried out by the tower by the updraft and eventually deposited on the surrounding terrain. Cooling tower vendors are guaranteeing a state-of-the-art drift rate of no greater than 0.002% of the circulating water flow, or about 5 gpm of liquid water. It is important to note that this guarantee and the following analysis are based on design conditions which occur only 3 or 4 days of the year.

Annual average salt concentration in the Patuxent River at Chalk Point is about 7 parts per thousand (ppt). On a monthly basis, values range from a low of 1 ppt to a high of 13 ppt. By adjusting

blowdown (water returned to the river) to equal evaporation loss, salt concentration in the circulating water would be twice river salinity. During the tobacco growing season, roughly April through September, the solid salt emission rate from the tower should be about 0.6 lb/minute (4.54 gm/sec). Based on typical summer values for atmospheric mixing layer height (500 meters) and the mean wind speed (3 mps), salt deposition rates of up to 3 lb/acre-mo (.34 gm/m^2-mo) can be predicted over a 1500 acre (6.1 X 10^6 m^2) area in an annular ring 0.9 to 1.4 miles (1.45 to 2.25 km) from the tower. Since sodium chloride is 60% chloride by weight, this region would receive an average of about 1.8 lb of chloride ion/acre-month (2.04 gm/m^2-mo).

According to one expert,[1] total chloride ion settling on any area growing tobacco should not exceed 1.5 lb/ac-mo (1.7 gm/m^2-mo) at least until better data are available to ascertain tobacco tolerance to salt. Furthermore, this guideline should apply throughout the year, since salt accumulation in the soil is at least as important as direct deposition on the leaf.

The above analysis, based on many assumptions which critically affect the results, is presented merely to indicate the magnitude of the drift problem. Clearly, as more cooling towers are built in the United States, it will be increasingly important to understand how cooling tower drift is transported through the atmosphere and deposited on the ground.

CHAPTER II

LITERATURE REVIEW

Basic Features of Cooling Towers

There are many simple models currently used to estimate the performance of cooling towers. Although these models will not be as accurate as more detailed analyses such as Woods and Betts[2], or Chilton[3], one can see the important physical processes and can calculate the heat rejection rate and water vapor flux from a tower for various weather conditions

Figure 2-1 shows a typical natural draft tower. Hot water from the condenser is sprayed onto a baffle called the fill or packing. Air is drawn through the fill mixing with the falling water. The water cools by evaporative and convective heat transfer to the air. The cool water collects in the basin and is pumped back into the condenser. Since the warm moist air above the fill is lighter than the cooler, drier air outside the tower, it rises out of the tower forming a buoyant, water laden plume.

Figure 2-2 shows a typical mechanical draft cooling tower. The evaporative cooling process is the same as in the natural draft tower except the air is induced to flow through the tower by a fan located on top of the tower.

As the air passes through the fill, small drops of liquid water are entrained and carried along with the air. In order to prevent the entrained drops from leaving the tower, drift eliminators are used as shown in Figures 2-1 and 2-2. The air stream is forced to make an abrupt turn; since the momentum of the liquid is much greater than that

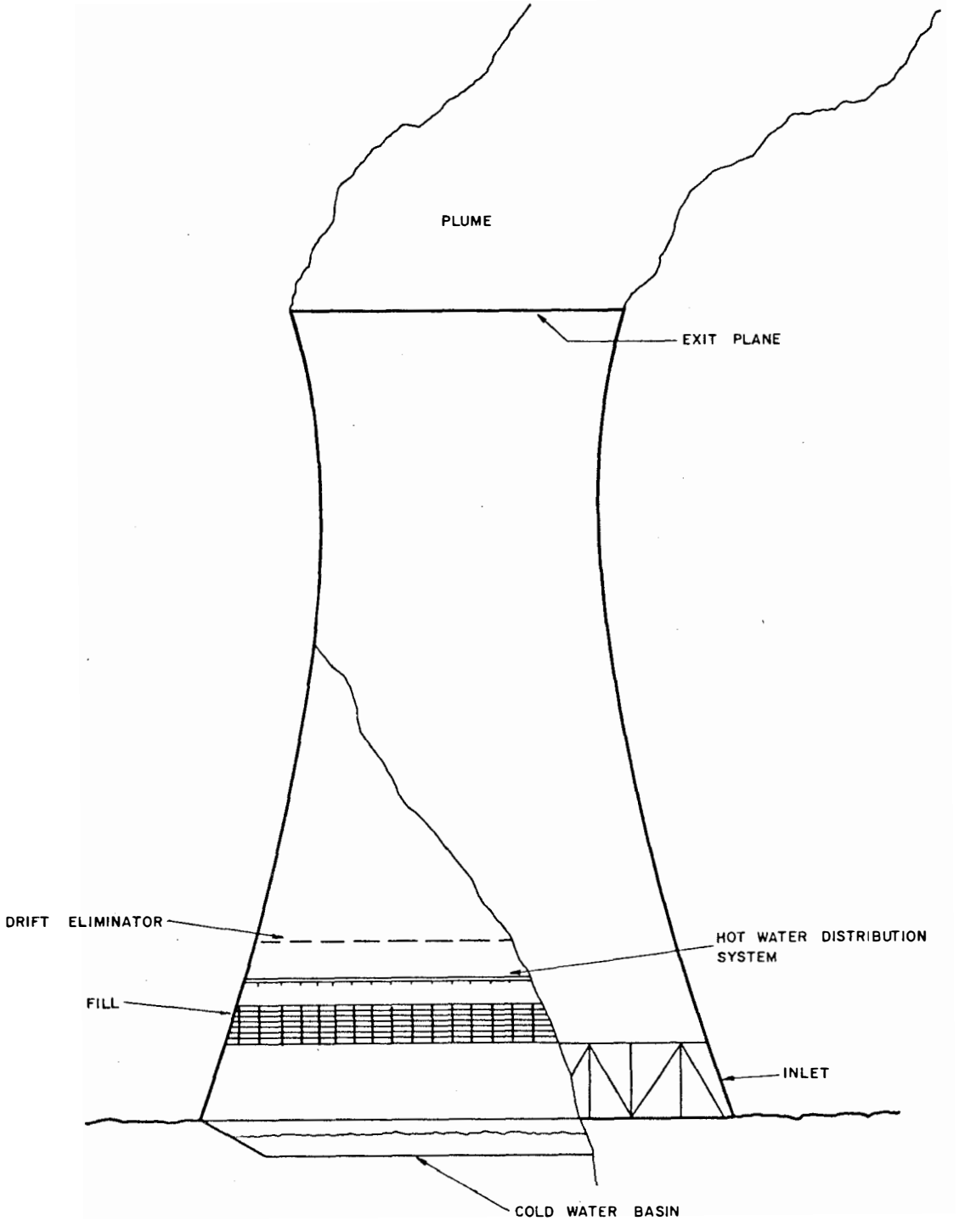

Figure 2-1. Natural Draft Cooling Tower

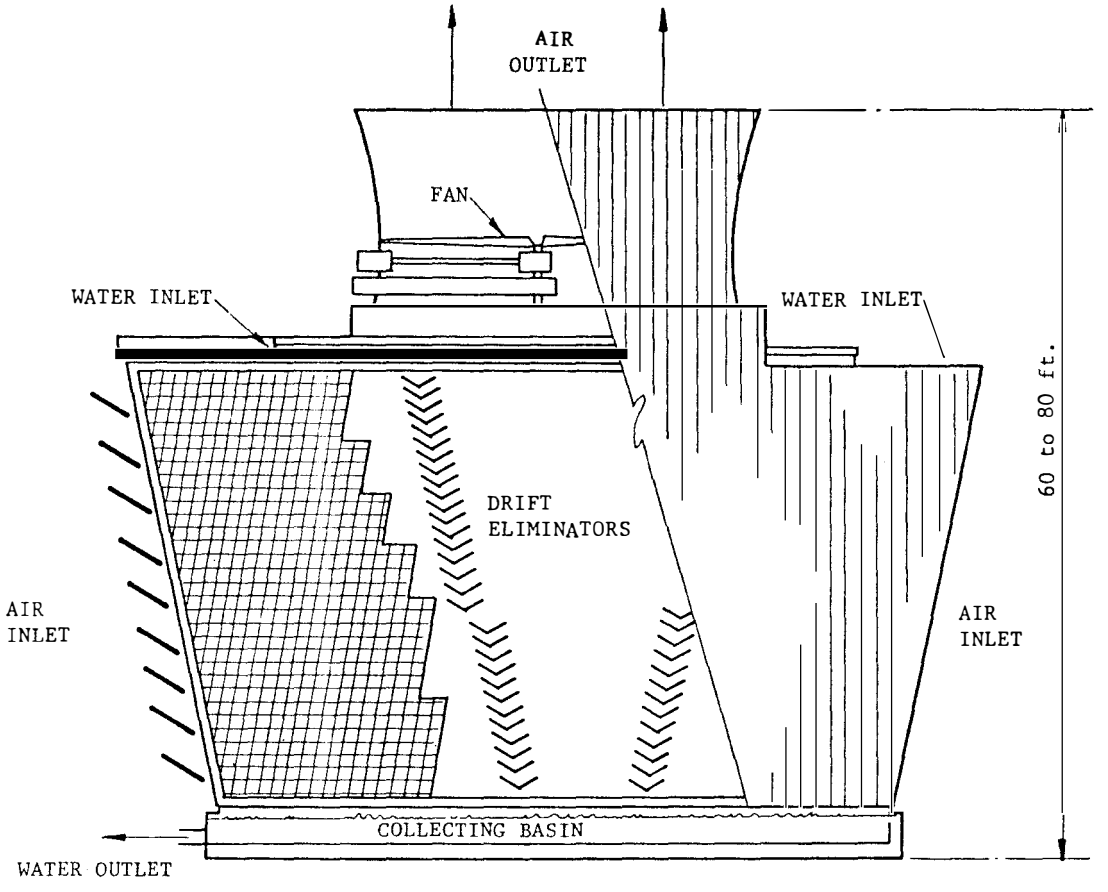

Figure 2-2. Mechanical Draft Cooling Tower

of the air, the large drift drops impact on the drift eliminators and are returned to the basin. More than 90% of the mass of the liquid water entrained in the air is removed and returned to the basin.

As the water heats the air, a small percentage of the water evaporates carrying away its latent heat of vaporization. This evaporative cooling accounts for the majority of the total heat transfer from the water.

General Plume Features

Basic flow features occur whether the plume is issuing into a moving or a stationary atmosphere. Figure 2-3 is a schematic representation of the flow near the exit plane of a tower. The merging of two flows at the tower tip results in the formation of a shear layer. Instability of this shear layer results in a turbulent mixing region for most practical cases. This turbulent mixing action consumes the undisturbed plume flow or so-called "potential core" until the entire plume cross-section is a turbulent mixing region. For the surrounding medium at rest, the submerged plume case, a region of similar mean velocity profiles occurs following a short transition region (i.e., the velocity may be expressed as $u/\{u_o - U\cos\beta\} = f\{r/a\}$). If the far field solution only is of interest, the plume is often considered to have originated from a point disturbance at an apparent source.

The primary effects of a cross flow on a plume are illustrated in Figure 2-4 taken from the test of Abramovich[4]. The cross flow deflects the plume downwind and deforms the cross-section to a kidney shape in a few plume diameters. Counter rotating vortices are formed behind the plume. These vortices significantly increase the mixing process, and

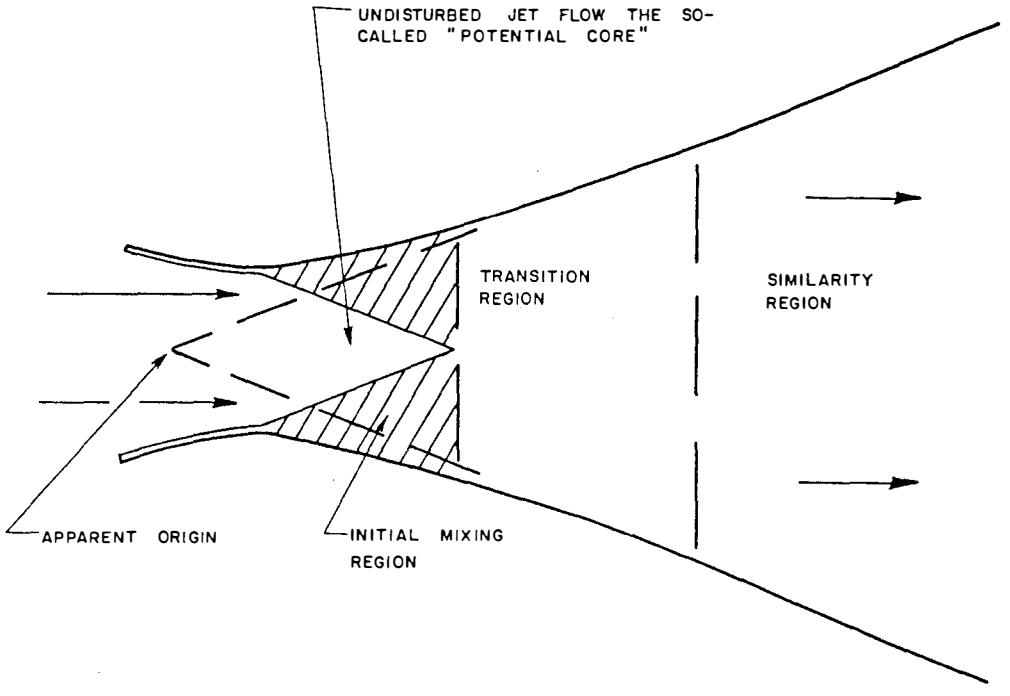

Fgiure 2-3. Schematic Representation of Flow Near the Cooling Tower Exit Plane

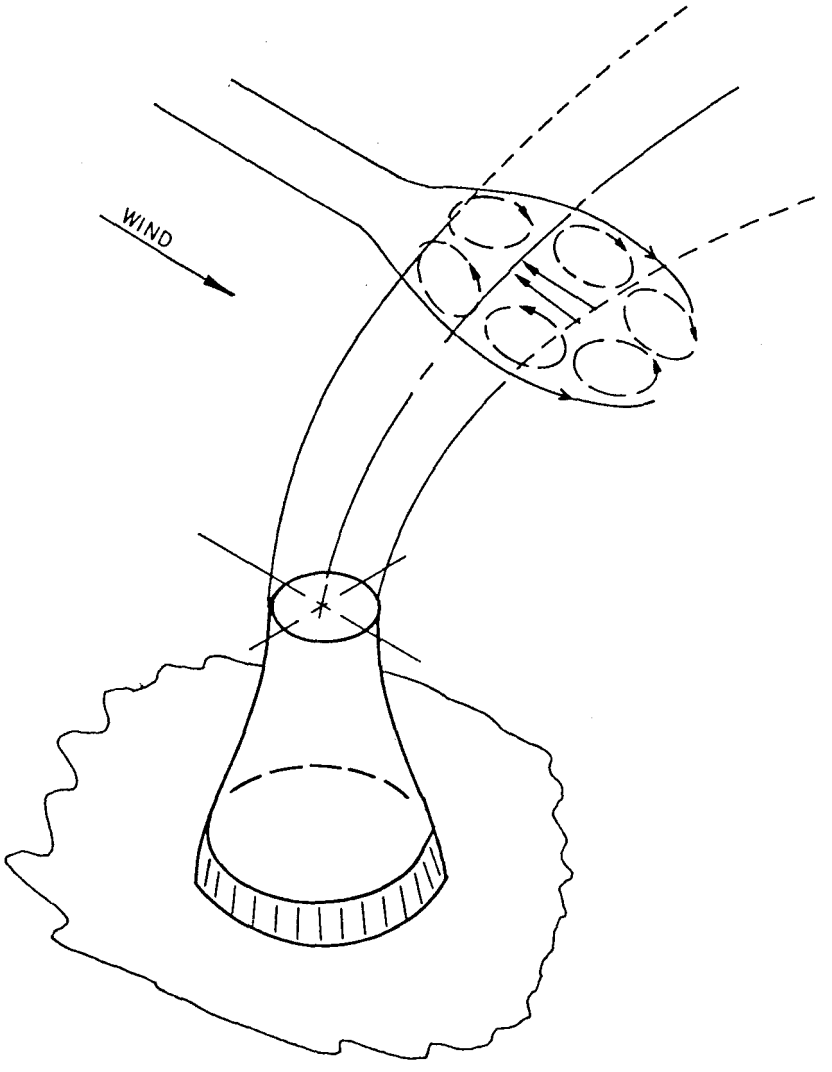

Figure 2-4. Schematic of a Plume in Cross Flow

at several diameters from the tower are the dominant flow disturbances. It is important to keep in mind the important effect of cross flow on a buoyant plume which deforms a circular plume to a kidney shape in a few plume diameters downwind. Most plume models appearing in the literature assume that circular cross-sections remain circular.

Basic Plume Assumptions in the Literature

There are several basic assumptions common to almost all plume rise theories. Continuity of mass must be satisfied, and the loss of mass due to particle fallout is usually neglected. Energy is assumed to be conserved; that is, the motion of the plume is considered to be adiabatic. Thus, potential temperature* of each element of gas is taken to be constant. Latent heat must be taken into account since plume rise from a large cooling tower includes much water vapor; condensation is likely to occur, particularly near the outer edge of the plume boundary. Most models account for latent heat by assuming a uniform distribution of water vapor and temperature in a cross-section of the plume.

Pressure is assumed to be constant. Forces arising from molecular viscosity are also neglected. Since the Reynolds number of a

---

*The potential temperature, θ, is defined as the temperature that a sample of air would acquire if it were compressed adiabatically to some standard pressure (usually 1000 millibars). The potential temperature is a convenient measure of atmospheric stability since

$$\frac{\partial \theta}{\partial z} = \frac{\partial T}{\partial z} + \Gamma$$

where Γ = 5.4°F/1000 ft = 9.8°C/km. Thus, the potential temperature gradient is positive for stable air, zero for neutral air, and negative for unstable air.

full-scale plume is of the order of 10^6, based on its diameter and rise velocity, the rising motion of the plume is fully turbulent and the bulk properties of the motion are nearly independent of viscosity. However, in neglecting the details of the turbulent motion and the viscous forces which intimately relate to its microstructure, it is necessary to introduce an assumption about the bulk effect of the turbulence on the plume motion in order to obtain mathematical closure of the equations. One means of doing this is by an assumption about the turbulent entrainment of ambient fluid into the plume.

With the basic assumptions made above, Morton[5] and Briggs[6] derive equations for the continuity of the fluxes of volume, momentum, buoyancy, water vapor, specific humidity and liquid water mixing ratio; i.e., $\forall$, $w\forall$, $b\forall$, $q\forall$, and $\sigma\forall$, respectively. The volume flux, $\forall$, is assumed to equal wR^2 during calm conditions and vR^2 during windy conditions. The initial flux $\forall_o$ is defined as $w_o R_o^2$ in both cases. The liquid water mixing ratio σ is defined as the mass of liquid water per unit mass of air. For example, if the liquid flux $\sigma\forall$ is multiplied by the plume air density ρ_p, then the mass of liquid water passing through a given plume cross-section per unit time is obtained. The buoyancy parameter b is defined as $(\frac{g}{T})(T_p - T_e)$. The set of equations for an unsaturated plume is ($q_p < q_{ps}$, $\sigma = 0$)

$$\frac{\partial}{\partial z} w\forall = \frac{\forall}{w}\left[b + .61g(q_p - q_e)\right] \quad \text{momentum} \qquad (2\text{-}1)$$

$$\frac{\partial}{\partial z} b\forall = -SP(\forall) \quad \text{buoyancy} \qquad (2\text{-}2)$$

$$\frac{\partial}{\partial z}(q_p - q_e) = -\forall \frac{\partial q_e}{\partial z} \quad \text{water flux} \qquad (2\text{-}3)$$

If the plume is saturated, then the equations take the form

$$\frac{\partial}{\partial z} w \forall = \frac{\forall}{w}\left[b + .61 g (q_p - q_e) - g\sigma\right] \quad (2-4)$$

$$\frac{\partial}{\partial z} b \forall = -S P(\forall) - \frac{g L \forall}{c_p T} \frac{\partial q_{PS}}{\partial z} \quad (2-5)$$

$$\frac{\partial}{\partial z}(q_p - q_e) = -\forall \frac{\partial q_e}{\partial z} - \forall \frac{\partial q_{PS}}{\partial z} - \text{RAINOUT} \quad (2-6)$$

Expressions for rainout and the variation of saturation specific humidity q_{ps} with height and temperature are required. In the numerical models using the above equations the empirical formula for $q_{ps}(T,z)$ suggested by the World Meteorological Organization[7] is commonly used. In analytical models, the Clausius-Clapeyron and hydrostatic equations are used to derive an analytical expression for $q_{ps}(T,z)$. The empirical formula agrees with observations better and is more easily used in a computer program, but is too long and unwieldy for analytical use. Rainout is approximated in the numerical model by an empirical expression suggested by Simpson and Wiggert[8]. Since Hanna[9] discusses these empirical assumptions in detail, they will not be given here.

Because of the nonlinearity of the above equations and the difficulties introduced by the water phase change terms, analytical solutions are very difficult. Hanna[9] discusses some particular problems associated with moist plume rise and presents general criteria for determining whether condensation will occur.

Hewett, Fay, and Hoult[10] use an integral approach to solve for the maximum plume rise. Using the nomenclature of Figure 2-5, the equation for conservation of mass along a plume may be written

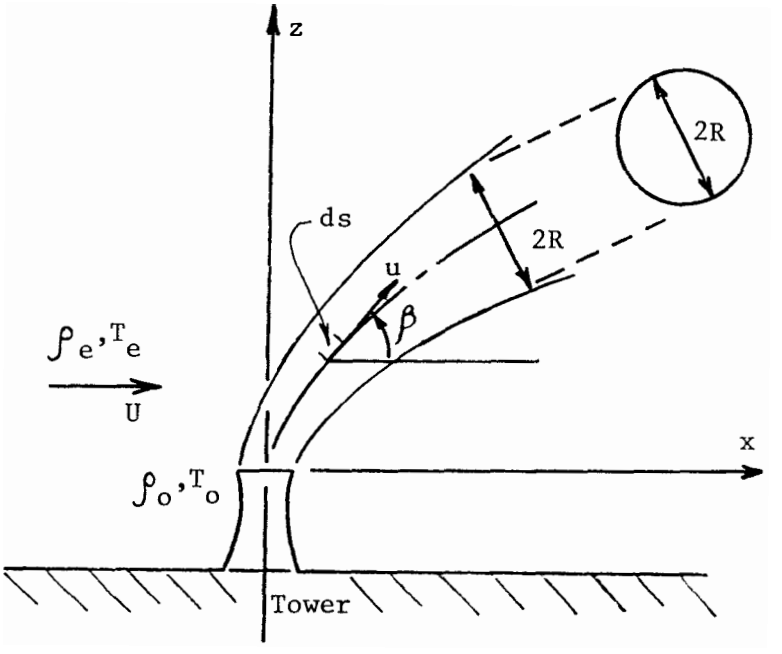

Figure 2-5 . Smokestack Plume showing Hewett, Fay, and Hoult's Coordinates

$$\frac{d}{ds}\int(\rho_p u)\,dA = \rho_e \varepsilon \qquad (2-7)$$

where ε is the rate of entrainment of the ambient flow and has the dimensions of volumetric flow rate per unit length of plume. All integrals are to be evaluated over the plume cross-section. Conservation of vertical momentum, assuming constant pressure, becomes

$$\frac{d}{ds}\int(\rho_p u)\,w\,dA = g\int(\rho_e - \rho_p)\,dA \qquad (2-8)$$

where the right side of the above equation gives the buoyant force per unit length of the plume. Conservation of horizontal momentum becomes

$$\frac{d}{ds}\int(\rho_p u)(u\cos\beta)\,dA = \rho_e U \varepsilon \qquad (2-9)$$

Neglecting changes in u^2 compared to changes in h, the enthalpy of the plume, the conservation of energy relation becomes

$$\frac{d}{ds}\int(\rho_p u)\,h\,dA = -g\sin\beta\int\rho_p u\,dA + \rho_e h_e \varepsilon \qquad (2-10)$$

Hewett, Fay, and Hoult[10] make assumptions concerning the rate of entrainment, ε, in order to solve the centerline of the plume and the

final plume rise. Since the solution of these equations is described in detail in reference[10], it will not be discussed further.

It may be noted at this point that the determination of plume behavior by Morton[5], Briggs[6], or Hewett, Fay and Hoult[10] does not yield the detailed velocity field within the plume which is necessary for an accurate determination of drift drop trajectories as discussed in Chapter VIII.

Thermodynamics of Moist Air Mixing

Consider mixing m kg of air at temperature T_1 and water vapor mass fraction q_1 with a kilogram of saturated air at temperature T_2. Equilibrium thermodynamics can be used to calculate the final state of mixing the two masses of air. Since this gives the maximum condensation of vapor, it is the first step in making an estimate of precipitation from plumes. The final state of the mixture is computed using the equations for conservation of air, total water, and energy, and the equilibrium assumption. For small mass fractions of liquid and vapor, the enthalpy of the mixture is given by

$$h = c_p(T - T_{ref}) + q_\ell L \qquad (2-11)$$

Thus, from conservation of energy, the final temperature of the mixture is*

*See Appendix B for derivations of equations presented in this section.

$$T_3 = \frac{m T_1 + T_2}{m + 1} + \left[\frac{m q_1 + q_2 - (m+1) q_3}{m + 1}\right] \frac{L}{C_p} \quad (2-12)$$

The last quantity in the above expression is the mass of liquid water in the final state, q_3, and is an unknown. Using the equilibrium assumption, q_3 must be less than or equal to the vapor mass fraction for saturated air at temperature T_3. If q_3 is less than this quantity, σ is zero; if it is equal, σ can be computed using the equation for conservation of water.

Brunt[11] found a convenient graphical scheme for solving these equations using a psychrometric chart shown in Figure 2-6. He assumed that the two masses of air initially mixed without condensation. This would have a temperature $T_{3'}$ given by

$$T_{3'} = \frac{m T_1 + T_2}{m + 1} \quad (2-13)$$

and a vapor fraction

$$q_{3'} = \frac{m q_1 + q_2}{m + 1} \quad (2-14)$$

This state is on the line connecting state 1 with state 2 such that the distance to each state is inversely proportional to the original masses. If point 3′ is above the saturation line as in the Figure 2-6, a small fraction of the vapor, $\delta q = \sigma$ will condense, and its latent heat

PSYCHROMETRIC CHART

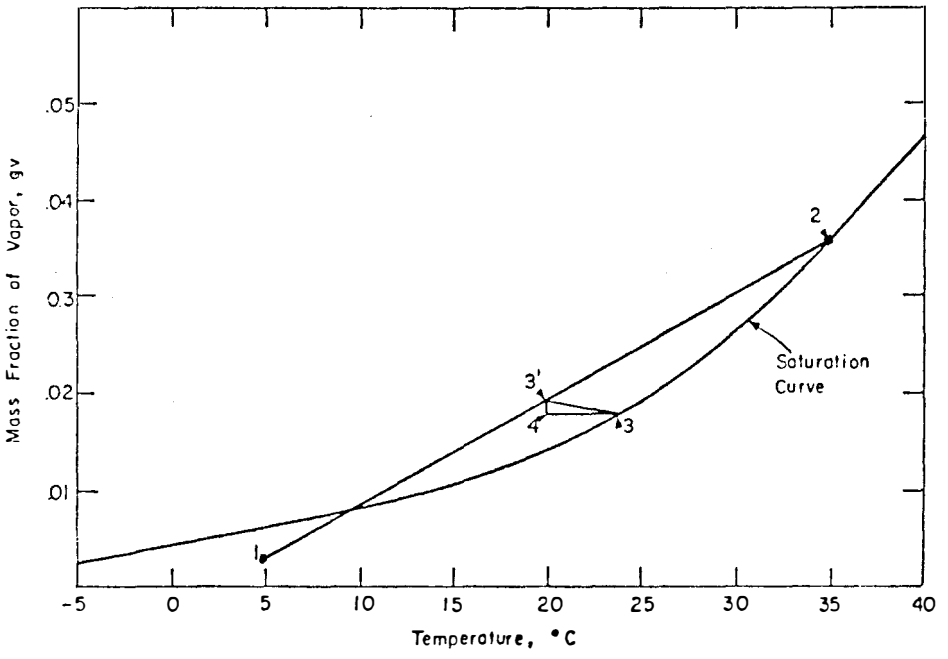

Figure 2-6. Vapor Mass Fraction versus Temperature

increases the temperature of the mixture by an amount δT. The amount of heat released by the condensing vapor in going from point 3′ to point 4 is

$$_{3'}Heat_4 = m_a(q_4 - q_{3'})L = m_a \delta q L \quad (2\text{-}15)$$

as shown in Figure 2-7. The amount of heat gained by the mixture in going from point 4 to point 3 is

$$_4Heat_3 = (q_3 \cancel{-} q_4)c_{Pv}\delta T + m_a c_{Pa}\delta T \quad (2\text{-}16)$$

$$0$$

as shown in Figure 2-7. The amount of heat released by the condensing vapor is equal to the heat gained by the mixture; equating equations (2-15) and (2-16), the process from point 3′ to point 3 has the slope

$$\frac{dq}{dT} = -\frac{c_P}{L} \quad (2\text{-}17)$$

and is along the line 3′ to 3. The amount of liquid condensing per mass of dry air is $q_{3'} - q_3$ or *

$$\sigma = \frac{m q_1 + q_2 - (m+1) q_3}{m+1} \quad (2\text{-}18)$$

---

*See Appendix B for derivations of equations presented in this section.

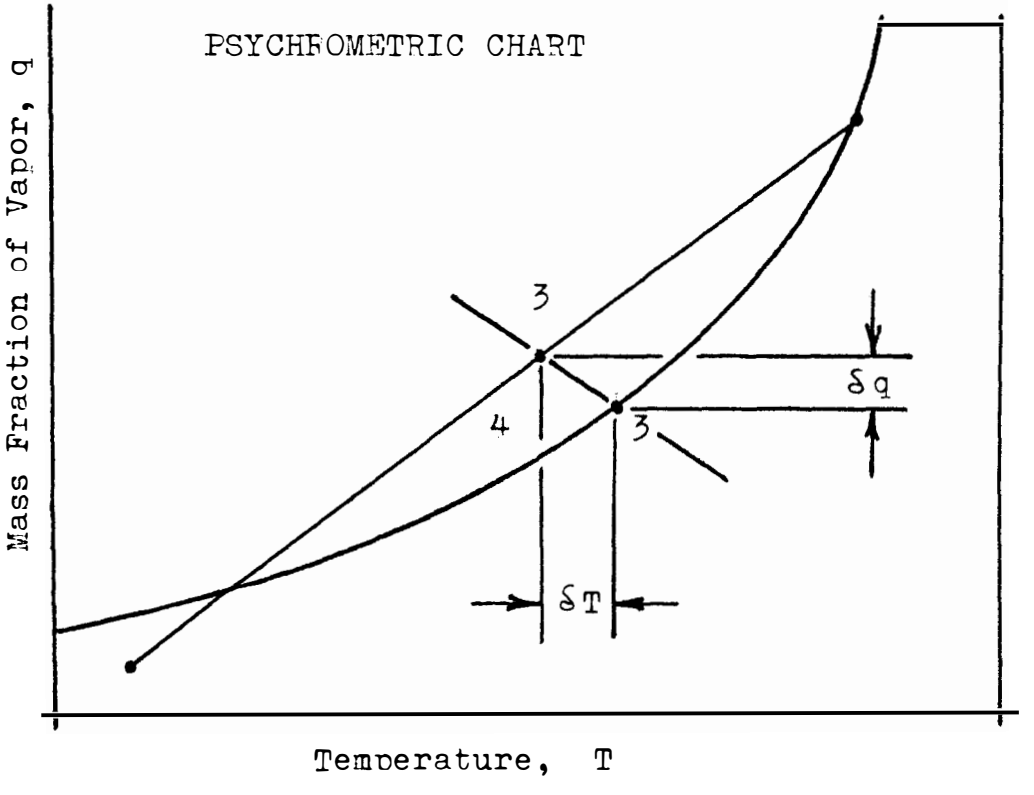

Figure 2-7 . Heat Balance for Air-Vapor Mixture

which is the distance from 3 to 4 in Figure 2-6. If 3 lies below the saturation line, there is no condensation and it is the equilibrium state. Differentiating equation (2-18) with respect to m, one obtains

$$\frac{d\sigma}{dm} = \frac{q_1 - q_2}{(m+1)^2} \qquad (2-19)$$

This method shows two important ideas. From equation (2-19) one can see that the mass fraction of liquid water as a function of the mixing ratio, m, for given initial states is greatest when m is of the order of one to three, and thereafter decreases as m increases. The other is that the maximum liquid mass fraction increases as T_1, the ambient temperature, decreases. These ideas imply that any precipitation from condensing vapor in plumes must occur before significant dilution of the plume by entrained air occurs, and it will increase as the plume temperature decreases.

As the moist air leaves the cooling tower it mixes with the cooler, drier air around it. At first this mixing causes the condensation of a fraction of the water vapor forming minute fog droplets. Eventually the plume becomes sufficiently dilute so that the droplets evaporate cuasing the plume to vanish at some distance downwind of the tower. The details of this process depend on the temperature and humidity of the air leaving the tower and of the surrounding air, the rate of entrainment of air into the plume, and the rates at which droplets condense and evaporate.

Usually the air leaving the cooling tower is saturated and contains some liquid water. Then point 2 in Figure 2-6 may be above

the saturation line which further complicates the mixing process.

Clearly, the classical thermodynamic approach is incomplete because it ignores the rate processes in droplet formation. It tells the maximum amount of liquid water in the mixture without saying how large the droplets become. To complete this model, the results from cloud physics must be used to determine how fast drops form.

Drops form by condensation of water vapor and coalescence of smaller drops. Overcamp and Hoult[12] indicate that in the cooling tower plume condensation cominates for drops of radius 20 μm or less and coalescence for larger ones. The minimum size for rain drops is around 100 μm; drops of this size will fall out of the plume but may evaporate before reaching the ground.

Overcamp and Hoult[12] assumed that no liquid water leaves the cooling tower and droplets initially formed by condensation. Calculations showed that the time for a droplet to grow to a radius of 20 μm is of the order of 10^3 - 10^4 seconds for a supersaturation of 0.05 percent which is considered the upper limit for natural clouds. For a constant supersaturation of 0.5 percent, the time is still of the order of 10^2 seconds. The residence time for a fluid element in the plume is of the order of the length of the visible plume divided by the wind speed. This length can be computed using the mixing calculations if the rate of entrainment of air into the plume is known. For typical conditions, this length is 10^3 m or less, and the wind speed at the top of the tower is about 10 m/sec or greater. This gives a residence time in the plume of 10^2 seconds or less. Since the supersaturation is undoubtedly less than 0.5 percent, the resident time in the plume is less than that required to form only 20 μm droplets. Thus, a significant number of

large raindrops cannot form by condensation in a plume based on the analysis of Overcamp and Hoult[12].

Measurements indicate that droplets are emitted from cooling towers. But since the plume has neither the long residence time for fluid particles nor the updrafts and depth of a rain cloud, it is improbable that these droplets can coalesce to form large drops except under very extreme conditions. Therefore, there are no large drops in the plume unless they passed through the drift eliminator.

Drift Deposition Models in the Literature

The factors affecting the transport and deposition of drift droplets ejected from cooling towers have been identified by a few investigators. These factors can be conveniently grouped into those intrinsically rooted in the design and operation of the cooling tower, and those related to atmospheric conditions. They are listed in Table 2-1. The number and complex nature of the factors involved require simplification of the models being used for the prediction of drift deposition.

Different approaches have been taken by investigators attempting to quantify the deposition of drift drops on ground surfaces. Some use a simple analogy with the deposition of industrial dust[13,14] and others use a combination of plume rise theories with the Gaussian diffusion model[15,16]. The ground deposition is then calculated by multiplying the ground level air concentrations by the corresponding fall velocities of the drift droplets. A simplified computational technique for the estimation of salt drift deposition has been developed by Hosler[17]. The major factors considered in each of the computational

TABLE 2-1.

FACTORS AFFECTING TRANSPORT AND DEPOSITION OF DRIFT

Factors associated with the design and operation of the cooling tower	Factors related to atmospheric conditions	Other factors
Volume of water circulating in the tower per unit time	Atmospheric conditions including humidity, wind speed and direction, temperature, Pasquill's stability classes, which affect plume rise, dispersion and deposition.	Collection efficiency of ground for droplets
Salt concentration in the water		
Drift Rate		
Mass size distribution of drift droplets	Tower wake effect which is especially important with mechanical draft towers	
Moist plume rise influenced by tower diameter, height and mass flux	Evaporation and growth of drift droplets as a function of plume atmospheric conditions and the ambient conditions	
	Plume depletion effects	

procedures will be described below. It is generally flet by meteorologists[18] that the diffusion models are applicable to drop sizes less than 80 micrometers in diameter and the trajectory models are used to describe the motion of the larger drops. Hence the diffusion will not be considered in detail.

1. The Bosanquet Method[19]

The Bosanquet method was applied originally to the deposition of one-size solid particles. The deposition equation incorporates plume rise, source term, particle fall velocity, wind speed and wind direction frequency. It can be applied to the calculation of deposition from a cooling tower providing the fall velocity is corrected to account for evaporation and growth of the droplet, which is not an elementary task. The mass fraction within each droplet size group has to be considered. The effect of size and density of the drop is characterized by the fall velocity which is expressed by Stokes' equation

$$V_d = \frac{2 \rho_d g R_d}{\mu_g} \qquad (2-20)$$

Thus, the ground deposition is found by summing the individual terms. Although the Bosanquet equation can give results which are comparable with other methods, difficulties are encountered when the equation is applied to drift droplets. The major one is due to the fact that the fall velocities are discrete values which do not incorporate the continuous change resulting from droplet evaporation.

2. The Gaussian Diffusion Model

This method is widely used in describing the diffusion of gases

discharged from stacks. It has been adapted to predict the deposition of small drift droplets from cooling towers[15,16]. Original calculations of particulate matter have been done using the modified Sutton equation[14,20]. The computational method incorporates plume rise, source term, particle fall velocity, atmospheric stability conditions, diffusion coefficients and stability parameters. The equation accounts for changes in plume axis due to the fall of the droplets by subtracting their vertical path from the actual plume height at different points downwind. The diffusion equation, while over-simplified for drift deposition, has the advantage of showing the effects of dispersion not included in the Bosanquet treatment. The Gaussian deposition method is applicable to droplet sizes less than 80 micrometers in diameter.

3. The Hosler Method[17]

Hosler, et.al, has developed a trajectory method for predicting the deposition of large drift drops from cooling towers. The basic principle of the Hosler method is the use of the trajectory (momentum) equation for each droplet size group incorporating fall velocity and wind speed. The time it takes for a droplet to evaporate to the size in equilibrium with the environmental vapor pressure is considered to allow a correction for the fall velocity as a function of time. Results are presented in graphical form from which salt deposition from a natural draft cooling tower can be estimated. Three cases are considered:

a) 100% relative humidity and no evaporation is possible.

b) relative humidity within the range of 50 to 100% when droplets will evaporate to a saturated solution.

c) relative humidities below 50% when droplets will evaporate completely leaving a solid particle .

For each of these cases, a different nomogram has to be used.

For a known plume rise and relative humidity conditions, the height h_e at which a droplet will reach equilibrium with the environment is determined. This height is compared with the maximum height h_r achieved by a droplet. If $h_r < h_e$, the droplet will reach the ground before evaporation occurs. If $h_r > h_e$, the droplet will reach equilibrium size after falling a distance $h_r - h_e$ beyond which no evaporation takes place for relative humidities higher than 50%. Below 50% the droplets will evaporate completely while falling the distance $h_r - h_e$ and will reach the ground as a solid particle.

The graphs in Figures 2-8 and 2-9 allow the calculation of the relations between h_e and h_r. For calculation purposes, it is assumed that each size group is extended over an interval of 50 micrometers. The three nomograms are presented in Figures 2-10,2-11, and 2-12 respectively. The lines with arrows and numbers illustrate the use of these nomograms. The ground deposition values are calculated by determining the width of concentric rings around the tower in which the respective size ranges will fall. A sample calculation will be made using Hosler's model in a later section for comparative purposes.

The deficiencies in this computational approach are that dispersion is solely a trajectory problem, variations in atmospheric stability are almost wholly absent, and calculated deposition values for a given concentric ring around the tower do not include superposition of deposition values due to different droplet sizes. The final plume rise and the mean vertical velocity in the plume are used to calculate the maximum rise of each particle. A very crude assumption is made that the particle remains in the plume until it reaches zero vertical velocity

and then it falls freely in the environment. Hence the details of the velocity field within the plume are completely ignored.

Although there are several deficiencies in his approach, Hosler's model provides an engineering solution to a very complicated computational problem. For comparison purposes, a sample calculation utilizing Figures 2-8 through 2-12 is presented in Chapter IX.

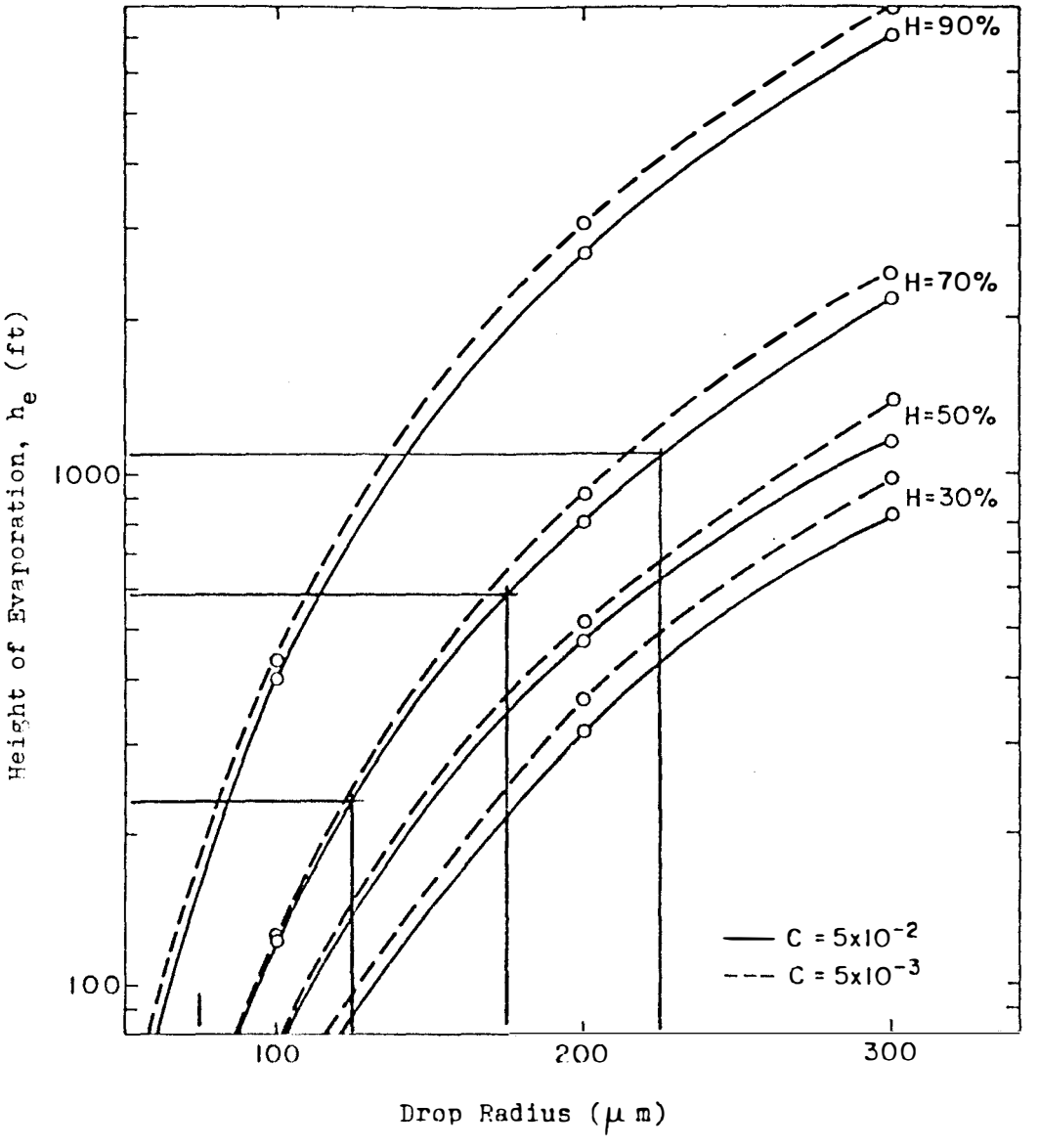

Figure 2-8. Height, h_e, a Drop of Initial Radius Must Fall To Reach the Equilibrium Size for Different Relative Humidities and Different Initial Salt Concentrations[17]

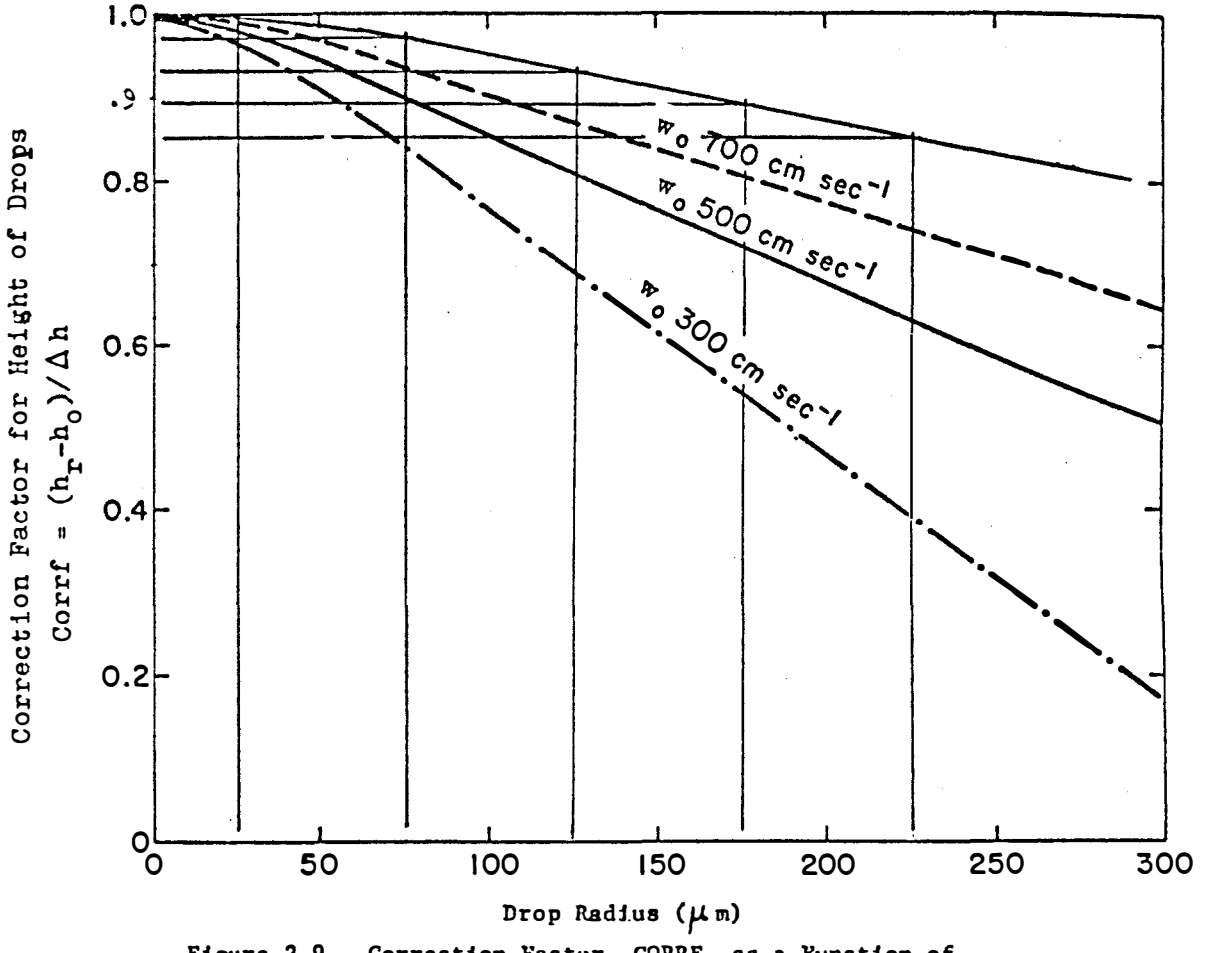

Figure 2-9. Correction Factor, CORRF, as a Function of Radius For Three Different Air Flow Velocities, w_o, from the Tower[17]

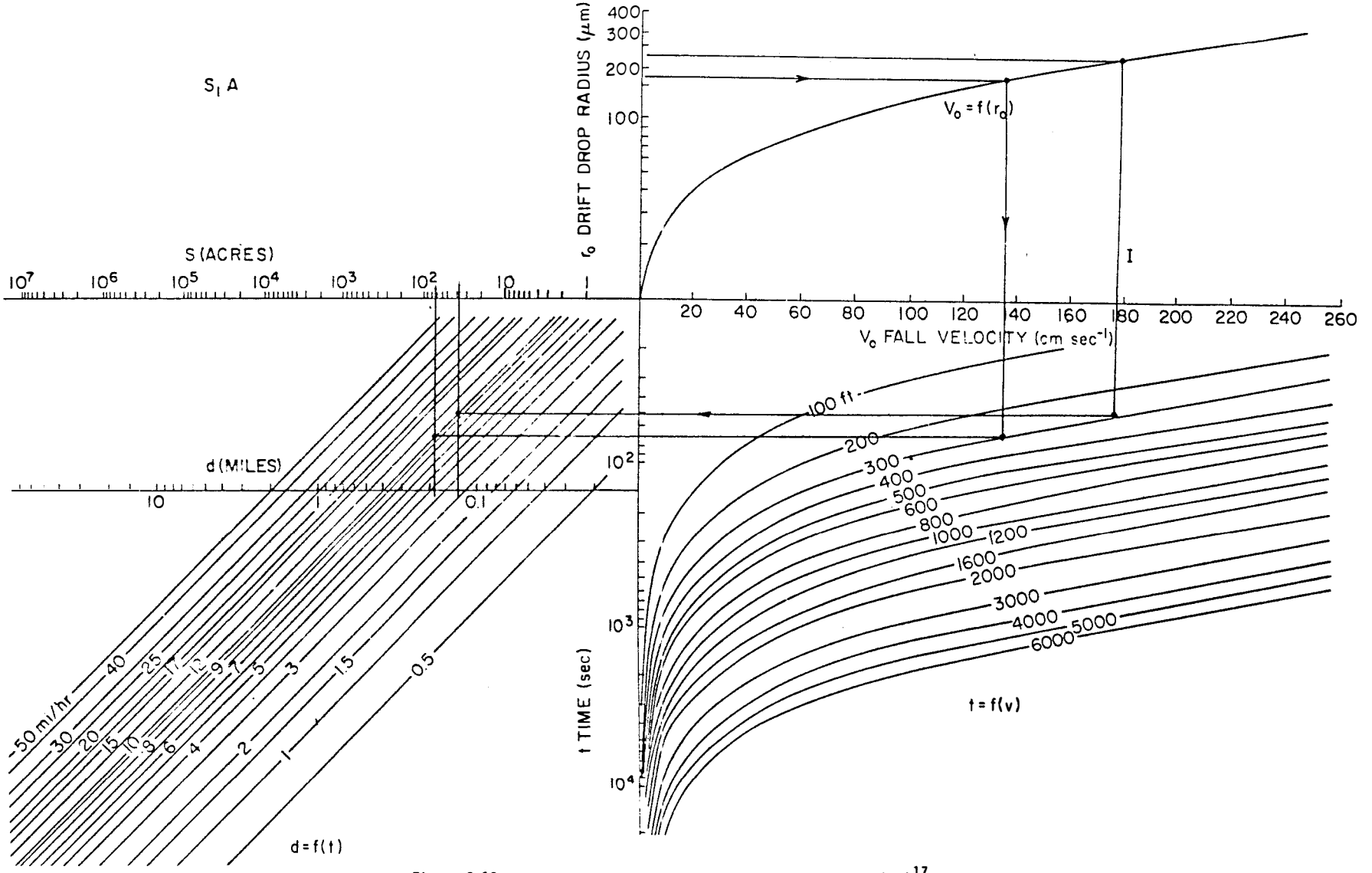

Figure 2-10. Nomogram for Salt Deposition Calculations ($h_r < h_e$)[17]

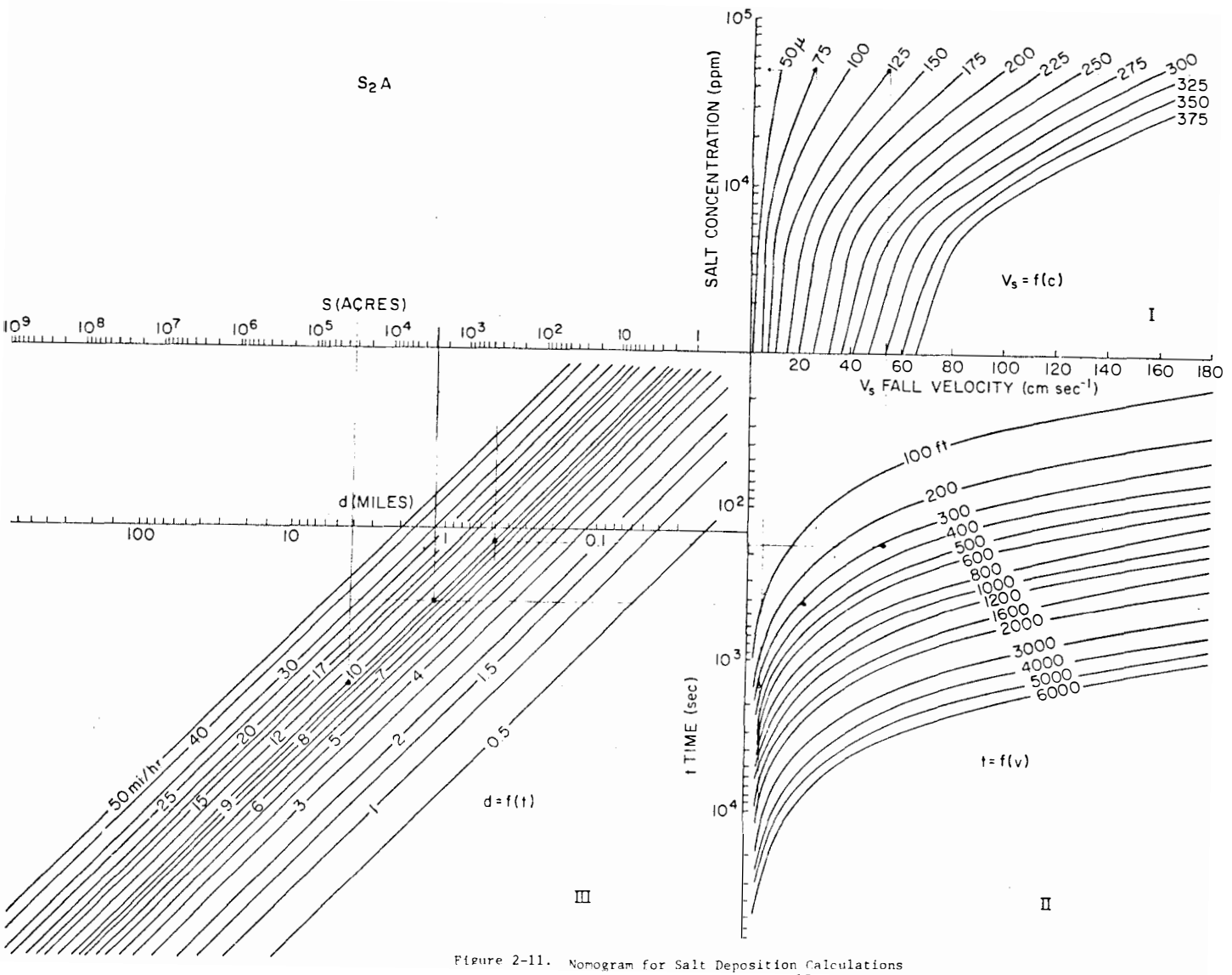

Figure 2-11. Nomogram for Salt Deposition Calculations (saturated droplets, $h_r > h_e$)[17]

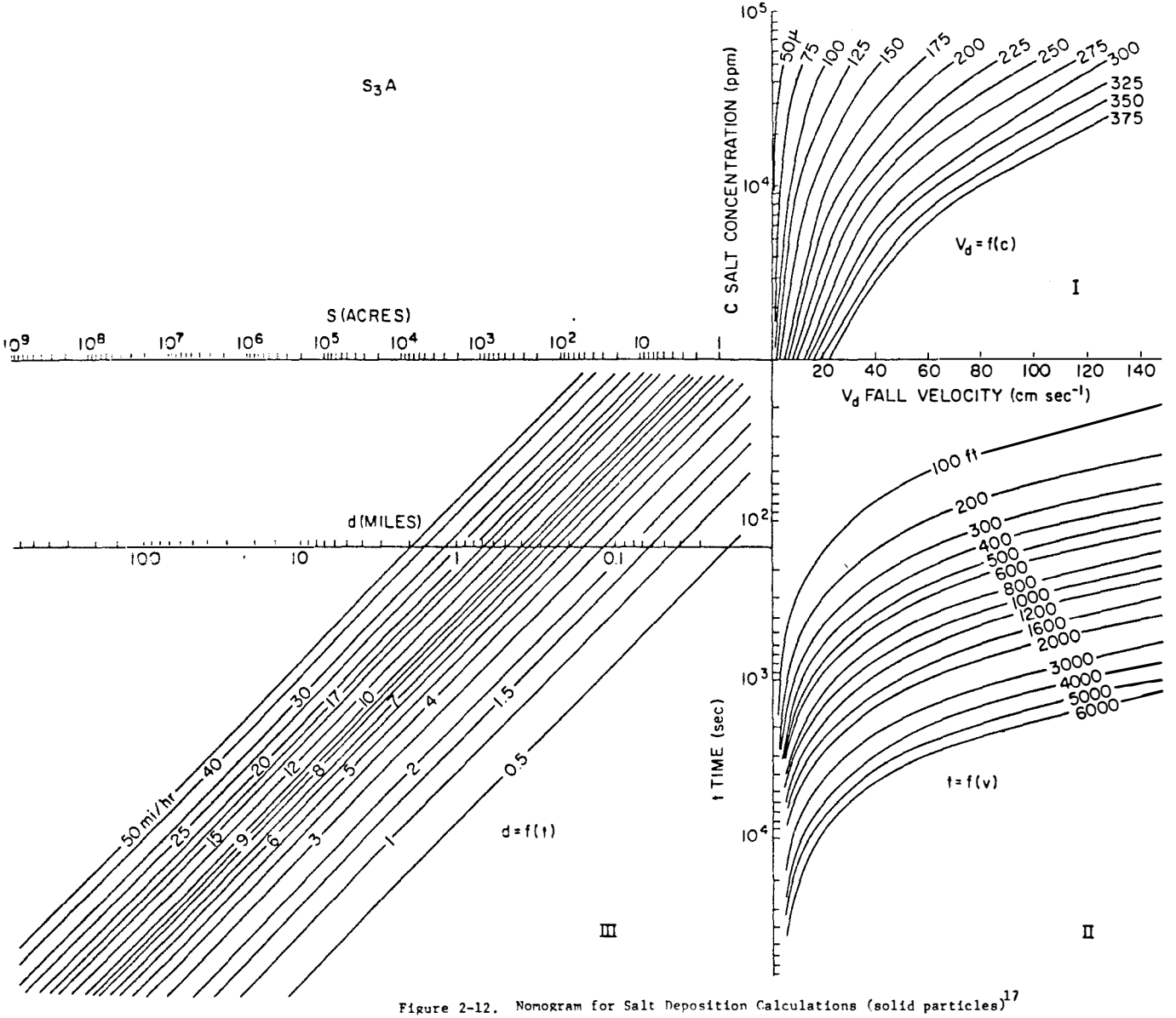

Figure 2-12. Nomogram for Salt Deposition Calculations (solid particles)[17]

CHAPTER III

DEVELOPMENT OF THE EQUATION OF MOTION

The equation of motion (Newton's second law of motion) is applicable to a system consisting of a fixed quantity of mass. The equation of motion relates the resultant force acting on the system to the rate of change of linear momentum of the cneter of mass of the system. For a system of mass m, the equation of motion is

$$\Sigma \bar{F} = \frac{d}{dt}(m \bar{V}) \qquad (3-1)$$

where $\Sigma \bar{F}$ is the resultant force acting on the system, m is the system mass, and $\bar{V}$ is the velocity of the center of mass. When applying equation (3-1) to an evaporating liquid drop, the system consists of liquid and vapor, the sum of whose masses is constant.

Consider the system consisting of liquid mass M, vapor of mass m, and velocity of the center of mass of the liquid and vapor $\bar{V}_M$ and $\bar{V}_m$ respectively. The equation of motion for this system may be written

$$\Sigma \bar{F} = \frac{d}{dt}(m \bar{V}_m + M \bar{V}_M) \qquad (3-2)$$

Since the mass of liquid and vapor is constant, m + M = constant and

$$\frac{dm}{dt} = -\frac{dM}{dt} \qquad (3-3)$$

Expanding the right side of equation (3-2) and introducing equation (3-3) gives

$$\Sigma \bar{F} = M \frac{d\bar{V}_M}{dt} + m \frac{d\bar{V}_m}{dt} + \frac{dM}{dt}(\bar{V}_M - \bar{V}_m) \qquad (3-4)$$

The system consisting of the liquid drop and vapor is shown in Figure 3-1. In the absence of evaporation, the flow around the liquid drop would be a boundary layer flow formed by the fluid external to the drop. The drag force acting on the drop is due to the boundary layer shear stresses acting at the surface of the drop. With evaporation occurring, the boundary layer external to the drop will experience transpiration due to the vapor transfer occurring at the surface of the drop. The experimental data of Le Clair, et.al.,[26] indicates that for evaporating water drops in air at moderately low temperatures the transpiration rate is sufficiently small to have a negligible effect on the boundary layer structure around the drop and hence the drag force. Thus the drag coefficient expression to be employed subsequently will be the same as for a non-evaporating spherical drop, i.e., a solid sphere (see Chapter IV).

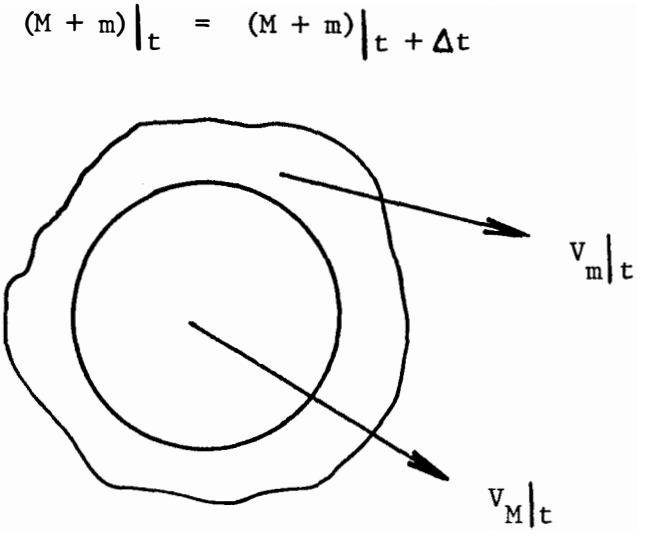

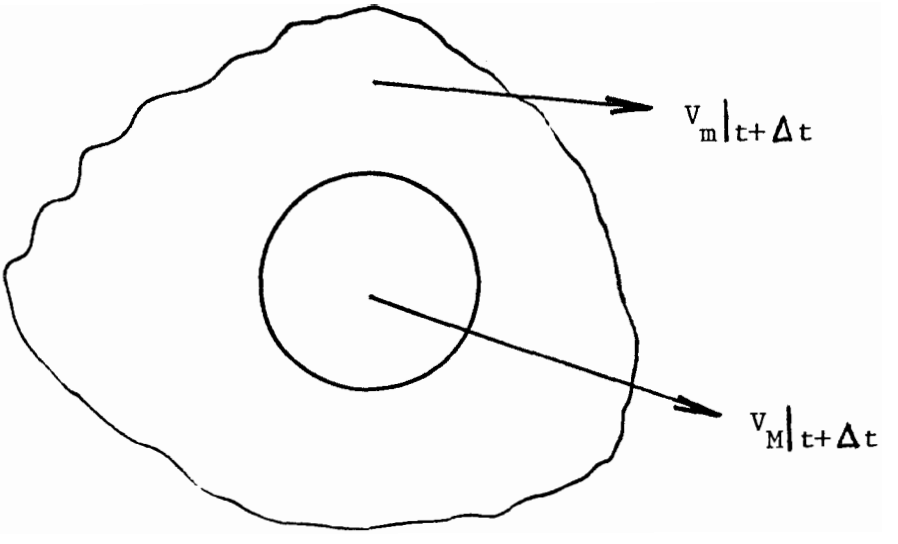

Figure 3-1. Drop at Time t and Time t + Δt.

The term $\Sigma\bar{F}$ on the left hand side of equation (3-3) represents the sum of all external forces acting on the liquid drop and vapor system. The forces acting on the liquid drop will be the body force due to gravity and the drag force. Thus, the forces acting on the liquid and vapor portions of the system may be separated as

$$\Sigma\bar{F} = \bar{F}_{BM} + \bar{F}_{DM} + \Sigma\bar{F}_m = M\frac{d\bar{V}_M}{dt} + m\frac{d\bar{V}_m}{dt} + \frac{dM}{dt}(\bar{V}_M - \bar{V}_m) \quad (3-5)$$

where $\bar{F}_{BM}$ is the body force acting on the liquid drop, $\bar{F}_{DM}$ is the drag force acting on the liquid drop, and $\Sigma\bar{F}_m$ is the resultant force acting on the vapor.

The term $(\bar{V}_M - \bar{V}_m)$ in equation (3-5) represents the velocity of the center of mass of the liquid drop relative to the center of mass of the vapor. A small fraction of the vapor of the system is contained within the boundary layer surrounding the liquid drop while the remainder of the vapor is in the free stream flow external to the drop boundary layer. Thus, the velocity of the center of mass of the vapor will approximately equal the velocity of the air surrounding the drop, $\bar{V}_a$. Thus, if the approximation $\bar{V}_m = \bar{V}_a$ is made, it follows that

$$\frac{d\bar{V}_m}{dt} \simeq \frac{d\bar{V}_a}{dt} = 0 \quad (3-6)$$

and

$$\Sigma \bar{F}_m = 0 \qquad (3-7)$$

Equation (3-6) follows because the velocity of the air surrounding the drop is constant in this model. Equation (3-7) follows from the assumption that most of the vapor is in the flow external to the boundary layer and is not being accelerated; therefore, the resultant force is zero.

Substituting equations (3-6) and (3-7) into equation (3-5) gives

$$\bar{F}_{BM} + \bar{F}_{DM} = M \frac{d\bar{V}_M}{dt} + \frac{dM}{dt}\left(\bar{V}_M - \bar{V}_a\right)$$

The literature on the dynamics of evaporating drops indicates that the second term on the right hand side of equation (3-8) has not been previously considered. The details of the treatment of the force terms $\bar{F}_{BM}$ and $\bar{F}_{DM}$ are discussed in Chapter VIII.

CHAPTER IV

DRAG COEFFICIENTS

For the purpose of this study, liquid water drops of varying sizes will be divided into three basic categories, (1) those that lie in the Stokes' law region or slightly above (Reynolds numbers 0 to 1), (2) those moving with sufficient speed to ventilate adequately the transition layer of vapor (Reynolds numbers 1 to 2000), and (3) those that move so fast as to be deformed from their normal sperical shape (Reynolds numbers greater than 2000). Ordinary drift drops fall within the first and second categories (Reynolds numbers 0 to 400).

The dynamic behavior of a water drop as it falls in still air has been studied by many authors. The resistance coefficient has been plotted in Figure 4-1 from several sources [21-26] where

$$C_D = \frac{F_D}{\frac{1}{2}\rho V^2 A_P} \qquad (4-1)$$

For a complete description of the physical processes involved in the transport of water drops in air, a simultaneous solution of the Navier-Stokes equations of motion and the continuity or energy (equation is required). By considering the steady, imcompressible creeping flow of a fluid past a sphere ($Re \ll 1$), it is easy to show that the inertia forces may be neglected so that the equation of motion takes the form

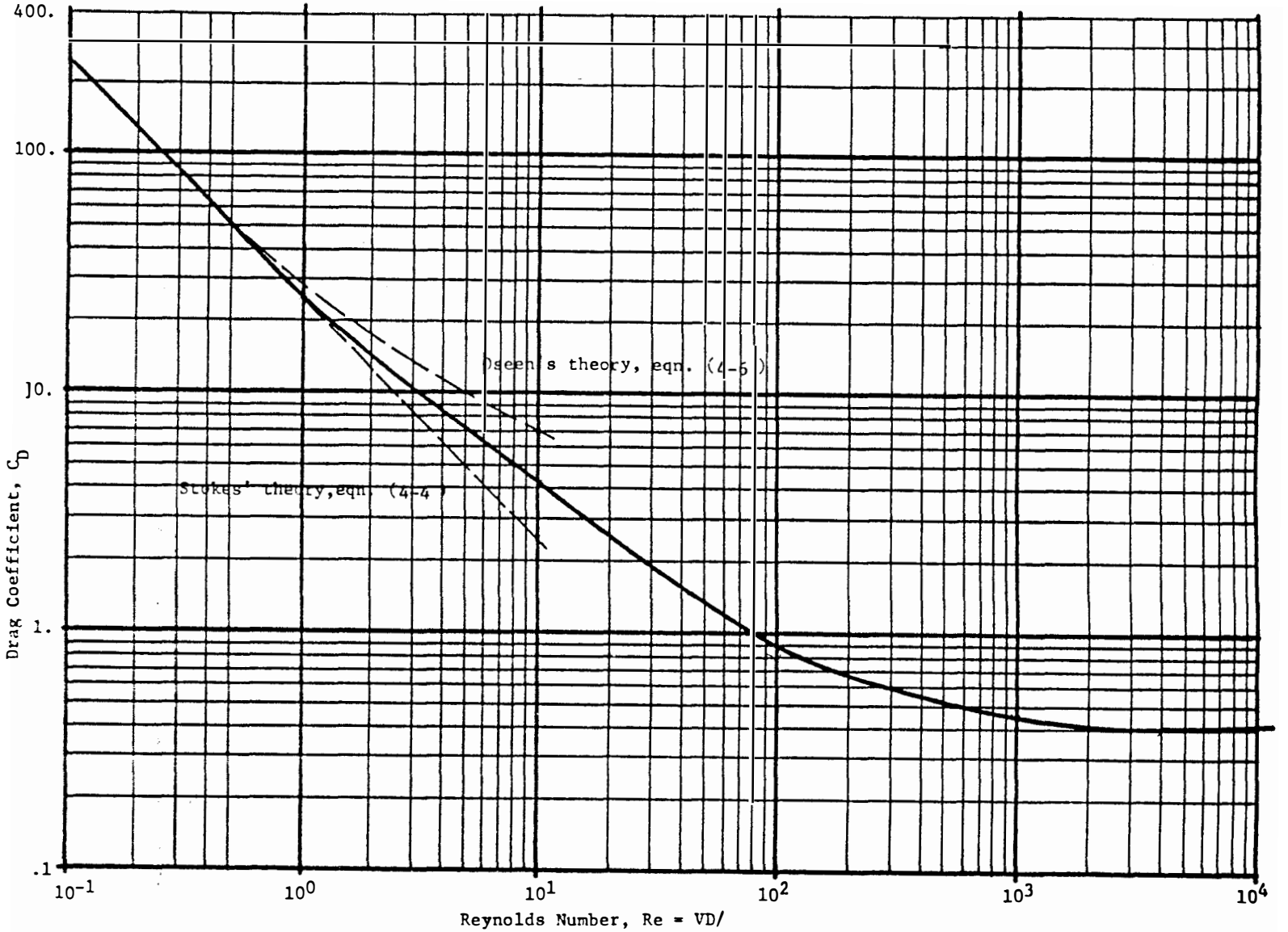

Figure 4-1. Drag Coefficient for Spheres as a Function of Reynolds Number

$$\overline{\nabla} P = \mu \nabla^2 \overline{V} \qquad (4-2)$$

and continuity becomes

$$\nabla \cdot V = 0 \qquad (4-3)$$

Solution of equations (4-2) and (4-3) for the velocity field and pressure distribution show that Stokes' classical linear approximation[27,28] to the drag coefficient

$$C_D = 24/Re \qquad (4-4)$$

is valid. It is obvious that Stokes' law can only be used with small Reynolds numbers; the error is almost proportional to Re and is about 1.7% at Re = 0.1. According to the conclusions of Stokes' law and deviations from the basic equations of the dynamics of viscous fluids, it was assumed that the following conditions prevailed:

1) No evaporation of the drop
2) Infinite fluid reservoirs
3) Small velocity movements.
4) Rigidity of the spherical particle.
5) No slip condition at the surface.

Proceeding to fluid droplets, several new factors appeared. A large droplet can be noticeably deformed by the action of the medium's resistance. Also, a circulation of the fluid developing in a moving droplet and directed at the droplet surface counter to its movement reduces the friction between the droplet and the medium. Hence the resistance decreases. The resistance of the medium to the movement of spherical liquid drops is expressed by

$$C_D = \frac{24}{Re}\left\{\frac{1 + 2\mu/3\mu_d}{1 + \mu/\mu_d}\right\} \qquad (4-5)$$

where μ is the viscosity of the medium and μ_d is the viscosity of the liquid drop.[28,30]. Due to the fact that the viscosity of air is considerably lower than the viscosity of water, the correction in the present case is insignificant.

Oseen[31] made a second approximation by considering the convective inertia term in the equation of motion; his correction appears as

$$C_D = \frac{24}{Re}\left\{1 + \frac{3}{16}Re\right\} \qquad (4-6)$$

As the Reynolds number increases beyond 0.5, the wake behind a sphere moving relative to the medium is no longer laminar. Very regular vortex patterns are formed. The flow field becomes very complex and solution of the Naview-Stokes equations and the continuity equation

for the velocity and the pressure fields becomes extremely difficult. At still higher Reynolds numbers, the vortex patterns become irregular and turbulent in character. Figure 4-1 shows that even Oseen's second approximation is poor in the present range of interest.

Various authors have presented a great number of emperical equations relating C_D and Re. However, the most successful equation among them for simplicity and degree of approximation is the one of L. Klyachko[32],

$$C_D = \frac{24}{Re} + \frac{4}{\sqrt[3]{Re}} \qquad (4-7)$$

which in the range of $3<Re<400$, offers variations not exceeding 2% of those in Figure 4-1. Equation (4-7) will be used to calculate the drag coefficient, C_D, in subsequent equations.

The assumption of modeling a drift drop from a cooling tower by a rigid water sphere is well justified for the present problem as long as $Re<400$. Le Clair, et.al.,[26] have shown that for an evaporating water drop the transpiration rate is sufficiently small to have a negligible effect on the boundary layer structure around the drop and hence the drag force. Thus the drag coefficient expression for a solid sphere can be used as an approximation to the drag coefficient for an evaporating water drop within the range of interest. The error associated with this approximation is less than 0.5%.

CHAPTER V

EVAPORATION OF DROPS

The drift drops from cooling towers are in an environment where partial or even complete evaporation will occur. This evaporation must be accounted for if accurate drop trajectories are to be calculated.

The rate of evaporation from liquid drops at rest has been explored theoretically and experimentally by Langmuir[33], Topley and Whytlaw-Gray[34], and Houghton[35]. These writers assumed the classical relation

$$\frac{dM'}{dt} = D \frac{d\rho}{dx} \qquad (5-1)$$

giving the time rate of mass transport of vapor per unit area, dM'/dt, in terms of the molecular diffusion coefficient, D, and the space gradient of vapor density, $d\rho/dx$. Accordingly, the time rate of change of mass for an evaporating spherical drop is

$$\frac{dM}{dt} = 4\pi R^2 D\left(\frac{d\rho}{dr}\right)\Big|_{r=R} \qquad (5-2)$$

where $(d\rho/dr)\big|_{r=R}$ is the vapor density gradient established at the surface of the drop. Equation (5-2) is successful in describing the evaporation of drops at rest whose radii are large compared to the mean free path of the environmental fluid.

Houghton's study[35] of the evaporation of small stationary drops suspended on fine wire or glass fibers showed that the vapor density gradient can be approximated with excellent accuracy by

$$\left(\frac{d\rho}{dr}\right)\Big|_{r=R} = - \frac{\rho|_R - \rho_\infty}{R} \qquad (5-3)$$

Assuming the vapor acts like an ideal gas an neglecting the small temperature difference, equation (5-3) may be written in terms of the vapor pressure as

$$\left(\frac{d\rho}{dr}\right)\Big|_{r=R} = - \frac{P_d - P_\infty}{\mathcal{R}\, T_d\, R} M_{w_v} \qquad (5-4)$$

Combining equations (5-2) and (5-4), the evaporation of stationary drops may be described by

$$\frac{dM}{dt} = - \frac{4\pi R D M_{w_v}(P_d - P_\infty)}{\mathcal{R}\, T_d} \qquad (5-5)$$

The very complicated problem of describing the evaporation when drops are falling through air at different velocities has been studied experimentally by Takahasi[36] and by Frössling[37] who examined drops varying in diameter from .02 to .18 cm with air velocities ranging from .2 to 7 m/sec. Both experimenters supported the drops on a fiber or wire, and thus introduced aritificalities into the normal mode of evaporation. Frössling showed that the motion of air past the

drops introduced further evaporation that increased linearly with the square root of the Reynolds number. He also gave data for the rate of sublimation from solid spheres as a function of the angle measured from the stagnation point. This data revealed a marked dependence of evaporation rate upon the details of air flow about the supported spheres. Takahasi[36] and Frössling[37] state that their measurements of evaporation rates of ventilated water drops are described by the formula

$$\frac{dM}{dt} = -\frac{4\pi R D M w_v (P_d - P_\infty)}{\mathcal{R} T_d}\left[1 + C(Re)^{1/2}\right] \quad (6\text{-}6)$$

where C is a constant. Both Houghton[35] and Frössling[37] assumed evaporating drops to be at the temperature of a wet-bulb thermometer, and the value of the water vapor pressure at the surface of the drop to be the saturation pressure at the temperature of the drop. Houghton used the temperature of a wet bulb in stationary air, while Frössling employed the ventilated wet-bulb temperature. Measurements of Kinzer and Gunn[38] (to be discussed later) showed that the temperature of the freely falling drops are very close to the ambient wet-bulb temperature.

In this work, the value of the water-vapor pressure is taken to be the saturation pressure at the temperature of the drop. The effect of salt concentration will be discussed later. The diffusion coefficient, D, will be treated as a function of the air pressure and the temperature of the falling waterdrop. Thus, in accord with the International Critical Tables[7],

$$D = D_o (T_d/T_o)(P_o/P) \quad (5-7)$$

where D_o = 0.220 cm^2/sec, T_o = 273.16°K, n-1.75, T_d is the absolute temperature of the ventilated wet-bulb, p_o is one atmosphere, and p is the pressure of the environmental air.

Kinzer and Gunn[38] considered both theoretically and experimentally the evaporation of freely falling drops that moved at their terminal velocity relative to the environmental air. Such freely falling drops rotate, vibrate and deform like natural drops, and their results were more applicable to the calculation of natural drop evaporation than studies where drops were attached to supporting wires or fibers. The measurements of Kinzer and Gunn[38] were made over the range of drop sizes from those so small that Stokes' law was obeyed, up to and including drops so large that they were non-spherical. It was found that the evaporation of drops varying over such a wide range of sizes must be considered in three different categories, (a) those that lie in the Stokes' law region or slightly above (Reynolds numbers 0 to 1), and which by virtue of gaseous viscosity entrain sufficient air to reduce effectively the evaporation rate toward that characteristic of a drop at rest; (b) those that fall with sufficient speed (Reynolds numbers 1 to 2000) to ventilate adequately the transition layer of vapor; and (c) those that fall so fast that they are deformed from their normal spherical shape (Reynolds number greater than 2000), and whose description requires special analysis. Drift drops from cooling towers fall into the first two categories since the drift eliminators effectively

remove the larger drops from the air stream. In this study drops with Reynolds numbers less than 1000 will be considered.

In determining the rate of transport of vapor, Kinzer and Gunn noted that the radial gradients surrounding the drop, when it is at rest, have finite values out to distances which are large compared to the radius of the drop. But when the drop is falling freely, the vapor and cooled air at its surface are continually replaced by environmental air. The net effect of increasing ventilation is to sweep away the vapor around the drop, thus increasing the surface gradients of vapor density and temperature and the rates of transport of vapor. The movement of air near the drop was examined in order to evaluate the effective gradients at the surface and the dependence of these gradients upon the velocity. A transient state was considered in which the vapor was allowed to diffuse into successive packets of fresh environmental air as each packet moved within a diffusion zone around the drop for a calculable period of time. This period of effective contact was approximated by the diameter of the drop divided by the velocity of ventilation. By summing up the transport to all packets of air making contact, the total vapor exchange was estimated and used to determine the equilibrium evaporation rate of the drop.

In order to account for the evaporation due to the movement of the drop relative to its surroundings, equation (5-5) is multiplied by a convection factor to give

$$\frac{dM}{dt} = - \frac{4\pi R D M_{w_v} (P_d - P_\infty)}{\mathcal{R} T_d} (cf) \quad (5-8)$$

Kinzer and Gunn[38] found that the convection factor depended very strongly on the Reynolds number, Re, and the Schmidt number, Sc, of the drop. The expression for the convection factor is

$$cf = 1 + VF\,(Re \cdot Sc/4\pi)^{1/2} \qquad (5\text{-}9)$$

where VF is the ventilation factor. The functional relationship found by Kinzer and Gunn for the ventilation factor, VF, is shown in Figure 5-1. The Schmidt number is commonly used to describe the mass transfer from a body in a fluid medium; it is the ratio of the kinematic viscosity of air, ν, to the diffusivity of water vapor in air, D. Hence,

$$Sc \equiv \nu / D \qquad (5\text{-}10)$$

Equations (5-8) and (5-9) will be used to describe the evaporation rate of drift drops exiting from cooling towers. The functional relationship found by Kinzer and Gunn[38] will be used to evaluate the ventilation factor in equation (5-9).

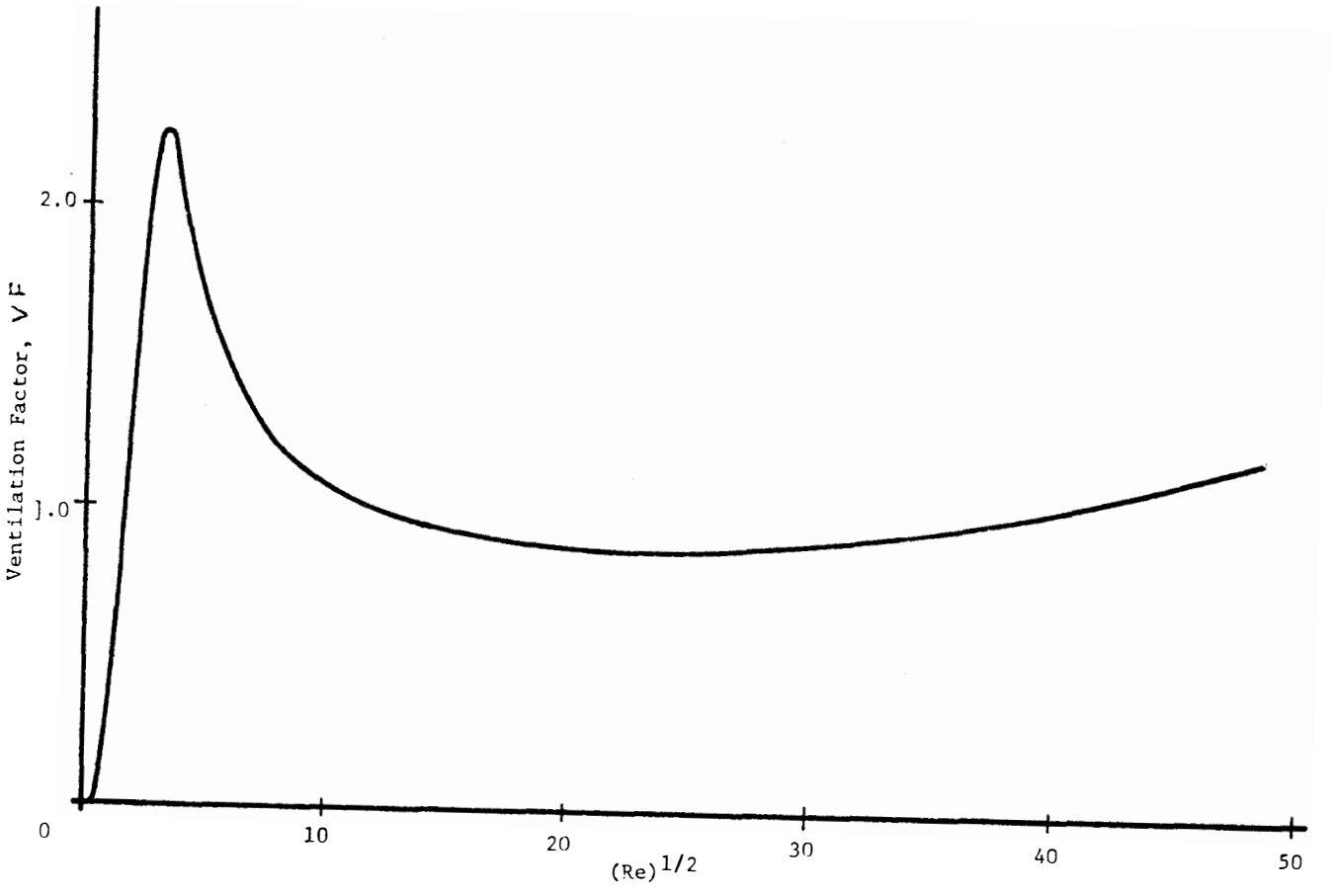

Figure 5-1. Ventilation Factor as a Function of Reynolds Number[38]

CHAPTER VI

DROPLET VAPOR PRESSURE

The difference between the droplet surface vapor pressure and the environment vapor pressure provides the driving force of the evaporation process. Both the salt concentration and the radius of curvature will affect the droplet vapor pressure.

In order to determine the effect of curvature on the droplet surface vapor pressure, consider a liquid in equilibrium with its vapor at temperature T as shown in Figure 6-1. P_s is the equilibrium pressure of the vapor on the flat surface. If a capillary tube is placed into the liquid as shown in Figure 6-2, the vapor/liquid interface is curved and is depressed a distance d below the flat interface outside the tube. The pressures across the interface are P_1 and P_2 as shown in Figure 6-2. If γ_l is the specific weight of the liquid, then from hydrostatics in the liquid,

$$P_2 = P_s + \gamma_l d . \qquad (6-1)$$

From a force balance on the curved surface,

$$\frac{2S}{R} = \gamma_l d + (P_s - P_1) \qquad (6-2)$$

where R is the radius of curvature and S is the surface tension.

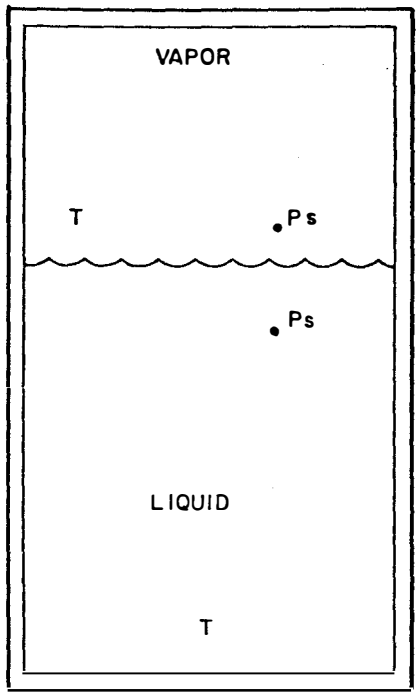

Figure 6-1. Vapor Pressure Over a Flat Surface

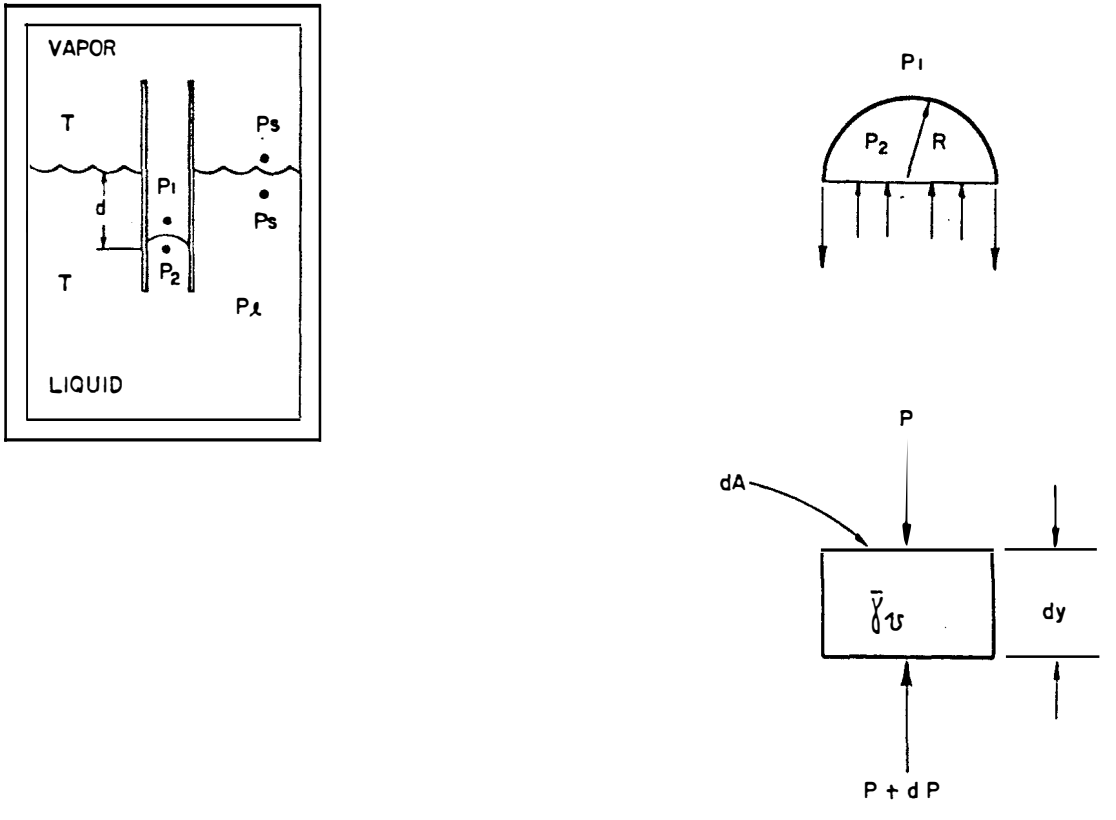

Figure 6-2. Vapor Pressure Over a Curved Surface

Now,

$$P_s - P_1 \cong - \bar{\gamma}_v \, d \qquad (6-3)$$

where $\bar{\gamma}_l$ is the specific weight of the vapor in the capillary. Thus,

$$P_s - P_1 << \gamma_l \, d. \qquad (6-4)$$

From equation (6-2), the depth of the depression of the curved interface is

$$d \cong \frac{2S}{R \gamma_l} . \qquad (6-5)$$

Consider an element of vapor of length dy in the capillary. Then a force balance gives

$$\frac{dP}{dy} = \gamma_v = \rho_v \, g/g_c \qquad (6-6)$$

Assuming that the vapor is an ideal gas and

$$\frac{P}{\rho} = \frac{RT}{M_w} = \text{constant} = \frac{P_s}{\rho_v} \qquad (6-7)$$

where ρ_v is the density of the saturated vapor over the flat surface. Combining equations (6-6) and (6-7), one obtains

$$\frac{dP}{P} = \frac{g \rho_v dy}{g_c P_s} \qquad (6-8)$$

Integrating equation (6-8) from y=0 to y=d and combining the result with equation (6-5), one obtains

$$\frac{P_1}{P_s} = e^{\frac{2S}{R\rho_l RT}} \qquad (6-9)$$

Equation (6-9) expresses the vapor pressure over a drop of radius R as a function of the surface tension, S, the drop density, ρ_l, the surface temperature, T, and the vapor pressure over a flat surface of pure water, P_s.

The effect of salt concentration on the droplet vapor pressure is important because as the droplet evaporates, its salt concentration level increases and consequently, the evaporation rate diminishes. Rault's law relates the vapor pressure over the solution to the vapor pressure over pure water by the equation

$$P/P_s = \text{mol. fraction of water} \qquad (6-10)$$

where p is the vapor pressure over the solution and p_s is the vapor pressure over pure water. In calculating the mole fraction care must be

taken to include the van't Hoff factor, n, which takes account of the disassociation of inorganic salts. This factor is not a constant, but varies to some extent with concentration. Figure 6-3 shows the variation in vapor pressure above the surface of the liquid for a 1 molar solution of a non-electrolyte, non-volatile solvent in water.

The vapor pressure over the surface of a liquid depends upon the number of solute paritcles in a given weight of the solvent. With non-electrolytes, 1 mole refers to the same number of particles, namely, 6.02×10^{23} molecules. But in the case of an electrolyte a mole refers to a larger number of particles. The "apparant" molecule, NaCl, is not a molecule but a pair of ions, Na^{+1}, Cl^{-1}. This means that 58.5 grams of NaCl contains not 6.02×10^{23} molecules, but 6.02×10^{23} Na^{+1} ions and 6.02×10^{23} Cl^{-1} ions. The data in Table 6-1 shows that for the electrovalent type of electrolyte, the number of particles in a mole is twice, three times, four times, etc., the number in a mole of a non-electrolyte solution.

The van't Hoff factor, n, is the number of apparent ions per molecule in an electrolyte solution. Table 6-2 shows that the van't Hoff factor is very near 2 for very dilute solutions of NaCl and decreases as the concentration increases. Figure 6-4 shows the variation in the van't Hoff factor as a function of concentration for a solution of NaCl and water.

In order to determine the effect of salt concentration on droplet vapor pressure, consider a drift drop of radius R containing a dissolved mass of salt m_s of gram-molecular weight Mw_s. Then, the number of apparent moles of salt in the drop is

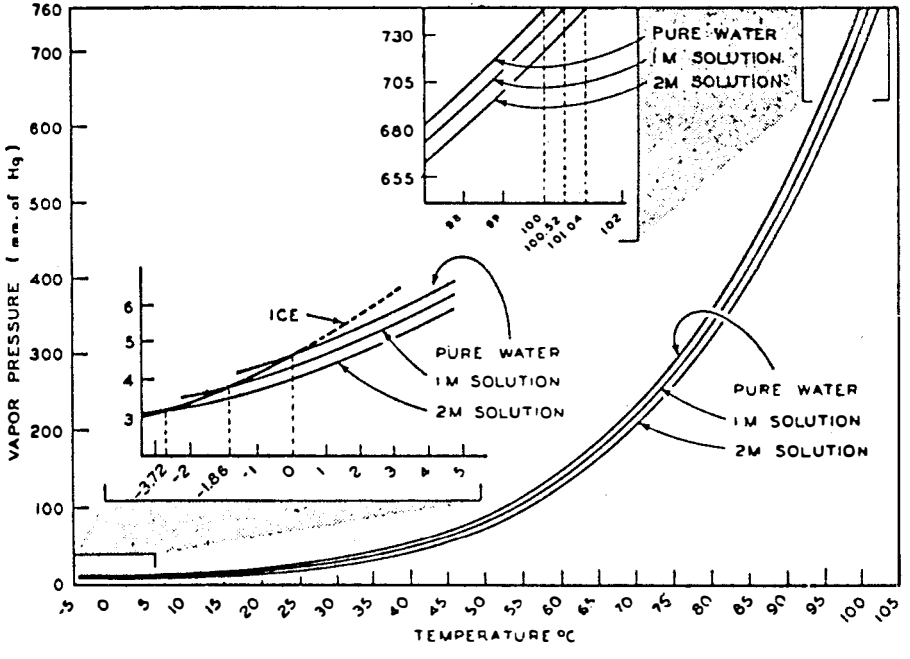

Figure 6-3. Comparison of the Vapor Pressures of Pure Water, a One Molal (1 M) Solution, and a Two Molal (2 M) Solution[39]

Table 6-1. Number of Particles in 1 Mole for Various Salts[39]

Formula	Particles Represented by Formula	Weight of 1 Mole	No. of Particles in 1 Mole
NaCl	Na^{+1}, Cl^{-1}	58.5 g.	$2X6.02X10^{23}$
KNO_3	K^{+1}, NO_3^{-1}	101.0 g.	$2X6.02X10^{23}$
$CaCl_2$	$Ca^{+2}, Cl^{-1}, Cl^{-1}$	111.0 g.	$3X6.02X10^{23}$
$NaSO_4$	$Na^{+1}, Na^{+1}, SO_4^{-2}$	142.0 g.	$3X6.02X10^{23}$
AlF_3	$Al^{+2}, F^{-1}, F^{-1}, F^{-1}$	84.0 g.	$4X6.02X10^{23}$

Table 6-2. Comparison of Freezing-Point Lowering by Ionic Electrolytes and Non-Electrolytes in Water[39]

Electrovalent Type of Electrolyte	No. of Ions per Apparent Molecule	Comparison at the Molal Concentrations Indicated			
		0.005	0.010	0.050	0.10
NaCl	2	1.94	1.93	1.89	1.87
KCl	2	1.96	1.94	1.88	1.86
$MgSO_4$	2	1.69	1.62	1.43	1.42
K_2SO_4	3	2.86	2.77	2.57	2.46

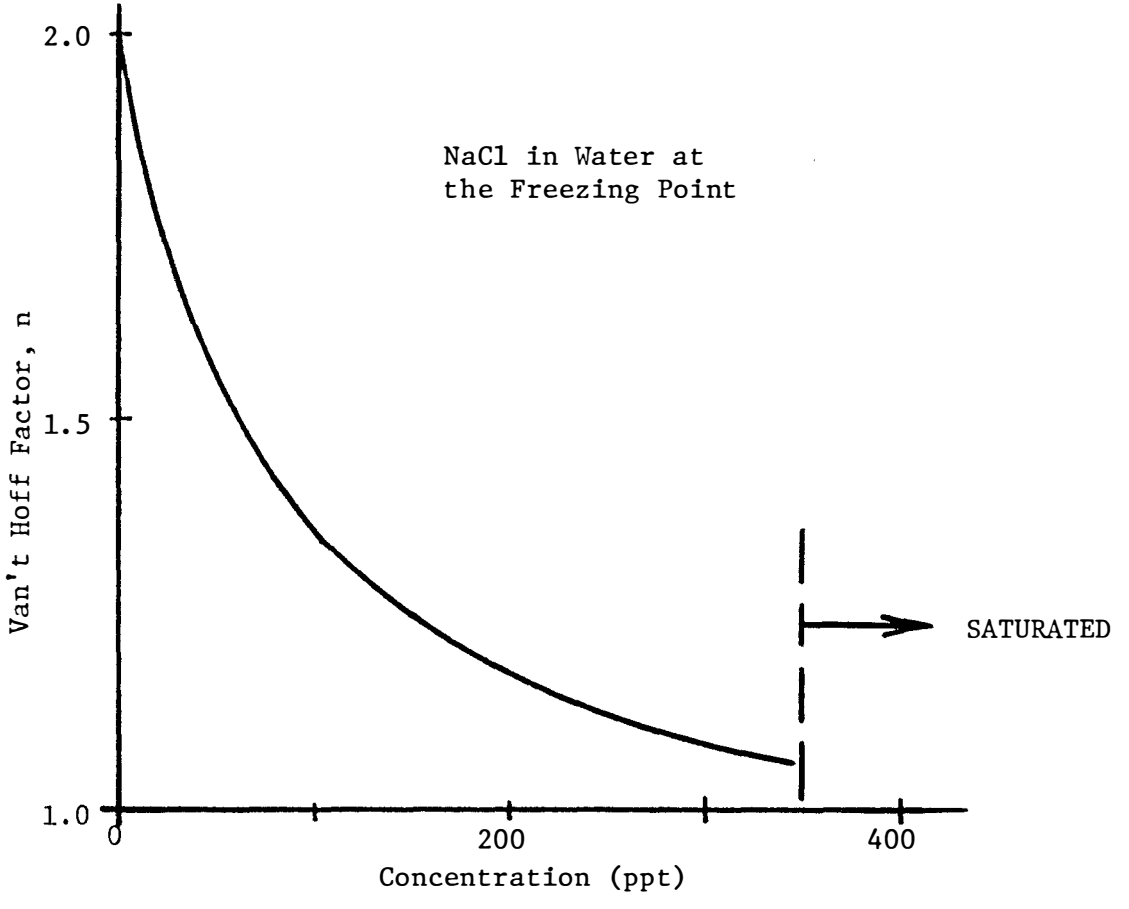

Figure 6-4. Van't Hoff Factor versus Concentration

$$n\, m_s / Mw_s$$

where n is the van't Hoff factor. The number of moles of water in the drop is

$$\left(\frac{4}{3}\pi R^3 \rho_l - m_s\right) / Mw_{H_2O}$$

Rault's law may be expressed as

$$\frac{P}{P_s} = \frac{\left(\frac{4}{3}\pi R^3 \rho_l - m_s\right) / Mw_{H_2O}}{\left(\frac{4}{3}\pi R^3 \rho_l - m_s\right) / Mw_{H_2O} + n\, m_s / Mw_s} \qquad (6-11)$$

or

$$\frac{P}{P_s} = \left[1 + \frac{n\, m_s\, Mw_{H_2O}}{\left(\frac{4}{3}\pi R^3 \rho_l - m_s\right) Mw_s}\right]^{-1} \qquad (6-12)$$

In terms of concentration, c,

$$\frac{P}{P_s} = \left[1 + \frac{n\, c\, Mw_{H_2O}}{Mw_s}\right]^{-1} \qquad (6-13)$$

Combining equations (6-9) and (6-13), one obtains

$$\frac{P}{P_s} = \left[\exp\left(2S/\mathcal{R}\rho_l RT\right)\right]\left[1 + \eta C\, Mw_{H_2O}/Mw_s\right]^{-1} \qquad (6-14)$$

Equation (6-14) expresses the vapor pressure over a drop of radius R containing a mass of dissolved salt m_s in terms of the saturated vapor pressure over a flat surface of pure water. The first bracket in equation (6-14) represents the curvature or Kelvin effect and the second bracket the osmotic effect. Equation (6-14) is not valid for concentrations greater than the saturation values indicated in Figure 6-5.

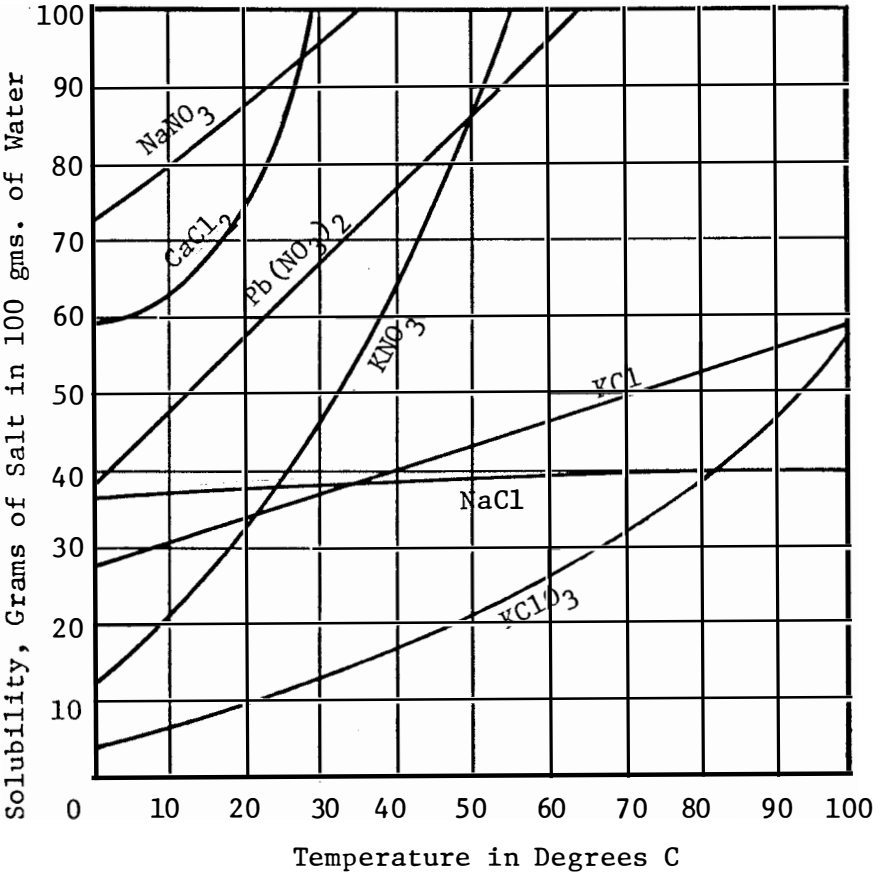

Figure 6-5. Solubilities of Certain Solids at Different Temperatures[39]

CHAPTER VII

PLUME BEHAVIOR

In order to describe the motion of a drop, it is necessary to know the details of the velocity field within the plume. The basic equations describing the motion in the plume are the continuity equation,

$$\frac{\partial \rho}{\partial t} + \bar{\nabla} \cdot (\rho \bar{V}) = 0 \qquad (7-1)$$

the momentum equation,

$$\rho \left[\frac{\partial \bar{V}}{\partial t} + (\bar{V} \cdot \bar{\nabla}) \bar{V} \right] = \bar{F}_B + \bar{\nabla} \cdot \bar{\bar{\sigma}} \qquad (7-2)$$

and the energy equation

$$\rho C_p \frac{DT}{Dt} = \frac{DP}{Dt} + \frac{\partial Q}{\partial t} + \hat{\Phi} - \bar{\nabla} \cdot \bar{q} \qquad (7-3)$$

Although several simplifying assumptions can be made (i.e., steady, incompressible flow, no energy generation, no radiation) the solution of the above equation in 3-dimensions is very complex. Many of the terms are nonlinear and the equations are coupled. Even in 2-dimensions the solution of the equations may involve lengthy numerical integrations or a difficult finite difference solution.

As discussed in Section II, simplified integral approaches have been used to solve equations (7-1) through (7-3) for the coordinates of the plume centerline, the mean horizontal and vertical velocity components and the final plume rise. None of these approaches will yield the details of the velocity field within the plume.

In this case a qualitative approach can be made using a simplified model which yields a reasonable analytical attack. Consider the flow field described by the superposition of a three dimensional source and a uniform stream. Using only that portion of the flow field above the tower exit plane and between the stream lines intersecting the outside diameter of the tower exit plane as shown in Figure 7-1, one can describe the velocity at any point wihtin the flow field. By adjusting the free stream velocity and the strength of the source, one can model almost any plume shape. The stream function and velocity potential are

$$\psi = -\frac{1}{2} U R^2 \sin\theta' + \frac{Q'}{4\pi} \cos\theta' \qquad (7-4)$$

and

$$\Phi = -UR\cos\theta' + \frac{Q'}{4\pi R}, \qquad (7-5)$$

The velocity components are

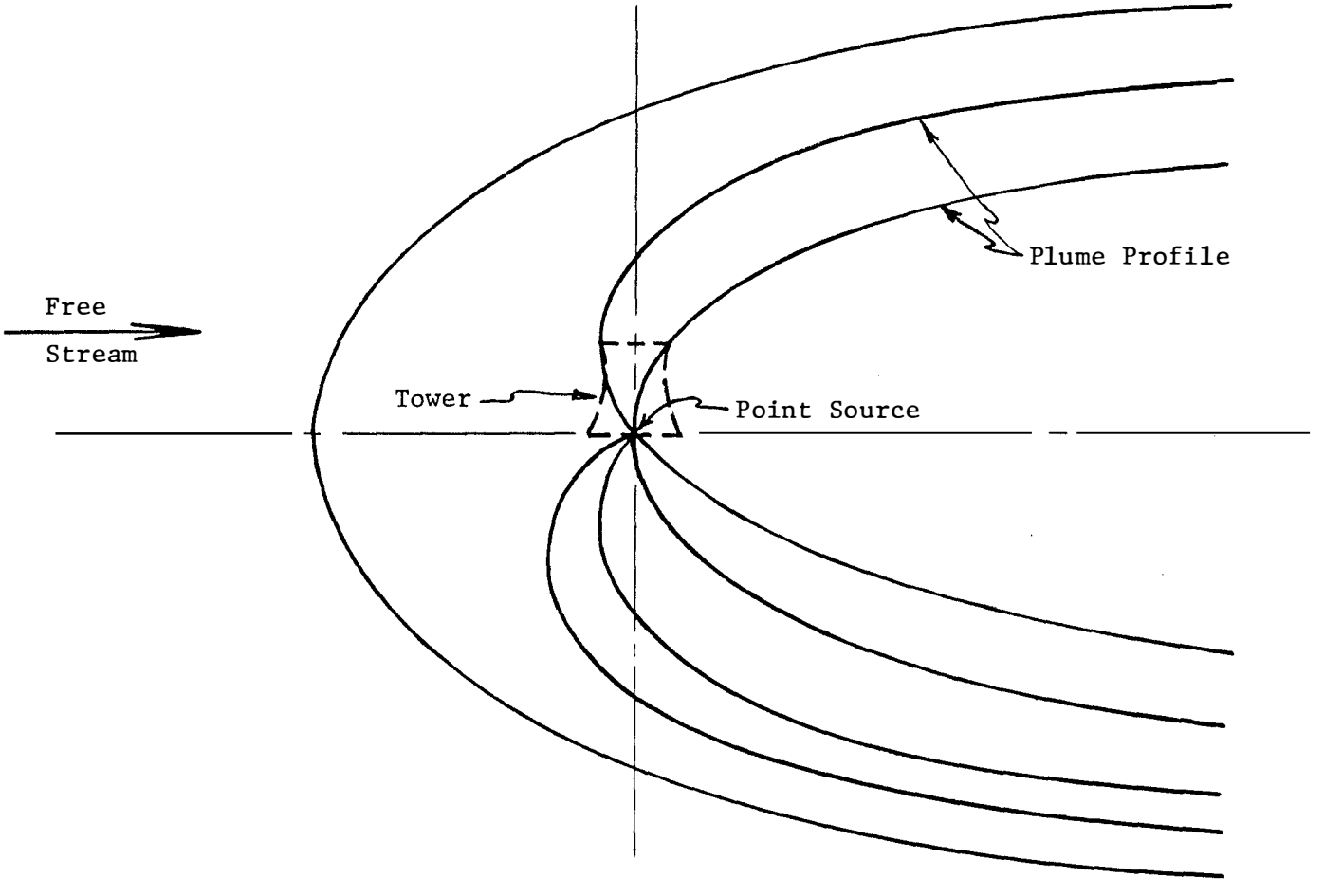

Figure 7-1. Plume Profile

$$v_r = U \cos\theta' + \frac{Q'}{4\pi R^2} \qquad (7-6)$$

$$v_\theta = -U \sin\theta' . \qquad (7-7)$$

In terms of the coordinates x, y, and z as shown in Figure 7-2, the velocity components within the plume are

$$v_x = U + \frac{Q' x}{4\pi (x^2 + y^2 + z^2)^{3/2}} \qquad (7-8)$$

$$v_y = \frac{Q' y}{4\pi (x^2 + y^2 + z^2)^{3/2}} \qquad (7-9)$$

$$v_z = \frac{Q' z}{4\pi (x^2 + y^2 + z^2)^{3/2}} \qquad (7-10)$$

Dimensionaless parameters may be defined which are convenient to work with. Hence, the dimensionless velocity ratio, vr, and the dimensionless stream function, ψ', may be defined as

$$(vr)^2 = Q'/4\pi U \qquad (7-11)$$

and

$$\psi' = -4\pi\psi/Q' . \qquad (7-12)$$

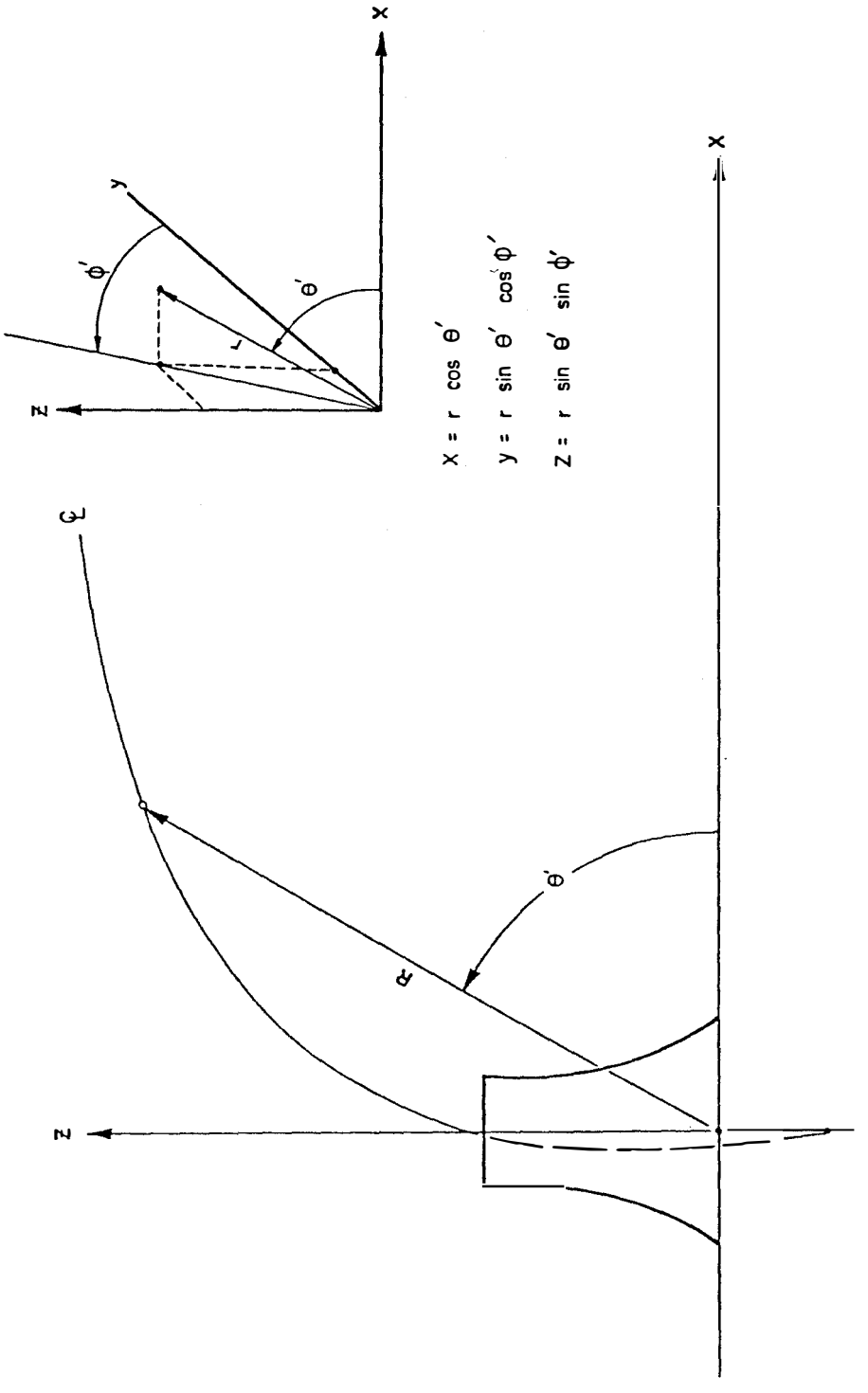

Figure 7-2. Coordinate System

Therefore, equation (7-4) becomes

$$\psi' = \frac{1}{2}\left(\frac{r}{vr}\right)^2 \sin^2\theta' - \cos\theta' \qquad (7\text{-}13)$$

In order to relate the potential flow variables and the meteorological conditions, the source strength will be defined as

$$Q' = 4\pi \, \mathbb{Z}P_o \, W_o^2 \qquad (7\text{-}14)$$

where w_o is the mean exit velocity from the cooling tower and $\mathbb{Z}P_o$ is defined in Figure 7-3. The maximum rise of the streamline passing through the center of the cooling tower exit plane will be related to Briggs'[6] maximum plume rise by

$$\mathbb{Z}P_{MAX} = (vr)\sqrt{2 + U/W_o} = \Delta h + \mathbb{Z}P_o \qquad (7\text{-}15)$$

Therefore, the velocity ratio becomes

$$vr = \frac{\Delta h}{\sqrt{2 + U/W_o} - \sqrt{U/W_o}} \qquad (7\text{-}16)$$

where Δh is calculated from Briggs' plume rise formulas.

The plume boundary may be defined by the locus of streamlines passing through the edge of the cooling tower exit plane. Consider

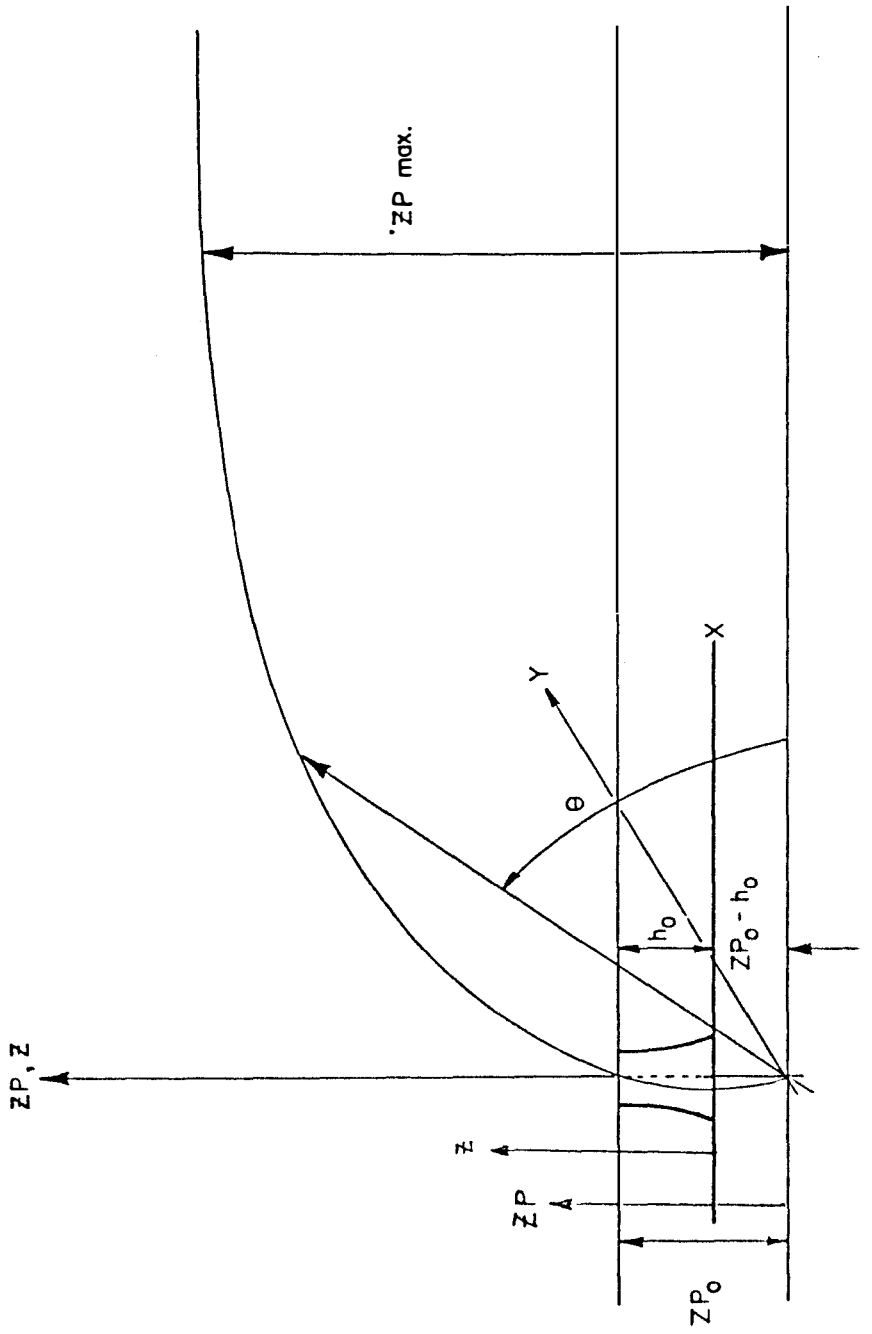

Figure 7-3 . Model Parameters

the x-z plane passing through the centerline of the cooling tower. The stream function at the edge of the plume is defined by the coordinates of the cooling tower exit plane. At any downwind location, x, equation (7-13) may be reduced to a sixth order polynominal in terms of the known constants ψ', vr, zp_o, h_o, and x, i.e.,

$$4(vr)^4 x^2(\psi'^2 - 1) + 4(vr)^2 zp^2 \psi'[(vr)^2\psi' - x^2) + zp^4[x^2 - 4(vr)^2\psi'] + zp^6 = 0 \qquad (7-17)$$

where $z = zp - (zp_o - h_o)$. The above polynominal may be solved for the z coordinate by a Newton-Raphson method. Therefore, one may determine when the drift particle leaves the plume. While the drift particle is in the plume, the velocity field defined by equation (7-8) through (7-10) will be used. When the particle leaves the plume, the velocity field

$$V_x = U \qquad (7-18)$$

and

$$V_y = V_z = 0 \qquad (7-19)$$

will be used.

CHAPTER VIII

SOLUTION OF THE EQUATION OF MOTION

Finite Difference Solution

In Chapter III the equation of motion was developed for an evaporating particle. From equation (3-5)

$$\bar{F}_{D_M} + \bar{F}_{B_M} = M \frac{d\bar{V}_M}{dt} + \frac{dM}{dt}(\bar{V}_M - \bar{V}_e) \quad (8-1)$$

The z component of equation (8-1) is

$$F_{D_z} + F_{B_z} = M \frac{dV_{Mz}}{dt} + \frac{dM}{dt}(V_{Mz} - V_z) \quad (8-2)$$

The drag force may be expressed as

$$F_{D_z} = \pm \frac{1}{2} \rho_a (V_{Mz} - V_z)^2 C_D A_P \quad (8-3)$$

where the drag coefficient, C_D, has been determined for water droplets over a wide range of Reynolds numbers as discussed in Chapter IV. The body force, F_{B_z}, due to gravity is

$$F_{B_z} = -Mg \quad (8-4)$$

Combining equations (8-2) through (8-4) and dividing by M, one obtains

$$\pm \frac{1}{2M} \rho_a (V_{Mz} - V_z)^2 C_D A_P - g = \frac{dV_{Mz}}{dt} + \frac{1}{M}\frac{dM}{dt}(V_{Mz} - V_z) \quad (8-5)$$

Since each term in equation (8-5) is a function of time (except the body force term), one cannot solve for the velocity and position of the drop

as a function of time. However, an approximate solution of the equation of motion may readily be obtained by a finite difference technique. Equation (8-5) may be expanded to give

$$\frac{V_{MZ}}{M}\frac{dM}{dt} + \frac{dV_Z}{dt} = \pm C_1 V_{MZ}^2 \mp 2 V_{MZ} V_Z C_1 \pm C_1 V_Z^2 - g + \frac{V_Z}{M}\frac{dM}{dt} \qquad (8-6)$$

where $C_1 = \rho_a C_D A_P / 2M$.

Expanding the velocity at time t in terms of the velocity at $t+\Delta t$ in a Taylor series and neglecting higher order terms, one obtains

$$V(t) = V(t+\Delta t) - \left.\frac{dV}{dt}\right|_{t+\Delta t} \Delta t \qquad (8-7)$$

or in indicial notation

$$\left.\frac{dV}{dt}\right|_{I+1} = \frac{V(I+1) - V(I)}{\Delta t} \qquad (8-8)$$

Evaluating each term in equation (8-6) at I+1 and linearizing the first term on the right side by the approximation

$$C_1 V_{MZ}^2\Big|_{I+1} = C_1 V_{MZ}\Big|_J V_{MZ}\Big|_{I+1} \qquad (8-9)$$

Combining equations (8-6), (8-8) and (8-9) and solving for $V_{MZ}(I+1)$, one obtains

$$V_{MZ}(I+1) = \frac{V_{MZ}(I) + C_1 V_Z^2 \Delta t - g\Delta t + \frac{V_Z \Delta t}{M}\frac{dM}{dt}}{1 + \frac{\Delta t}{M}\frac{dM}{dt} + 2C_1 \Delta t\left[\pm V_Z \mp V_{MZ}(J)/2\right]} \qquad (8-10)$$

The velocity must be iterated because the denominator in equation (8-10) contains the linearized term V_{Mz} (J) where J=I on the

first iteration. Hence all terms on the right side of equation (8-10) are evaluated at station J=I on the first iteration and then at station J=I+1 during subsequent iterations.

The mass of the drop at station I+1 may be expressed as

$$M(I+1) = M(I) + \frac{dM}{dt}\Delta t \qquad (8-11)$$

The velocity of the drop in the x and y directions is similar to V_{Mz} except that the body force terms are zero. Hence

$$V_{Mx}(I+1) = \frac{V_{Mx}(I) \pm C_1 V_x^2 \Delta t + \frac{V_x \Delta t}{M}\frac{dM}{dt}}{1 + \frac{\Delta t}{M}\frac{dM}{dt} + 2C_1\Delta t\left[\pm V_x \mp V_{Mx}(J)/2\right]} \qquad (8-12)$$

and

$$V_{My}(I+1) = \frac{V_{My}(I) \pm C_1 V_x^2 \Delta t + \frac{V_y \Delta t}{M}\frac{dM}{dt}}{1 + \frac{\Delta t}{M}\frac{dM}{dt} + 2C_1\Delta t\left[\pm V_y \mp V_{My}(J)/2\right]} \qquad (8-13)$$

In order to solve for the position of the drop, Z(t), function of time, consider a Taylor series expansion of Z(t) at time t+Δt. Neglecting 2nd order terms, one obtains

$$Z(I+1) = Z(I) + V_{Mz}(I+1)\Delta t \qquad (8-14)$$

Similarly, expressions for the position coordinates X and Y of the particle are

$$X(I+1) = X(I) + V_{Mx}(I+1)\Delta t \qquad (8-15)$$

$$Y(I+1) = Y(I) + V_{My}(I+1)\Delta t \qquad (8-16)$$

Hence, the velocity and position of a particle may be calculated in terms of the velocity and position at the previous time station.

Initial Conditions

The initial conditions may be specified by defining the initial velocity and coordinates of the particle as it leaves the cooling tower exit plane.

It will be assumed that the initial velocity of the particle is perpendicular to the exit plane (i.e., $V_{Mx}(t=0)=0$) and that the exit velocity is equal to the equilibrium velocity corresponding to the drop radius. The equilibrium exit velocity may be determined from equation (8-1) by setting dM/dt and $dV_{Mz}/dt = 0$. The drag force is identically balanced by the body force acting on the drop. Hence,

$$F_{Dz} = M g \qquad (8-17)$$

From equations (8-3) and (8-4),

$$V_{Mz}(1) = V_z - \sqrt{\frac{8 \rho_d R g}{3 \rho_a C_D}} \qquad (8-18)$$

where V_z corresponds to the velocity of the plume at the exit plane. Therefore one can determine the initial velocity of the particle from equation (8-18). Since the drag coefficient, C_D, is a function of velocity, an iteration is necessary. On the first iteration, Stokes law, equation (4-4) may be used to calculate the first approximation. Thereafter equation (8-18) is iterated until $V_{Mz}(1)$ is within 1% of the final value where C_D is evaluated using equation (4-7).

The initial coordinate may be specified by defining x(1) and y(1). z(1) is equal to the height of the tower.

Sign on the Drag Term

A coordinate system has been defined in Figure 7-2. A positive drag force acts in the positive coordinate direction.

As a drift particle leaves the cooling tower exit plane, it is carried upward in the plume. As long as the drop remains in the plume, the drag force acting on the particle is positive since the absolute velocity of the drop is never greater than the plume velocity as shown in Figure 8-1.

If the velocity of the drop is positive when it leaves the plume, the drag force will change sign and become negative as in Figure 8-2. At some point throughout the trajectory of the drop, it will reach a maximum height at which time the vertical velocity component, V_{Mz}, is zero. After this point in time, the drag force becomes positive until it hits the ground or evaporates as in Figure 8-3.

A simple method of determining the sign of the drag term is by relating it to the sign of the velocity difference defined by

$$VD_z = V_z - V_{Mz} \qquad (8\text{-}19)$$

When $VD > 0$, $F_D > 0$ and when $VD < 0$, $F_D < 0$.

Equation (8-10) is

$$V_{Mz}(I+1) = \frac{V_{Mz}(I) + C_1 V_z^2 \Delta t - g\Delta t + \frac{V_z \Delta t}{M}\frac{dM}{dt}}{1 + \frac{\Delta t}{M}\frac{dM}{dt} + 2C_1 \Delta t \left[\pm V_z \mp V_{Mz}(J)/2\right]} \qquad (8\text{-}20)$$

When $VD_z < 0$, the term in brackets in the denominator is $[V_z - V_{MZ}(J)/2]$. When $VD_z \geq 0$, the term in brackets becomes $[-V_z + V_{MZ}(J)/2]$.

The velocity components V_{Mx} and V_{My} are evaluated in a similar manner.

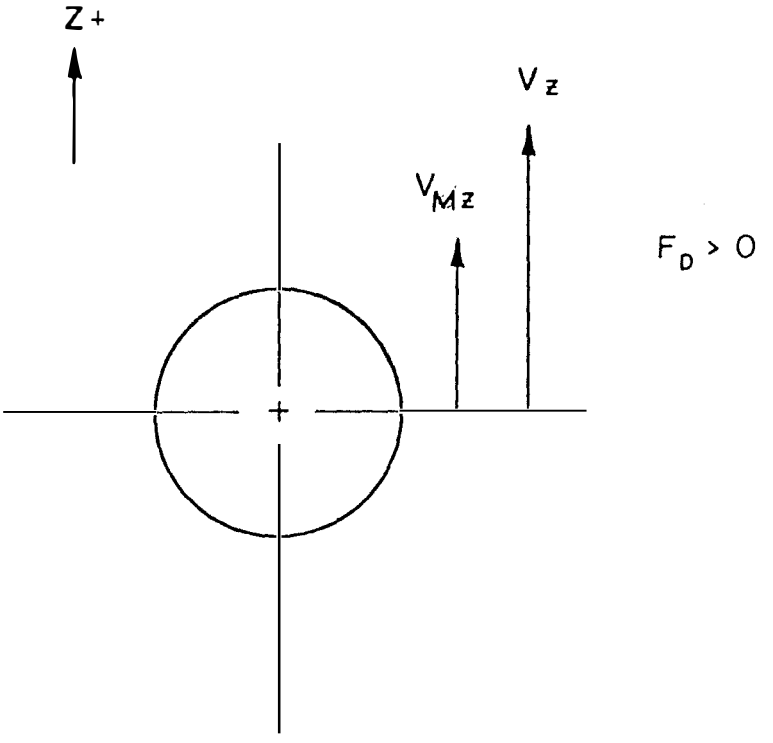

Figure 8-1 . Drift Drop in Plume

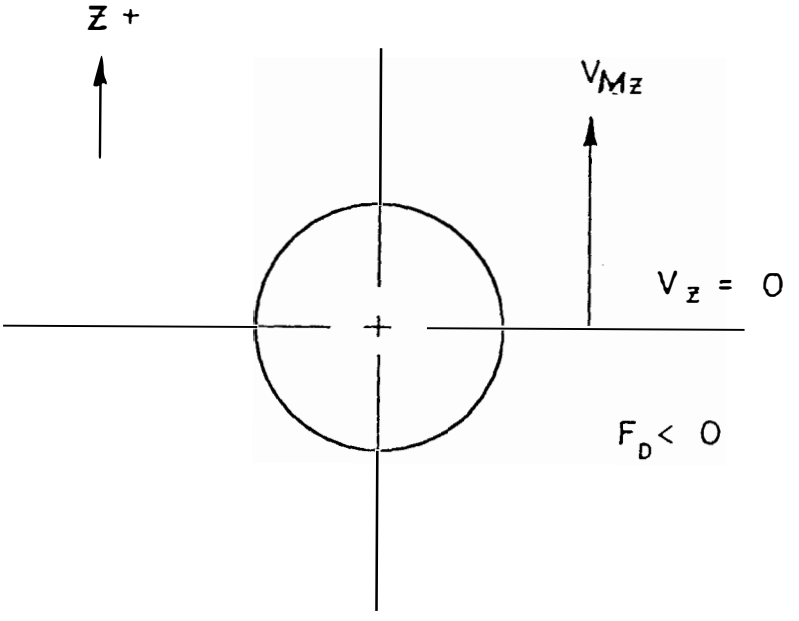

Figure 8-2 . Drift Drop Moving Up in Ambient Air

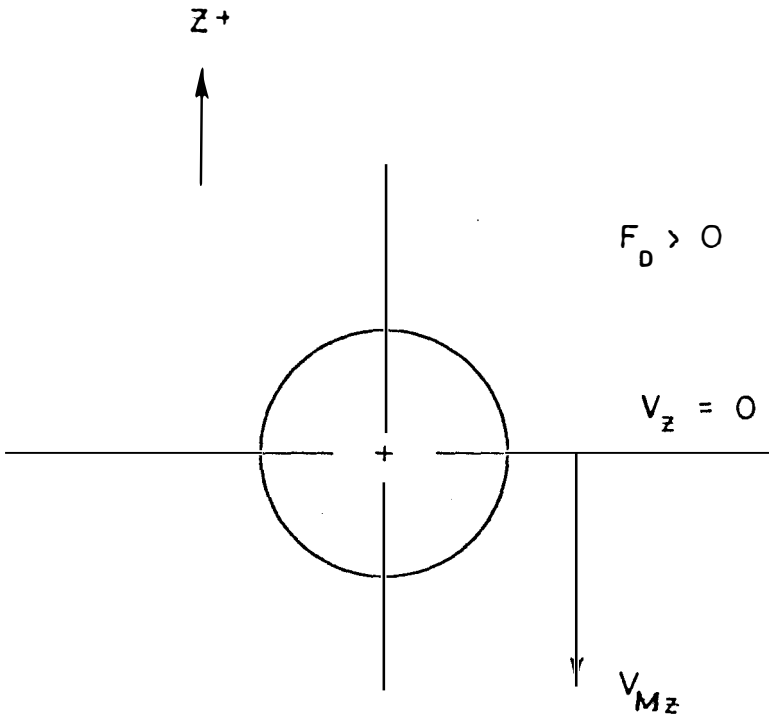

Figure 8-3 . Drift Drop Falling in Ambient Air

CHAPTER IX

DISCUSSION OF RESULTS

A computer program has been developed employing the concepts and equations presented in the previous chapters. The program calculates the trajectory of a drift drop as a function of cooling tower parameters and meteorological variables. For each drop size, the calculation terminates when the drop "effectively evaporates" (i.e., when the drop radius is 40 μm or less) or when it hits the ground. A complete listing of the program is given in Appendix A.

The input variables for the model can be broken down into two groups, cooling tower parameters and meteorological variables. The cooling tower parameters are

1. range (inlet water temp.-outlet water temp.)
2. approach (outlet water temp.-ambient wet bulb temp.)
3. tower height
4. exit radius
5. exit velocity
6. drift drop size distribution
7. drift drop mass distribution

The meteorological variables are

1. atmospheric stability condition
2. dry bulb temperature
3. wet bulb temperature
4. wind speed.

In addition to the variables mentioned above, there are several program variables and initial conditions which are important in calculating the drop trajectories. They are

1. the time increment
2. initial drop position
3. initial concentration.

Figures 9-1 through 9-4 illustrate the effects of some of the more important variables on the droplet trajectory.

Meteorologists describe turbulence in the atmosphere by classifying the states into various stability conditions. One common classification is the Pasquill Stability Classification[42] as shown in Table 9-1. The temperature gradient is a direct measure of the stability condition; the temperature gradient ranges for each of the Pasquill stability classes are indicated in the table. Condition A, B, and C are unstable, condition D is neutral, and conditions E and F are stable.

Figure 9-1 illustrates the effect of evaporation on particle trajectory. Curve 1 represents the trajectory of a drift drop of pure water. Very little evaporation occurs while the drop is in the plume. When the drop leaves the plume, it evaporates rapidly as it falls toward the ground. At a downwind distance of 186.2 meters, the drop has "effectively evaporated" (i.e., $R < 40\,\mu m$). Curve 2 represents the trajectory of a slat laden drift drop where the initial concentration is 66 ppt. The effect of the dissolved salt, as indicated in equations (5-8) and (6-12), is to reduce the vapor pressure over the drop and thereby reduce the evaporation rate. As expected, the drop falls to the ground at a downwind distance of 193 meters. The radius of the salt laden dorp when it hits the ground is $154\,\mu m$ and the concen-

Table 9-1. The Pasquill Stability Classification

Condition	Temperature Gradient ($\Delta T/\Delta z$) (°K/ meter)	
A	$\frac{\Delta T}{\Delta z} < -.02180$	unstable
B	$-.02180 \leq \frac{\Delta T}{\Delta z} < -.01593$	unstable
C	$-.01593 \leq \frac{\Delta T}{\Delta z} < -.01228$	unstable
D	$-.01228 \leq \frac{\Delta T}{\Delta z} < -.00273$	neutral
E	$-.00273 \leq \frac{\Delta T}{\Delta z} < +.01997$	stable
F	$+.01997 \leq \frac{\Delta T}{\Delta z}$	stable

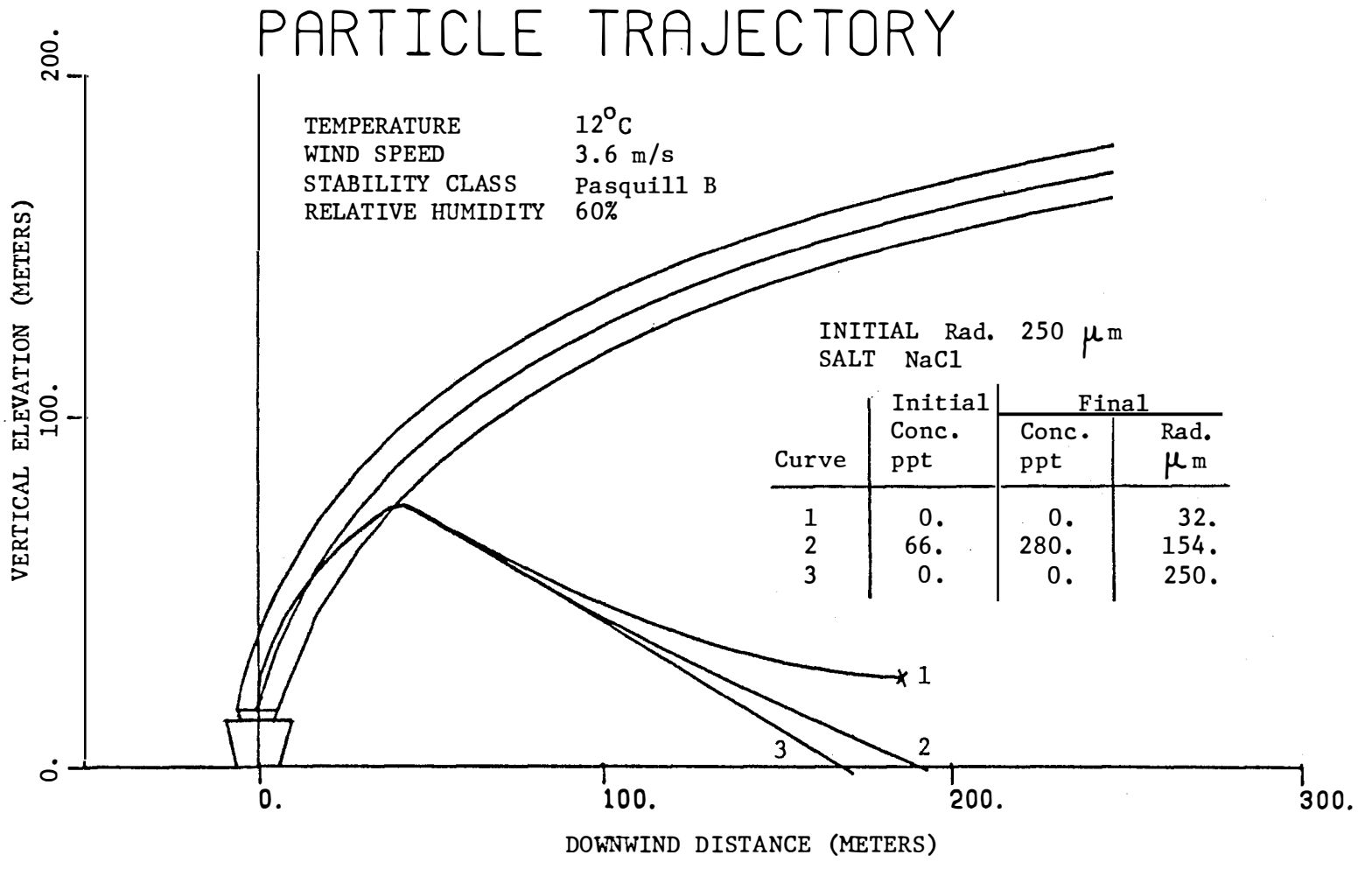

Figure 9-1. Drift Drop Trajectory

tration is about 280 ppt. For comparison purposes Curve 3 illustrates the trajectory of a solid drop where the density is the same as that of water. Curve 3 represents the limiting case of 1 and 2 since dM/dt = 0. The solid drop leaves the plume at about the same point as in Curves 1 and 2, but it contacts the ground at a downwind distance of 172 meters.

One may conclude from Figure 9-1 that the evaporation rate has a considerable effect on drift drop trajectory from a cooling tower and must be considered in calculating the deposition of drift drops. The reduced evaporation rate of the drift drop due to the salt concentration causes the drop to fall to the ground sooner and increases the deposition rate.

Figure 9-2 illustrates the effect of the initial coordinate position on particle trajectory. The droplets following trajectories 1, 2, and 3 all have the same initial conditions except that droplet 1 was emitted at x = -3 meters, droplet 2 was emitted at x = 0 and droplet 3 was emitted at x = 3 meters. Since droplet 1 remains in the plume longer than droplet 2 or 3, it is carried to a higher elevation and subsequently falls a greater distance through the ambient air. As a result, droplet 1 is carried further downwind and evaporates to a smaller size than droplets 2 or 3.

The droplet trajectories in Figure 9-2 are not straight lines since the drops are continuously evaporating and the fall velocities are decreasing. This is apparent by comparing curves 2 and 3 in Figure 9-1. Curve 3 in Figure 9-1 is a straight line outside the plume and it is apparent that curve 2 is slopped upward from curve 3. Curve 2 in Figure 9-1 is identical to curve 2 in Figure 9-2.

By considering initial positions at the edge of the cooling

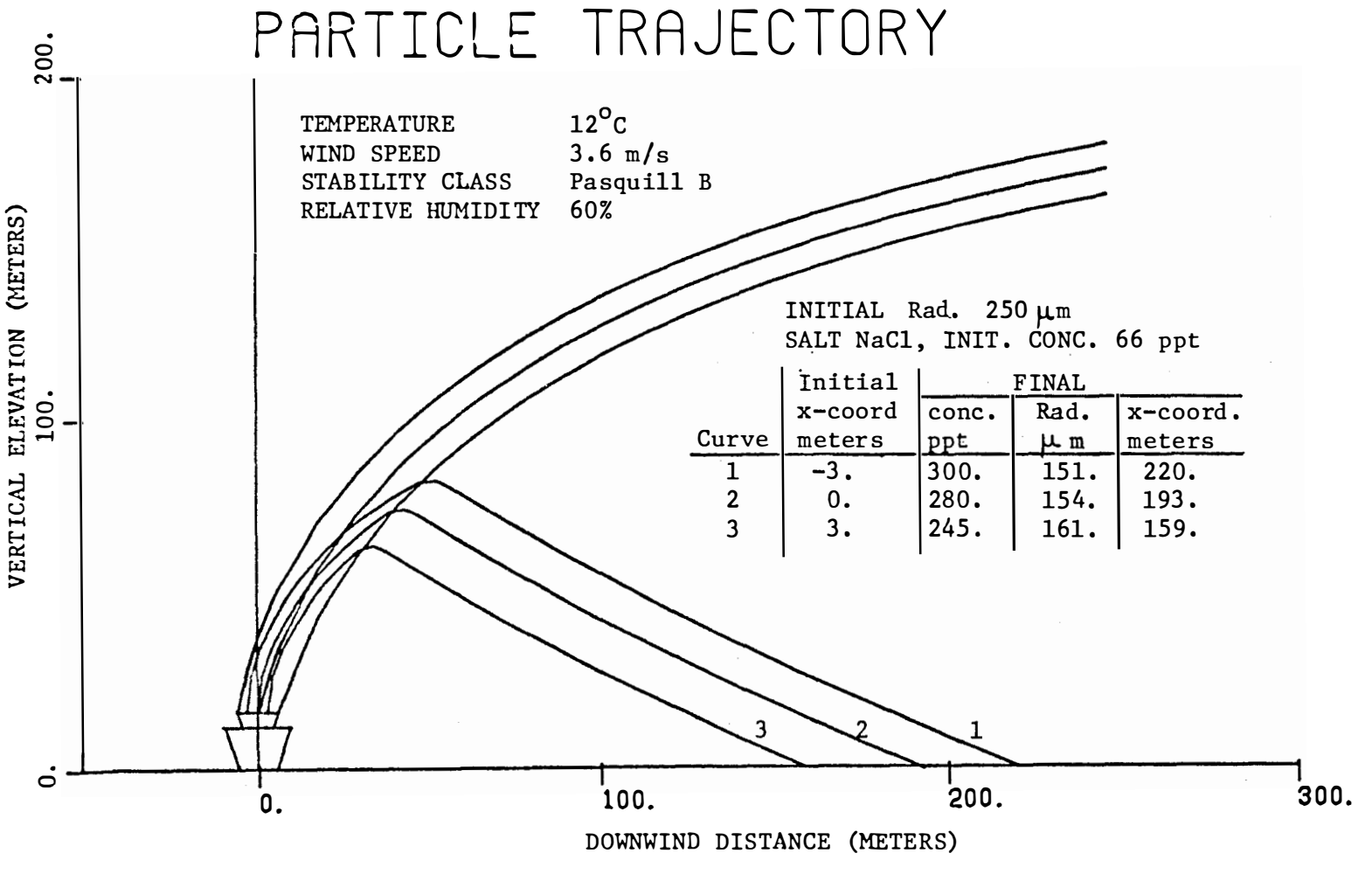

Figure 9-2. Drift Drop Trajectory Showing Effects of Initial Position

tower exit plane, the downwind distances at which the drops hit the ground may differ by as much as an order of magnitude depending on the drop size and meteorological parameters. Therefore, the initial position of the drops is important in calculating the deposition of drift drops from cooling towers.

Figure 9-3 shows the effect of salt concentration on the droplet trajectory. The droplets following curves 1, 2, and 3 have the same initial conditions except that droplet 1 has an initial concentration of 33 ppt, droplet 2 has an initial concentration of 66 ppt, and droplet 3 has an initial salt concentration of 132 ppt. All three droplets leave the plume at about the same point. Since droplet 1 has a smaller concentration than droplets 2 or 3, it evaporates more rapidly. Therefore the fall velocity of droplet 1 is less and it remains in the air longer than droplets 2 and 3 and is carried further by the wind as indicated in Figure 9-3. Under the conditions indicated in Figure 9-3, a 100% increase in salt concentration from 66 ppt to 132 ppt causes about an 8% decrease in the downwind distance that the drop hits the ground. In general, an increase in salt concentration increases the deposition near the tower.

Figure 9-4 illustrates the effect of the atmospheric stability condition on the drop trajectory. The meteorological conditions governing the behavior of the two plumes in Figure 9-4 are the same except that the dotted curves "B" represent the plume behavior under stability condition B and the solid curves "F" represent the plume behavior under stability condition F. Stability condition B represents an unstable environment where as condition F represents a stable condition. Curves 1 and 2

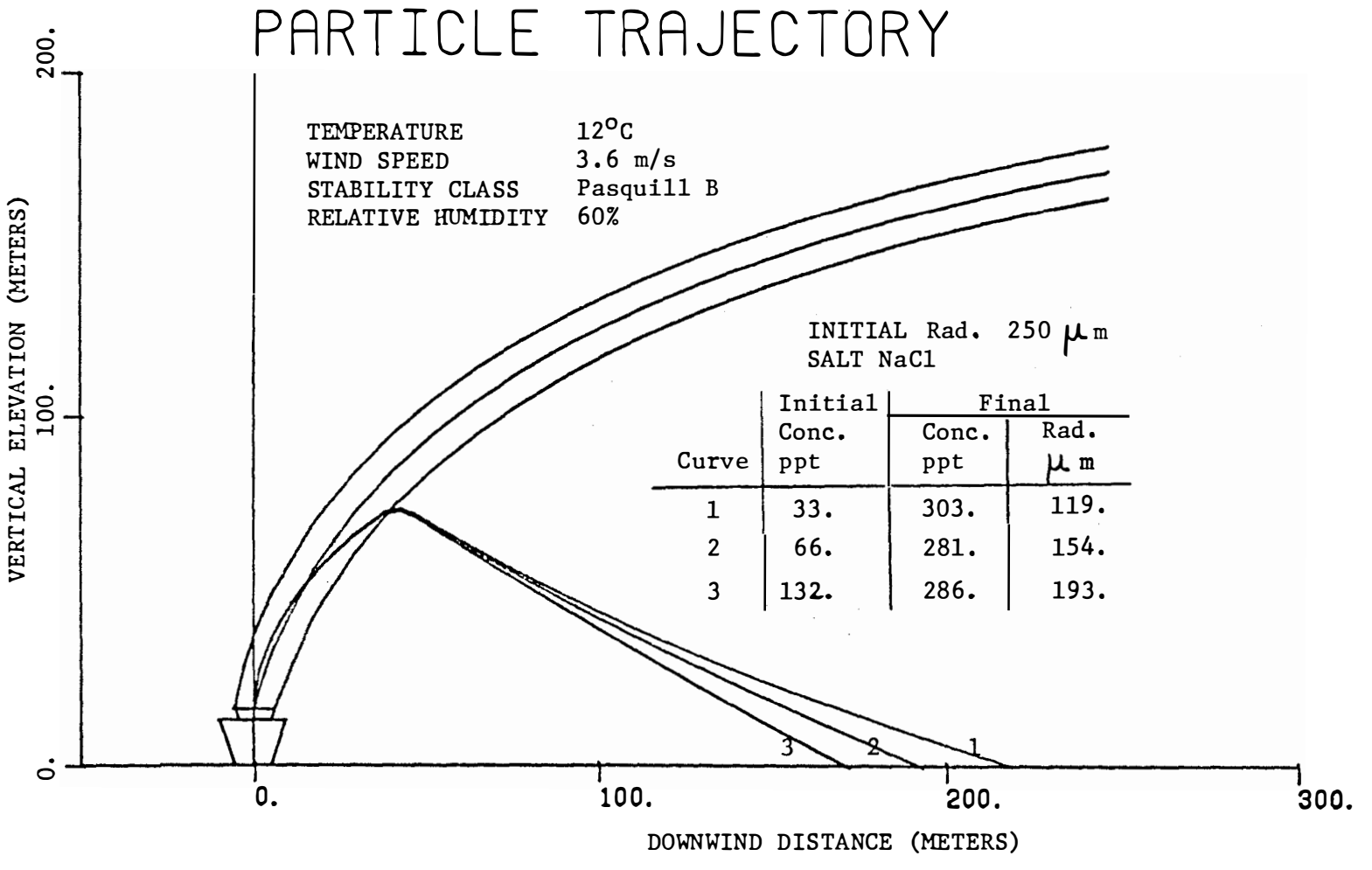

Figure 9-3. Drift Drop Trajectory Showing Effects of Salt Concentration

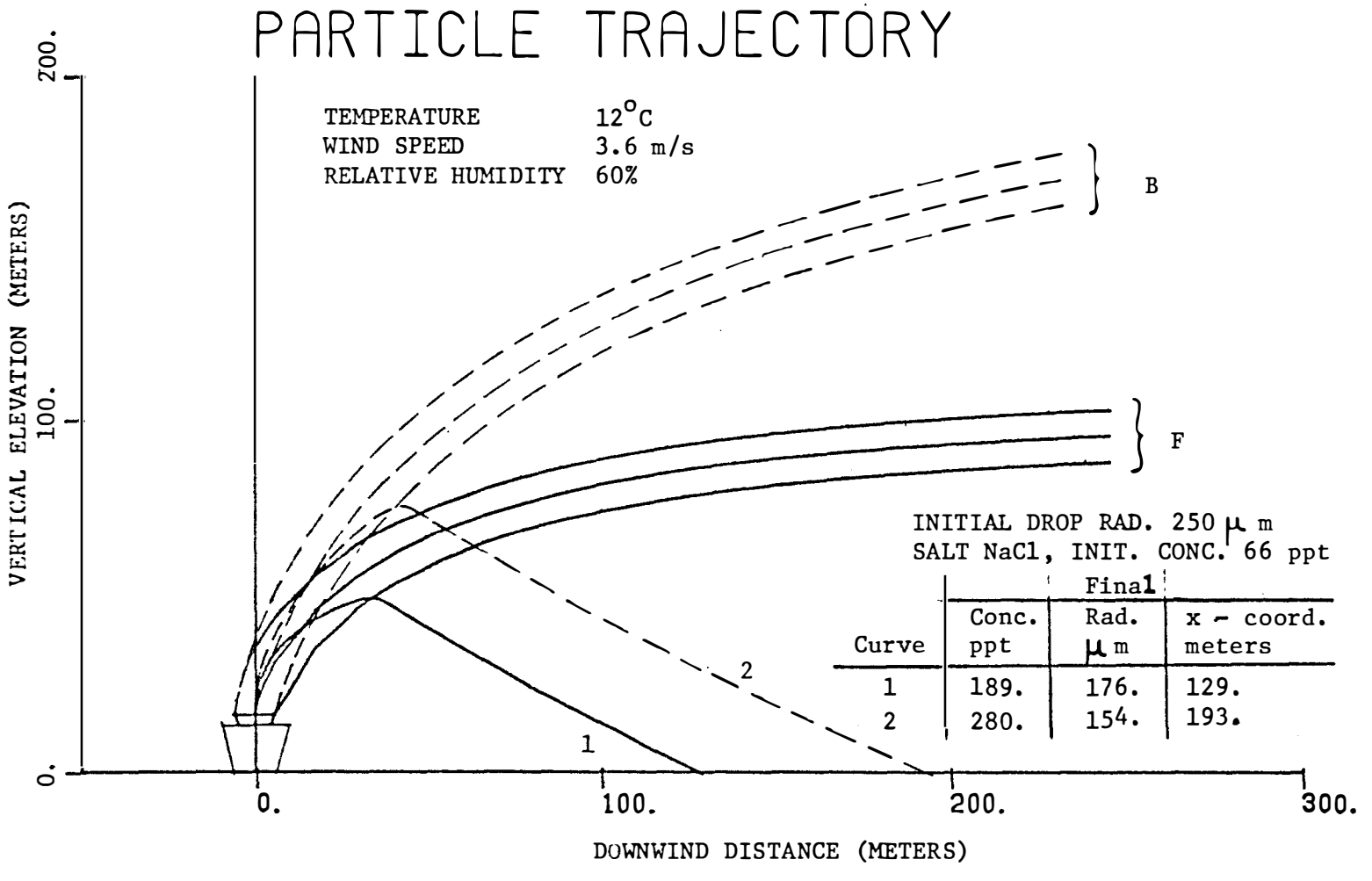

Figure 9-4. Drift Drop Trajectory Showing Effects of Stability Condition

represent the trajectories of a 250 μm drift drop with an initial salt concentration of 66 ppt. Curve 1 is the trajectory of the drift drop during stable conditions, Pasquill F, and curve 2 is the trajectory of the same drift drop during unstable conditions, Pasquill B. Since the plume rise is somewhat greater in an unstable atmosphere, a drift drop will rise to a greater height as indicated by curve 2 and fall a greater distance through the atmosphere. Droplet 2 hits the ground at a greater distance (193 meters) from the tower than droplet 1 (129 meters). Since droplet 2 is in the air longer, it evaporates to a smaller size (R=154μm) than droplet 1 (R=176μm). Therefore, the atmospheric stability condition has a significant effect on the droplet trajectory.

Very little information is currently available in the open literature on the trajectory of drift drops from a cooling tower. Wistrom and Ovard[39] have recently presented some information on drift drop trajectories as shown in Figure 9-5. The meteorological conditions in Figure 9-5 were a 17.3°C dry bulb temperature and 50% relative humidity with a stable atmospheric condition and a wind speed of 20 mph. The cooling tower was of mechanical draft design with a salt concentration in the drift equal to sea water. In order to provide some basis of comparison with the above result, a similar calculation was made for a 300 μm radius drop and a 225 μm radius drift drop using the present model and the above data. In addition, it was assumed that the height of the tower was 70 feet.

Using the present model, Figure 9-6 shows the predicted trajectory of a 225 m and 300 m radius drift drop. The drift drop with an initial radius of 300 m evaporated to a radius of 127μm and a saturated

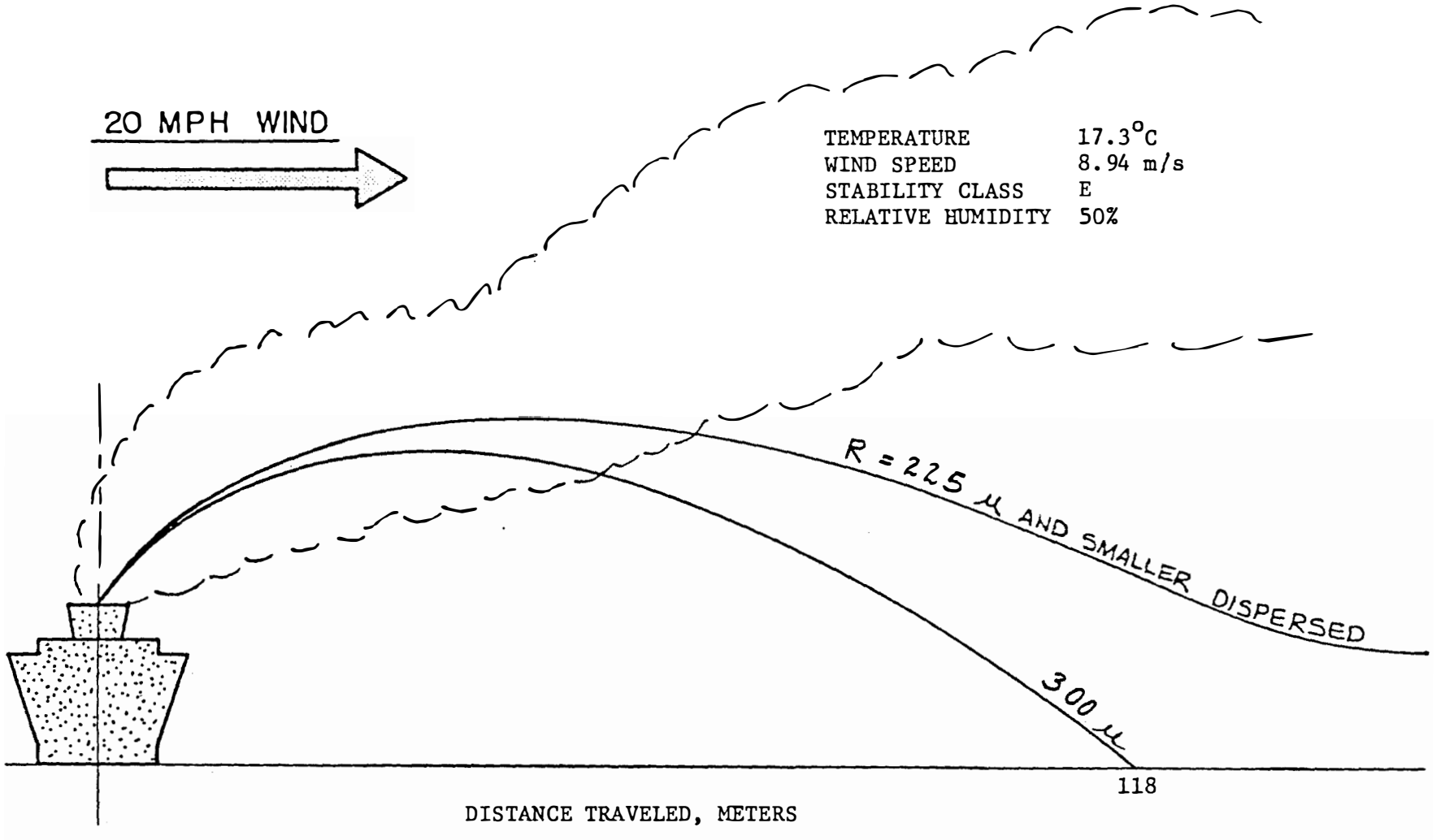

Figure 9-5. Drift Drop Trajectory of Wistrom and Ovard[40]

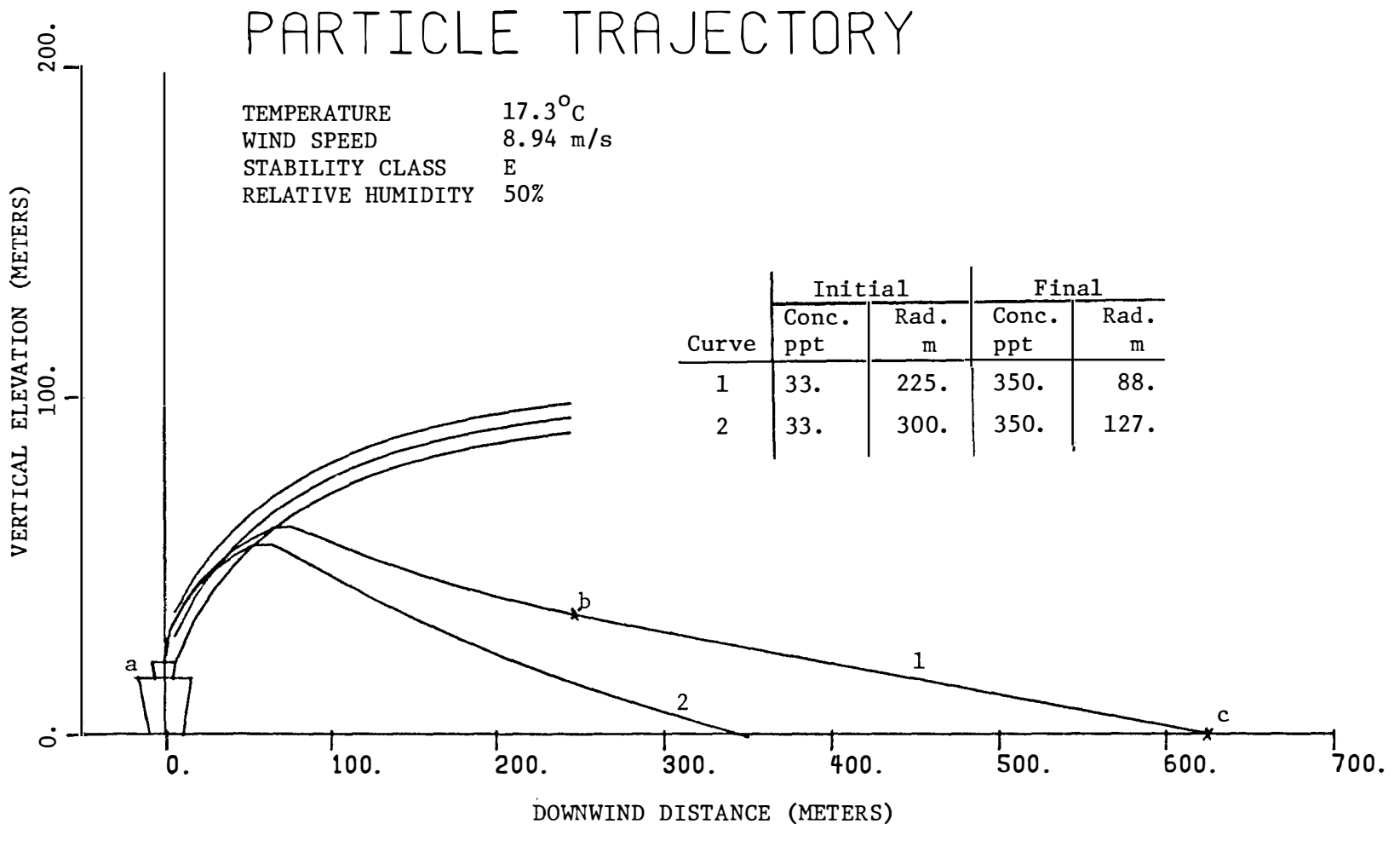

Figrue 9-6. Drift Drop Trajectory by UT Model

concentration of 350 ppt and traveled to a downwind distance of 351 m. This distance is more than twice the 118 m of Wistrom and Ovard.

A greater difference occurs in the case of the 225 μm drift drop. As indicated in Figure 9-5, Wistrom and Ovard[40] predict that a 225 μm drop will "effectively evaporate". However, the present model predicts that a 225 μm radius drop will hit the ground at a downwind distance of 624 m. Under the meteorological conditions indicated in Figure 9-6 and a salt concentration of 33 ppt, a 225 μm radius evaporates to a saturated drop at a downwind distance of 246 m. At this point many authors neglect the effects of salt precipitation within the drop. A saturated drop will continue to evaporate if the ambient vapor pressure is sufficiently low. In order to take into account the effects of precipitation within the drop, it may be assumed that the initial amount of salt remains dissolved until a saturated condition is reached. From that point on, the drop concentration is equal to the saturated concentration as specified in Figure 6-5. The excess salt is assumed to precipitate out as a solid crystal. The volume of the solid salt and the saturated water is easily determined and the corresponding radius may be calculated. For example, consider the 225 μm drift drop mentioned above with an initial NaCl concentration of 33 ppt. At a downwind distance of 246 m the drop has evaporated to a saturated radius of 102.2 μm radius. The saturation concentration is about 350 ppt. When the drop hits the ground, the radius is 88.5 μm. Figure 9-7 illustrates the condition of the 225 μm drop at points a, b, and c in Figure 9-6. Note that the total mass of salt remains constant.

Since the downwind distance at which a given size drop hits the ground can be calculated under any conditions, the mass fraction

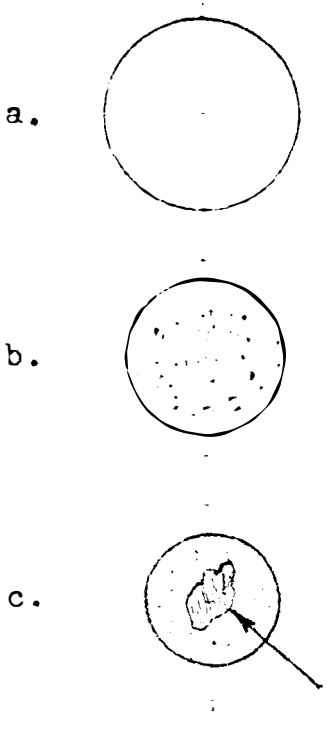

	Mass of				Volume x 10^{-6}		
		Salt(NaCl)					
	Water μgm	dissolved μgm	solid μgm	Conc. ppt	water cm^3	salt cm^3	Rad. μm
a.	47.7	1.57	0	33.	47.7	0	225.
	dilute mixture						
b.	4.46	1.57	0	350.	4.46	0	102.2
	saturated drop						
c.	2.60	.91	.66	350.	2.60	.305	88.5
	saturated drop with solid salt crystal						

Figure 9-7. Salt Precipitation within a Drift Drop

and the deposition area associated with each drop size enables one to determine the total salt drift deposition from a cooling tower. In order to further illustrate the use of the particle trajectory in calculating the chemical deposition from a cooling tower, a sample calculation will be made using both Hosler's model[17] and the UT model listed in Appendix A. The meteorological conditions used in the calculations are shown in Table 9-2 and the cooling tower variables are indicated in Table 9-3.

Sample Calculation Using the Hosler, et. al., Model

Assume that the drift drop distribution is indicated in Table 9-3. The mass of salt in each class interval can then be calculated from the drift rate[17] and entered in Table 9-4.

The drift in the class interval r = 50 μm is distributed in the drop sizes between 25 and 75 μm, the 20% as 100 μm radius drops are distributed between 75 and 125 μm and so on.

From Figure 2-8[17] the values of h_e , the minimum height a drop must fall in order to evaporate to a saturated solution[17] drop, is obtained. These values are shown in Table 9-5. From Figure 2-9, the values of h_r, the height the drops rise in the plume, are obtained and shown in Table 9-5.

For drop sizes 175 and 225 μm, we have shown that $h_e > h_r$; these drops do not reach their equilibrium size[17], so, Figure 2-10 is used. For the 175 μm drop, one enters the figure at 175 μm and a horizontal line is drawn from the vertical axis to the curved line $V_o = f(r_o)$. A vertical line is then drawn down to the point where it crosses h_r = 297 ft. A horizontal line is constructed from this point to the

Table 9-2. Meteorological Conditions Used in Sample Calculations

Variable	Value
Dry Bulb Temperature	80°F (299.9°K)
Wet Bulb Temperature	63°F (290.7°K)
Relative Humidity	70%
Wind Speed	10 MPH (4.47 m/s)
Stability Condition	B
Frequency of Calm	.019

Table 9-3. Cooling Tower Variables Used in Sample Calculations

Variable	Value
Mechanical Draft Cooling Tower	
Range	20°F (11.11°K)
Approach	15°F (8.33°K)
Tower Height	21.2 m
Exit Radius	4.6 m
Exit Velocity	40 fps (12.2 m/s)
Circulating water flow rate	15,000 GPM ($2.48 \times 10^9 \frac{kg}{mo}$)
Drift Rate (% of Circulating water flow rate)	.01%
Concentration	50,000 ppm

Table 9-4. Mass Distribution Using Hosler, et. al., Model[17]

r μm	Mass Fraction	M_i kg/mo
50	.2	2480
100	.2	2480
150	.3	3720
200	.3	3720
	1.0	12400

$$\frac{\text{kg } H_2O}{\text{mo}} \quad X \quad 1 \quad X \quad \frac{\text{kg Salt}}{\text{kg } H_2O}$$

$$M = (2.48 \times 10^{9})(1 \times 10^{-4})(5 \times 10^{-4})(10^{-6})$$

$$= 12440 \text{ kg/mo}$$

Table 9-5. Maximum Height in Plume and Equilibrium Fall Height of Drops Hosler, et. al., Model[17]

	$r_{\mu m}$	h_e ft	h_e m	Corrf	h_r ft	h_r m
S_2A $h_e < h_r$	25	80	24.4	.99	324	98.42
	50					
	75	80	24.4	.97	317	96.86
	100	110	33.5	.95	312	95.2
	125	220	67	.93	306	93.74
	150					
S_1A $h_e > h_r$	175	580	176.7	.89	297	90.62
	200					
	225	1100	335	.85	287	87.5

10 mph wind speed line. The last line is constructed parallel to the vertical axis and the downwind distance at which the drop hits the ground is read off the axis as d = .18 miles. The curve is entered with the 225 μm drop size in a similar manner as shown in Figure 2-10.

For drop sizes 25, 75, and 125 μm, $h_e < h_r$, the drops reach their equilibrium size[17], so Figure 2-11 is used. Figure 2-11 is entered by constructing a horizontal line at the salt concentration of 50,000 ppm. For each drop size, veritcal lines are constructed from the intersection of the curved lines $V_s = f(c)$ and the horizontal concentration line. From this point on, the construction is the same as before as shown in Figure 2-11.

For each drop size, the distance from the tower at which the respective drops fall and the area covered are tabulated in Table 9-6. The deposition is obtained by simply dividing the mass contained in each drop size by the corresponding area.

The above calculation is for a uniform wind distribution. To account for the variation in the frequency of wind direction, the deposition is multiplied by the normalized fraction of time the wind blows in a specified direction. For simplicity, a uniform wind distribution is used and the results of the calculation have been plotted in Figure 9-8.

UT Model

The program listed in Appendix A incorporates the concepts presented in the previous chapters and calculates the coordinate position of a drift drop from the time it leaves the cooling tower to the time it hits the ground or evaporates. Consider a particle released from the leading edge of the cooling tower exit plane as shown in Figure 9-2;

Table 9-6. Deposition by Hosler, et. al., Model [17]

	r m	x miles	acres	acres	kg/mo	lb/mo	Q lb/ac-mo	kg/m^2-yr	$\bar{x}$ miles	meters
	25	4.1	31000							
	50			28000.	2480	5500	.196	.000264	2.6	4185.
S_2A	75	1.1	3000							
$h_e < h_r$	100			2550.	2480	5500	2.2	.00287	.79	1271.
	125	.48	450							
	150			378.	3720	8200	21.6	.0292	.33	531.
S_1A	175	.18	72.							
$h_e > h_r$	200			35.	3720	8200	234.	.315	.155	249.
	225	.13	37.							

From Nomograms

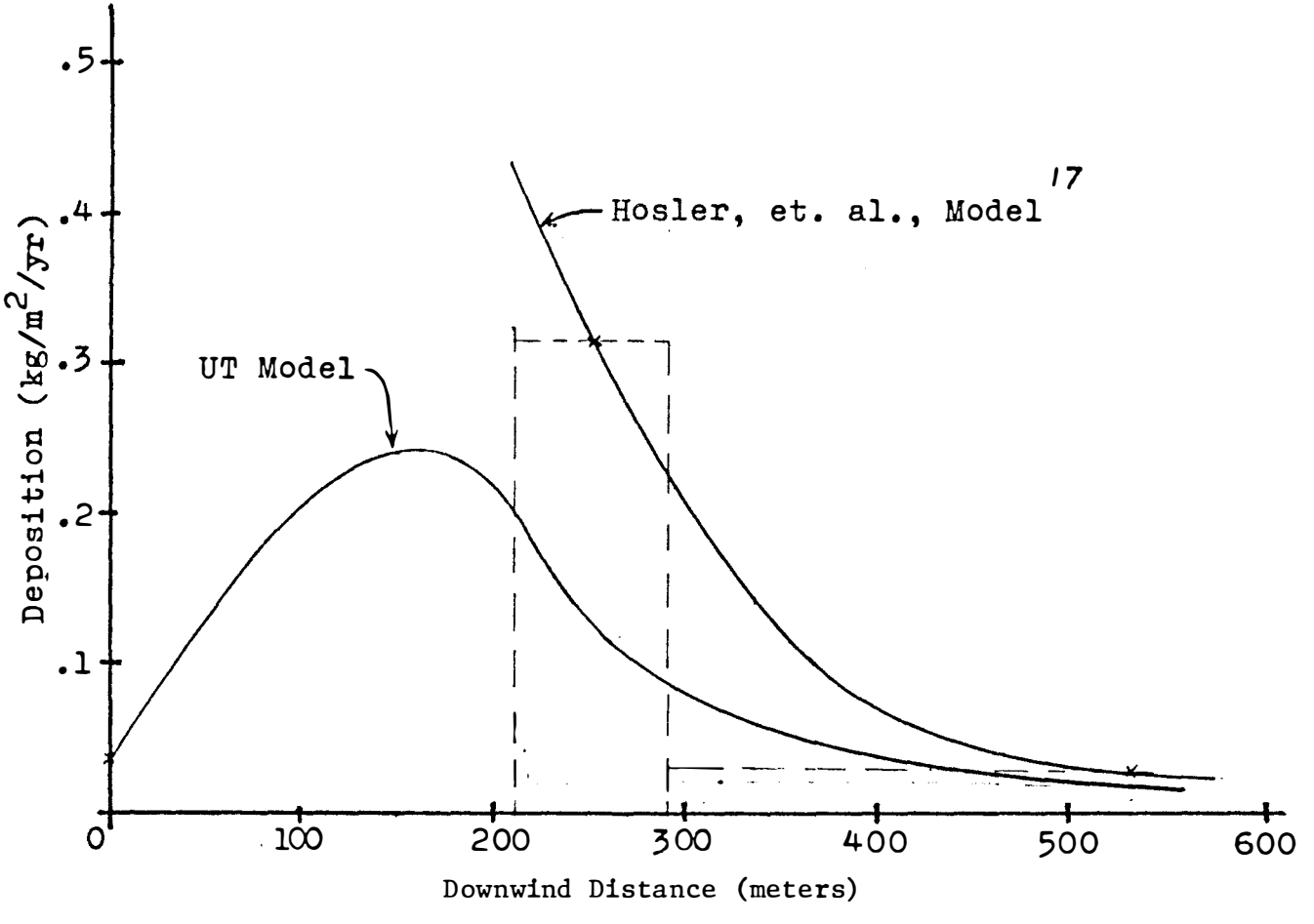

Figure 9-8. Comparison of Deposition from Hosler, et. al., Model and UT Model

the program calculates the maximum distance that a given size drop is carried downwind of the tower. Similarily, consider a drift drop of the same size released from the trailing edge of the cooling tower exit plane; the program calculates the minimum distance that a drop of given size is carried. The area over which drift drops of a specified size are distributed is thereby calculated and shown in Figure 9-2. The deposition is simply the mass flux divided by the area. This procedure is repeated for each drop size considered. The final deposition is obtained by summing individual deposition values over all the frequency classes considered.

In order to provide a basis of comparison, consider the same data used to illustrate Hosler's model in the previous section. The input variables for the computer program are listed and described in Table 9-7. The input cards for this particular example are shown in Table 9-8.

The mass distribution presented in Table 9-4 and the uniform wind distribution used in calculating the salt deposition by Hosler, et.al., model have been modified slightly as shown in Table 9-9 and 9-10 to account for calm conditions.

The results of the computer program using the above data have also been plotted in Figure 9-8.

Discussion of Sample Calculation

Comparison of the curves in Figure 9-8 illustrates several differences in calculating cooling tower deposition by the two methods.

Hosler's model predicts no salt deposition at distances less than 287 meters from the tower. The UT model not only predicts chemical deposition within this distance but it predicts a value of .035 kg/m^2-yr

Table 9-7 Program Input

Card	Field	Format	Program Designation	Description of Quantity
1	1-80	20 A4	LØC (I)	Title and information
2,3,4,5	1-80	8F 10.2	XME (I)	X coordinate values at which deposition is desired (meters)
6	1-10	I 10	NTP	Type of Plume 0 - Bouyant 1 - moment um
	11-20	F 10.2	HT	Height of Tower (m)
	21-30	F 10.2	Range	Range (°K)
	31-40	F 10.2	APP	Approach (°K)
	41-50	F 10.2	WØ	Tower exit vel. (m/s)
	51-60	F 10.2	RØ	Tower exit Rad. (m)
	61-70	F 10.2	GPM	Water Flow Rate thru tower (GPM)
7	1-10	F 10.0	C	Salt Concentration (PPT)
	11-20	F 10.5	Alpha	Drift Fraction (of GPM)
8	1-10	I 10	NP	Number of drift drop sizes
9	1-80	8F 10.4	RP(I)	Radius of Drift Drops (centimeters)
10	1-80	8F 10.4	xMF(I) xMF(I+1)	Mass Fraction Sum of Calms
11	1-64	16A4	LDIR(I)	16 Compass Directions
12	1-10	I 10	ISC	Pasquill Stability condition (1 = A, 2 = B, ...)
	11-20	F 10.4	TDBO	Dry bulb temperature (°K)
	21-30	F 10.4	B	Adiabatic Lapse Rate (°K/m)
	31-40	F 10.4	U	Wind Speed (m/s)
	41-50	F 10.4	RHØ	Relative humidity
	51-54	A 4	SEA	Season
	61-70	F 10.4	TWB	Wet bulb (°K)
13,14	1-80	8F 10.4	F(IDIB)	Frequency wind blows in resprictive directions
15	1-10	F 10.4	F(17)	Frequency of Calm

Table 9-8. Input Cards for UT Computor Program

Card No.	Card
1	MECHANICAL DRAFT TOWER, SALT DEPOSITION, KG/M**2/YR. Card No. 1, LOC(I)
	A Thru I
2	10.00 20.00 30.00 40.00 50.00 60.00 70.00 80.00
	A Thru I
3	90.00 100.00 200.00 300.00 400.00 500.00 600.00 700.00
	A Thru I
4	800.00 900.00 1000.00 2000.00 3000.00 4000.00 5000.00 6000.00
	A Thru I
5	7000.00 8000.00 9000.00 10000.00 Card No. 2-5, XME(I)
	A Thru I
6	1 21.20 11.11 8.33 12.20 4.60 15000.00
	A Thru I Card No 6
	J Thru R NTP HT RANGE APP WO RO GPM
7	50. .00010 Card No. 7, C and ALPHA
	A Thru I10 15
8	4 Card No. 8, NP
	A Thru I
9	.0050 .0100 .0150 .0200 Card No. 9, RP(I)
	A Thru I
10	.2000 .2000 .2810 .3000 .0190 Card No. 10, XMF(I)
	A Thru I
11	N NNE NE ENE E ESE SE SSE S SSW SW WSW W WNW NW NNW
	A Thru I Card No. 11, LDIR(I)
12	2 299.9000 -.0073 4.4700 .7000EXAMPLE 290.7000
	A Thru ISC TD BO B U RHO SEA TWB
	J Thru R Card No. 12
13	.0613 .0613 .0613 .0613 .0613 .0613 .0613 .0613
14	.0613 .0613 .0613 .0613 .0613 .0613 .0613 .0615
15	.0190 Card No. 13-15, F(I)
	A Thru I
	J Thru R
	S Thru Z

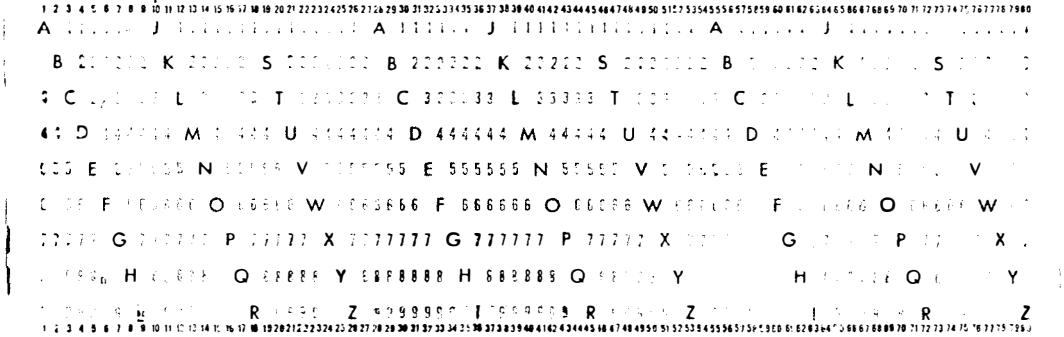

Table 9-9. Modified Mass Distribution for UT Model

r μm	Mass Fraction	M_i kg/mo
50	.2000	2480
100	.2000	2480
150	.2810	3500
200	.3000	3720
Calm	.0190	220
	1.0000	12400

Table 9-10. Modified Wind Distribution

Direction	Uniform Distribution	Modified Distribution
N	.0625	.0613
NNE	.0625	.0613
NE	.0625	.0613
ENE	.0625	.0613
E	.0625	.0613
ESE	.0625	.0613
SE	.0625	.0613
SSE	.0625	.0613
S	.0625	.0613
SSW	.0625	.0613
SW	.0625	.0613
WSW	.0625	.0613
W	.0625	.0613
WNW	.0625	.0613
NW	.0625	.0613
NNW	.0625	.0615
Calm	.0000	.0190
	1.0000	1.0000

very near the tower. This large difference can be attributed to the fact that the Hosler model does not present any realistic method for handling the calm conditions. The UT model easily accounts for the calm conditions by distributing the mass flux associated with the calm over the area defined by the minimum downwind distance of the largest drop.

Figure 9-9 represents unpublished data from the Oak Ridge National Laboratory[41] on chemical deposition from a similar mechanical draft cooling tower. Unfortunately no concurrent meteorological data was available for correlation with the present model. However, the data does indicate that a significant amount a chemical deposition occurs very near the cooling tower and prediction of this deposition represents an important part of any model.

Another significant difference occurs in the location of the maximum deposition. Hosler's model predicts a maximum deposition of .43 kg/m^2-yr at a distance of 287 meters whereas the UT model predicts a maximum deposition of .23 kg/m^2-yr at a distance of 170 meters. This difference can be attributed to the fact that Hosler uses the final plume rise in calculating the height the drop reaches in the plume. In effect, this means that the plume travels straight up until it reaches the height of the final plume rise and then travels downwind at the speed of the wind. The total time that it takes each particle to reach zero velocity in the plume and fall from rest to the ground is calculated and multiplied by the wind speed to obtain the downwind distance traveled. This technique overestimates the distance traveled and consequently underestimates the corresponding deposition. The UT model takes into account the transport of the drop within the plume by

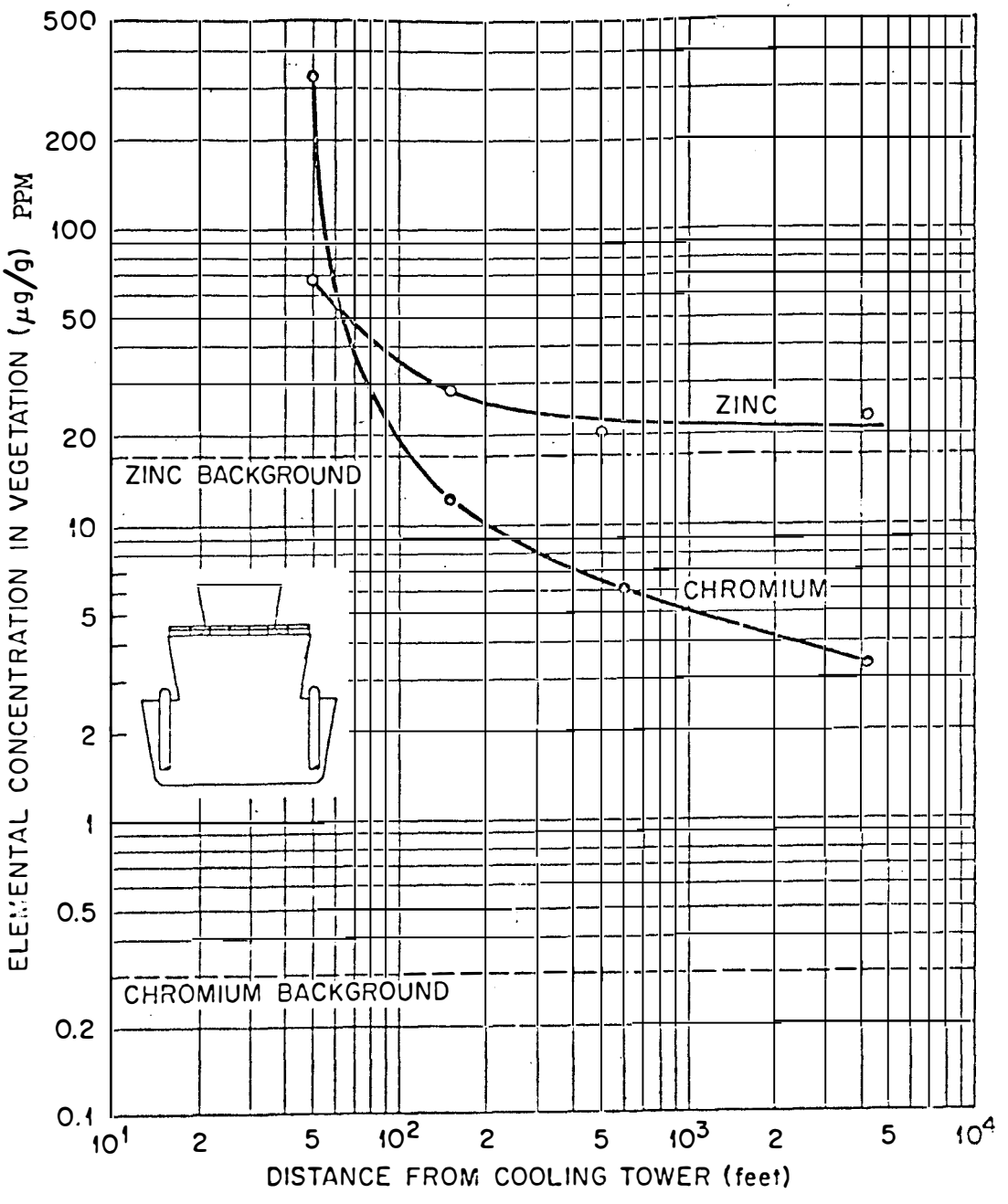

Figure 9-9 . Transfer of Chromium and Zinc to Vegetation from Cooling Tower Drift as a Function of Distance from the Tower. The Horizontal Lines (dashed) Indicate Levels of Concentration in Vegetation Remote from the Towers.

drag forces in both the horizontal and vertical directions. The plume rise is a function of the downwind distance. The drop can actually leave the plume while still traveling upward (this actually occurs with the smaller drops for the velocity field considered). Therefore, the drops leave the plume in a shorter amount of time and fall to the ground sooner.

Another difference in the models is the minimum size of particles considered to be transported by body forces and drag forces. Hosler, et.al.,[17] consider particles as small as 25 μm in radius. Based on the recommendation of Gifford and Hanna[18], the smallest drops considered to be transported by body forces and drag forces are those drift drops whose radii are greater than 40 μm. Inclusion of these small drop sizes in Hosler, et.al., model cause a slight overestimate a great distances from the tower. It is recommended that deposition of drift drops from cooling towers whose radii are less than 40 μm be calculated by a method discussed in detail by Chamberlandd[20] and in Meteorology and Atomic Energy.[42]

CHAPTER X

CONCLUSIONS

The primary purpose of this research has been to study the dynamic forces effecting the transport and deposition of large drift drops from evaporation cooling towers. The equation governing the motion of a drift drop after it leaves the cooling tower has been developed and solved by a finite difference method. A term was included in the equation of motion which has not been included by previous authors.

As pointed out in Chapter II, the mixing of a cooling tower plume with ambient air is a complicated process. Not only are there no known analytical models which accurately predict the detailed velocity, temperature, and specie concentrations fields within a plume, but there is no experimentally reproducible data to verify an analytical model.

In order to solve for the position coordinates of the drift drop as a function of time, it was necessary to know the details of the velocity field within the plume. Therefore, a simplified plume model was developed and presented in Chapter VII. Although this plume model was a very crude approximation to the actual mixing phenomenon, it yielded a reasonable velocity field which could be used to solve the differential equation of motion.

The effects of chemicals dissolved in the drift drop on the evaporation rate of the drop have been considered. Previous models considered only sodium chloride (NaCl) whereas the present model is general enough to consider any soluable inorganic salt.

The most significant difference between the UT model and previous models is that the UT employs a realistic method of treating the calm conditions whereas previous models do not account for the calm. Also, the UT model accounts for the time variations in the concentration of any salt dissolved in the drop as evaporation occurs. The agreement of the UT model with experimental results is good, especially near the tower.

An effort has been made to present the concepts which can be used to accurately predict the transport and deposition of drift drops when a more accurate description of the velocity field within a cooling tower plume becomes available. In the near future, more accurate measurements of the drift drop size distribution as well as concurrent meteorological and chemical deposition data will also become available so that the accuracy of the drift transport and deposition may be improved.

BIBLIOGRAPHY

BIBLIOGRAPHY

1. Brandt, C. S., Agricultural Specialist, Bureau of Air Quality Control, Md. State Dept. of Health and Mental Hygiene, Personal Communication, 1973.

2. Woods, B., and P. Betts, "A Contribution to the Theory of Natural Draught Cooling Towers," Proc. Inst. Mech. Engrs., 54-78, 1950.

3. Chilton, H., "Performance of Natural-Draught Water Cooling Towers," Proc. Inst. Elec. Engrs., 99, 440-456, 1952.

4. Abramovich, G. N., The Theory of Turbulent Jets, Cambridge: Massachusetts Institute of Technology Press, 1963.

5. Morton, B. R., "Buoyand Plumes in a Moist Atmosphere," J. Fluid Mech., 2, 127-144, 1957.

6. Briggs, G. A., Plume Rise, AEC Critical Review Series, TID-25075 form Clearinghouse for Fed. Scient. and Tech. Inform., U.S. Dept. of Comm., Springfield, Va.

7. World Meteorology Organization, Internat. Meteorol. Tables, WMO-188-TP-94, introd. to tables 4.6 and 4.7, 1966.

8. Simpson, J., and V. Wiggert, "Models of Precipitating Cumulus Towers," Mon. Wea. Rev., 97, 471-766, 1970.

9. Hanna, S. R., "Cooling Tower Plume Rise and Condensation," Proceedings Air Pollution, Turbulence, and Diffusion Symposium, Las Cruces, New Mexico, Dec. 7-10, 1971.

10. Hewett, T. A., J. A. Fay, and D. P. Hoult, "Laboratory Experiments of Smokestack Plumes in a Stable Atmosphere," Atmospheric Environment, Pergamon Press, Great Britain, Vol. 5, p. 767-789, 1971.

11. Brunt, D., " Condensation by Mixing," Q. J. Roy Soc., Vol. 61, Vol. 61, p. 213-217, 1935.

12. Overcamp, T. J., and D. P. Hoult, "Precipitation in the Wake of Cooling Towers," Atmos. Envir., Vol. 5, p. 751-766, 1971.

13. Southern Nuclear Engineering, Inc., An Evaluation of the Feasibility of Salt Water Cooling Towers for Turkey Point, SNE-54, February, 1970.

14. Sterm, A. C., Editor, Air Pollution, Vol. 1, Academic Press, New York, London, 1968.

15. GPU Service Corp., Program to Investigate the Feasibility of Natural Draft Salt Water Cooling Towers, Appendix to "Applicant's Environmental Report" for Forked River Unit 1, New York, 1972.

16. EG&G, Inc., "Potential Environmental Modifications Produced by Large Evaporative Cooling Towers," prepared for EPA Water Pollution Control Research Series 16130DNH01171, Boulder, Colo., 1971.

17. Hosler, C., Pena, J. and Pena, R., Determination of Salt Deposition Rates from Drift from Evaporative Cooling Towers, Dept. of Meteorology, Pennsylvania State University, 1972.

18. Gifford, F. A., and Hanna, S. R., discussions held at the Atmospheric Turbulence and Diffusion Laboratory, National Oceanic and Atmospheric Administration, Oak Ridge, Tennessee, Jan. thru March, 1973.

19. Bosanquet, C. H., Carey, W. F., and Halton, E. M., "Deposition of Solid Particles in Air," Proc. Inst. Mech. Engineers, 162:355, London, 1950.

20. Chamberlain, A. C., Aspects of Travel and Deposition of Aerosols and Vapor Clouds, Atomic Energy Research Establishment, AERE-HP/R1261, Harwell, Berkshire, England, 1961.

21. Wieselsberger, C., Zeitschr. Flugtech. Motorluftschiffahrt, 4, 140, 1914.

22. Morsi, S.A., and Alexander, A.J., "An Investigation of Particle Trajectories in Two-Phase Flow Systems," J. Fluid Mech., Vol. 55, Part 2, pp. 193-208, 1972.

23. Lewis, B., Pease, R.N., and Taylor, H.S. (editors), High Speed Aerodynamics and Jet Propulsion, Vol. II, p. 425, Princeton Univ. Press., Princeton, N.J., 1956.

24. Davies, C., "Definitive Equations for the Fluid Resistance of Spheres," Proc. of Phys. Soc. London, Vol. 57, p. 260, 1945

25. Beard, K. V., and Pruppacher, H. R.,"A Determination of the Terminal Velocity and Drag of Small Water Drops by Means of a Wind Tunnel," Journal of Atmospheric Science, 26:1066, 1969.

26. LeClair, B. P., A. E. Hamielec and H. R. Pruppacher, "A Numerical Study of the Drag on a Sphere at Low and Intermediate Reynolds Numbers," Journal of Atmospheric Science, 27:308-315, 1970.

27. Batchelor, G. K., An Introduction to Fluid Dynamics, Cambridge: Cambridge University Press, 1967.

28. Landau, L. D., and E. M. Lifschitz , Fluid Mechanics, New York: Pergamon Press, 1959.

29. Rybczinski, W., Anzeig. Akad. Krakau, s. 40, 1911.

30. Lamb, G., Hydrodynamics, Gostekhizdat, M.-L., Sect. 337, 1947.

31. Oseen, C. W., "Uber Die Stokessche Formel and Uber Die Verwandte Aufgabe in der Hydrodynamik," Arkiv for Mathematik, Astronomi Och Fysik, 6, 29, 1910.

32. Klyachko, L., Heating and Ventilation, No. 4, 1934.

33. Langmuir, I., "The Evaporation of Small Spheres," Physics Review, 12:368, 1918.

34. Topley, B. and R. W. Whytlaw-Gray, "Experiments on the Rate of Evaporation of Small Spheres as a Method of Determining Diffusion Coefficients," Philosophical Magazine, 4:873, 1927.

35. Houghton, H. G., "A Study of the Evaporation of Small Water Drops," Physics, 4:419, 1933.

36. Takahasi, Y., "Experiments on the Evaporation of Water Drops," Geophysics Magazine, 10:321, 1936.

37. Frossling, N., "Uber die Verdunstung Fallender Tropfen," Gerlands Beitreibung Geophysik, 52:170, 1938.

38. Kinzer, G. and R. Gunn, "The Evaporation, Temperature, and Thermal Relaxation Time of Freely Falling Water Drops," Journal of Meteorology, 8:71-83, 1951.

39. Wood, J. H., and Keenan, C. H., General College Chemistry, New York:Harper & Brothers, 1957.

40. Wistrom, G. K., and Ovard, J. C., "Cooling Tower Drift-Its Measurement, Control and Environmental Effects," Presented at Cooling Tower Institute Annual Meeting, Houston, Texas, Jan. 29-31, 1973.

41. Unpublished Experimental Data, Oak Ridge National Laboratory, Oak Ridge, Tennessee, 1972.

42. Slade, D. H. (editor), Meteorology and Atomic Energy, U. S. Atomic Energy Commission, Division of Technical Information, July, 1968.

APPENDIXES

APPENDIX A

For a copy of the computer deck described in this paper, please contact

Dr. W. T. Snyder, Head
Department of Engineering Science
& Mechanics
Perkins Hall
University of Tennessee
Knoxville, Tenn. 37916

APPENDIX B

Consider m_1 grams of air at temperature T_1 with specific humidity q_1 and 1 gram of air at temperature T_2 and specific humidity q_2. Let these two quantities of air mix without condensation as shown in Figure B-1. From the conservation of mass,

$$m_1 + 1 = m_3 \qquad (B-1)$$

and

$$m_1 q_1 + q_2 = m_3 q'_3 \qquad (B-2)$$

Combining equations B-1 and B-2, one obtains

$$q'_3 = \frac{m_1 q_1 + q_2}{m_1 + 1} \qquad (B-3)$$

From the conservation of energy,

$$m_1 c_{P_a}(T_1 - T_{ref}) + m_1 q_1 c_{P_v}(T_1 - T_{ref}) + c_{P_a}(T_2 - T_{ref}) + q_2 c_{P_v}(T_2 - T_{ref}) = m_3 c_{P_a}(T'_3 - T_{ref}) + m_3 q'_3 c_{P_v}(T'_3 - T_{ref}). \qquad (B-4)$$

Combining equations B-1, B-3, and B-4 and letting $T_{ref} = 0$, one obtains

$$m_1 c_{P_a} T_1 + m_1 q_1 c_{P_v} T_1 + c_{P_a} T_2 + q_2 c_{P_v} T_2 = (m_1 + 1) c_{P_a} T'_3 + (m_1 + 1) c_{P_v} \left(\frac{m_1 q_1 + q_2}{m_1 + 1}\right) T'_3 \qquad (B-5)$$

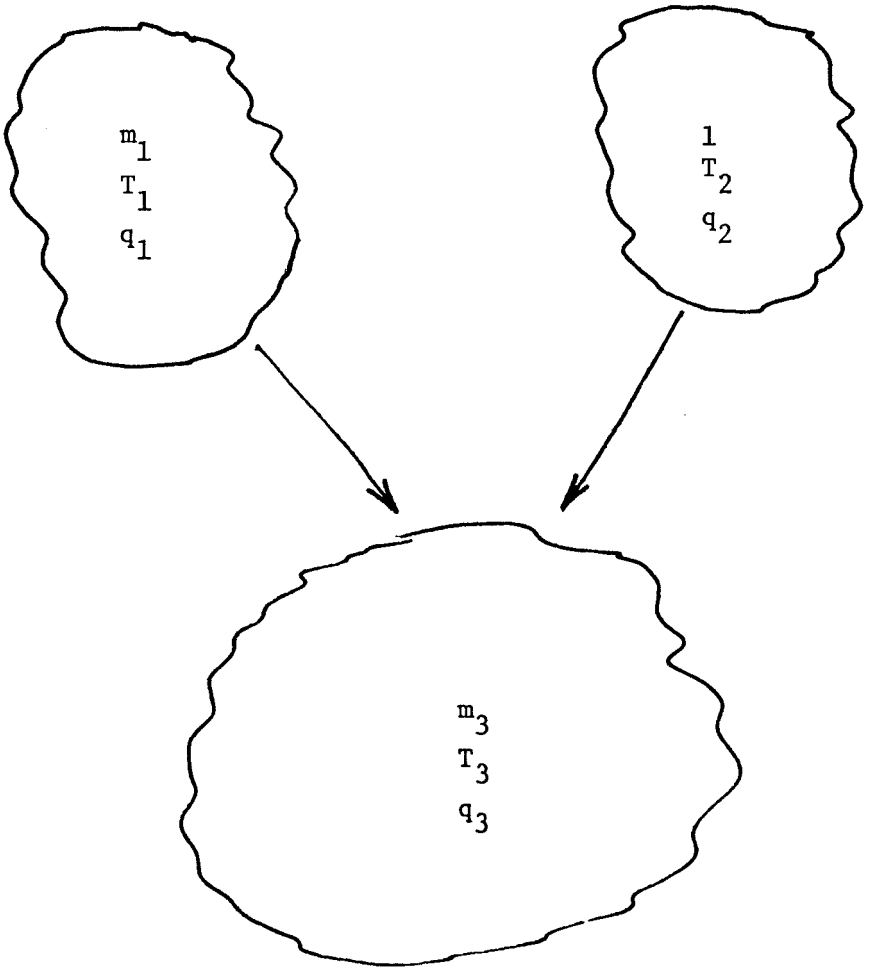

Figure B-1. The Mixing of Air

Solving equation B-5 for the temperature of the mixture, T_3', one obtains

$$T_3' = \frac{c_{Pa}(m_1 T_1 + T_2) + c_{PV}(m_1 q_1 T_1 + q_2 T_2)}{(m_1 + 1) c_{Pa} + (m_1 q_1 + q_2) c_{PV}} \quad (B-6)$$

For small amounts of water vapor in air, the second term in the numerator and the denominator are small and may be neglected. Hence, equation B-6 becomes

$$T_3' = \frac{m_1 T_1 + T_2}{m_1 + 1} \quad (B-7) \quad (2-13)$$

With condensation, $T_{ref} = 0$, and neglecting the enthalpy of the vapor, equation B-4 becomes

$$m_1 c_{Pa} T_1 + c_{Pa} T_2 = (m_1 + 1) c_{Pa} T_3 + [m_1 q_1 + q_2 - (m_1 + 1) q_3] L \quad (B-8)$$

where the second term represents the amount of latent heat released. Solving equation B-8 for the temperature of the mixture, one obtains

$$T_3 = \frac{m_1 T_1 + T_2}{m_1 + 1} + \left[\frac{m_1 q_1 + q_2 - (m_1 + 1) q_3}{m_1 + 1}\right] \frac{L}{c_{Pa}} \quad (B-9) \quad (2-12)$$

The term in brackets in equation B-9 represents the mass of liquid water condensed per unit mass of dry air, σ. Hence,

$$\sigma = \frac{m_1 q_1 + q_2 - (m_1 + 1) q_3}{m_1 + 1} \quad (B-10) \quad (2-18)$$

Differentating equation B-10 with respect to m_1, one obtains

$$\frac{d\sigma}{dm_1} = \frac{q_1 - q_2}{(m_1 + 1)^2} \qquad (B-10) \quad (2-19)$$

VITA

Edison A. Picklesimer, Jr., was born in Rahway, New Jersey, on December 5, 1941. He attended elementary schools in Verona, New Jersey, and was graduated from Verona High School in 1960. The following September he entered Georgia Institute of Technology, and in June, 1965, he received a Bachelor of Mechanical Engineering. In the summer of 1965, he accepted a teaching assistantship at Georgia Institute of Technology and began study toward a Master's degree. He received this degree in December, 1966.

He entered the Graduate School at the University of Tennessee in September, 1967, as a graduate research assistant and received the degree Doctor of Philosophy with a major in Engineering Science and Mechanics in August, 1974. He is a member of the American Society of Mechanical Engineers.

He is married to the former Linda Ann Patrick of Gainesville, Georgia. He has two sons, Patrick and Kent. His hobbies are golf and tennis.